TECHNICAL REPORT GL-83-14

IN SITU AND LABORATORY SHEAR DEVICES FOR ROCK: A COMPARISON

by

Glenn A. Nicholson

Geotechnical Laboratory
U. S. Army Engineer Waterways Experiment Station
P. O. Box 631, Vicksburg, Miss. 39180

October 1983
Final Report

Approved For Public Release; Distribution Unlimited

Prepared for Office, Chief of Engineers, U. S. Army
Washington, D. C. 20314

Under CWIS 31197

Unclassified

SECURITY CLASSIFICATION OF THIS PAGE (When Data Entered)

REPORT DOCUMENTATION PAGE

READ INSTRUCTIONS BEFORE COMPLETING FORM

1. REPORT NUMBER
Technical Report GL-83-14

2. GOVT ACCESSION NO.

3. RECIPIENT'S CATALOG NUMBER

4. TITLE (and Subtitle)
IN SITU AND LABORATORY SHEAR DEVICES FOR ROCK: A COMPARISON

5. TYPE OF REPORT & PERIOD COVERED
Final report

6. PERFORMING ORG. REPORT NUMBER

7. AUTHOR(s)
Glenn A. Nicholson

8. CONTRACT OR GRANT NUMBER(s)

9. PERFORMING ORGANIZATION NAME AND ADDRESS
U. S. Army Engineer Waterways Experiment Station
Geotechnical Laboratory
P. O. Box 631, Vicksburg, Miss. 39180

10. PROGRAM ELEMENT, PROJECT, TASK AREA & WORK UNIT NUMBERS
CWIS 31197

11. CONTROLLING OFFICE NAME AND ADDRESS
Office, Chief of Engineers, U. S. Army
Washington, D. C. 20314

12. REPORT DATE
October 1983

13. NUMBER OF PAGES
141

14. MONITORING AGENCY NAME & ADDRESS(if different from Controlling Office)

15. SECURITY CLASS. (of this report)
Unclassified

15a. DECLASSIFICATION/DOWNGRADING SCHEDULE

16. DISTRIBUTION STATEMENT (of this Report)
Approved for public release; distribution unlimited.

17. DISTRIBUTION STATEMENT (of the abstract entered in Block 20, if different from Report)

18. SUPPLEMENTARY NOTES
Available from National Technical Information Service, 5285 Port Royal Road, Springfield, Va. 22161.

19. KEY WORDS (Continue on reverse side if necessary and identify by block number)
Field tests
Rock strength
Rock tests (Laboratory)
Shear strength (Rock)

20. ABSTRACT (Continue on reverse side if necessary and identify by block number)
Shear strength parameters were measured using an assortment of testing devices. The results were compared and contrasted. The devices included machines routinely used by the U. S. Army Corps of Engineers and several machines with new or unusual features.

The tests were performed on rock simulant and Rangely sandstone. The tests on rock simulant used specimen suites that included smooth cast joints, joints with asperities, and intact material. The tests on the Rangely sandstone were performed on clean discontinuities. (Continued)

DD FORM 1 JAN 73 1473 EDITION OF 1 NOV 65 IS OBSOLETE

Unclassified

SECURITY CLASSIFICATION OF THIS PAGE (When Data Entered)

20. ABSTRACT (Continued).

All tests on the rock simulant were performed in the laboratory. One of the test suites on the sandstone was performed in situ; the remainder of the tests were performed in the laboratory.

The tests showed substantial differences in strength parameters due to test machine details. The study demonstrated the need for a reliable direct shear device capable of testing 6-in.-diam core.

PREFACE

This study was conducted by the U. S. Army Engineer Waterways Experiment Station (WES). The work was sponsored by the Office, Chief of Engineers (OCE), under Civil Works Investigation Study (CWIS) 31197, Determination of In Situ Strength of Rock Masses.

Mr. G. A. Nicholson, Engineering Geology and Rock Mechanics Division (EGRMD), Geotechnical Laboratory (GL), conducted the research and prepared this report under the general supervision of Mr. J. S. Huie, Chief, Rock Mechanics Applications Group, GL, and Dr. D. C. Banks, Chief, EGRMD. Mr. J. P. Sale and Dr. W. F. Marcuson III were Chiefs, GL, during the investigation. Mr. Paul R. Fisher was the OCE Technical Monitor.

Commanders and Directors during the study and report preparation were COL John L. Cannon, CE, COL Nelson P. Conover, CE, and COL Tilford C. Creel, CE. Technical Director was Mr. Fred R. Brown.

CONTENTS

CONVERSION FACTORS, U. S. CUSTOMARY TO METRIC (SI) UNITS OF MEASUREMENT

U. S. customary units of measurement used in this report can be converted to metric (SI) units as follows:

Multiply	By	To Obtain
cubic feet	0.02831685	cubic metres
feet	0.3048	metres
inches	2.54	centimetres
kips (force)	4.448222	kilonewtons
pounds (force)	4.448222	newtons
pounds (force) per square inch	6894.757	pascals
pounds (mass) per cubic foot	16.01846	kilograms per cubic metre
square inches	6.4516	square centimetres
tons (force) per square foot	95.76052	kilopascals

IN SITU AND LABORATORY SHEAR DEVICES FOR ROCK: A COMPARISON

PART I: INTRODUCTION

Background

1. The diverse localities of U. S. Army Corps of Engineers (CE) construction projects include many which have major structures founded in or on rock masses. The economical construction and continued safe maintenance of these structures require knowledge of the rock mass behavior under loading. Most rock masses encountered in civil engineering works possess internal surfaces of real or potential weakness. These zones of weakness are referred to as discontinuities.

2. The term "discontinuity" applies to many naturally occurring planes or near planar surfaces or zones of weakness, as well as fractures induced during excavation caused by blasting and stress relief. Relatively clean discontinuities include many joints, fractures, bedding planes, and foliation surfaces. Discontinuities may be open, closed, or healed (i.e., the joint surfaces are wholly or partially welded together).

3. Discontinuities may contain clay or some type of crushed or sheared material. The fill material is usually produced by shearing and weathering along the discontinuity or is deposited by groundwater flow. Other discontinuities may be formed by thin layers of weak material interbedded with hard intact rock (i.e., weak shale beds interbedded with sandstone and limestone).

4. The overall strength (and hence the stability of associated structures) of most rock masses is controlled not by the strength of the intact portions between discontinuities, but by the resistance of the separate portions of the mass to slippage over one another along the discontinuities. Factors controlling the shear of a discontinuity include body loads imposed on the interface, the macroroughness of the opposing surfaces, the frictional characteristics of the constituent minerals, the nature of the material intervening between rock blocks, and the pore water pressures in the discontinuity.

5. Even with extreme care during the sampling operation, seldom is the condition of specimens recovered for laboratory tests representative of the in situ conditions. Specifically, discontinuity surfaces are either damaged and lost, or the specimens are not of sufficient size. Often the "good rock" is tested rather than the "bad rock," and an unrealistically high factor of safety results from unconservative data sources. When parameters defining material properties can be obtained from in situ testing, then the degree of uncertainty caused by the recovery operation is minimized.

6. The in situ shear strength of discontinuities is usually determined from direct shear tests on in situ specimens isolated and prepared in a manner so that failure occurs along the discontinuity. Numerous cases have been reported in the literature describing in situ shear equipment, test procedures, and test results. Zeigler (1972) presents a comprehensive state-of-the-art discussion on in situ testing of rock masses. In this country, both the U. S. Army Corps of Engineers (Missouri River Division (MRD) and Ohio River Division (ORD)) and the U. S. Bureau of Reclamation have been active in in situ shear strength testing of discontinuous rock.

7. In situ tests, even under ideal conditions where representative specimens can be isolated and prepared with relative ease, are laborious and time consuming. In situations where test pits or test adits require extensive excavation to isolated and prepared representative specimens, the cost of in situ testing can be prohibitive. Because of the expense, in situ tests are usually reserved for those projects where the strength parameters are critical.

8. Shear strength parameters used for the design of most structures founded in or on rock are obtained from small laboratory shear tests, empirical application of index test, and intuition based on engineering judgment. Loading systems and specimen failures of small laboratory shear tests closely model in situ tests and failures in the field. It is, however, difficult to determine whether the data obtained with these devices are representative of the total field strength, even assuming the tests were conducted correctly. Additionally, it is not known how accurate the tests are, i.e., do the tests really give the correct shear strength parameters for the portion of discontinuity tested. The primary advantage of laboratory tests is cost (under ideal conditions approximately 10 to 100 times cheaper than in situ tests). Empirical techniques and intuition provide, at best, only approximations of in situ shear strength.

Purpose of the Study

9. The study reported herein was conducted to (a) define factors controlling in situ shear strength of discontinuous rock, (b) evaluate the various commonly used laboratory testing devices, and (c) to make recommendations for methods and equipment for field and laboratory tests. Test methods and equipment recommended as a result of this study will have direct future application in defining shear strength parameters of discontinuous rock for new projects and in the assessment and evaluation of existing structures or slopes.

Method of Approach

10. The results of large-scale direct shear tests, used as a standard, were compared with the results of small-scale shear tests made with devices commonly used by the CE. Attempts were made to rationalize any discrepancies between the test results and to determine which of the smaller shear tests produced the most reliable shear strength parameters as compared with the larger direct shear tests. The study was divided into four phases: (a) development of equipment and model material, (b) molding and testing of specimens, (c) data reduction, and (d) analysis of data. Each of the phases will be covered in detail in later parts of this report.

11. There are four factors which must be considered when comparing the data obtained with the various testing devices. These are: (a) scale effect, (b) mode of failure, (c) duplication of test specimens, and (d) the stiffness of the test devices.

12. In previous paragraphs the size of the test or specimen was frequently mentioned. It was implied that large tests were more reliable than small tests. The importance of specimen size is relative to the total surface area of the discontinuity considered. In naturally occurring discontinuities, surfaces exhibit irregularities or asperities which contribute added shearing resistance. Size or scale effect can best be explained by examining the hypothetical discontinuities illustrated in Figure 1. The test results from specimen A would not be the same as the results from specimen B, and in all probability, for this particular case, specimen A might better approximate the shear strength of the entire discontinuity. Specimen B may tend to give

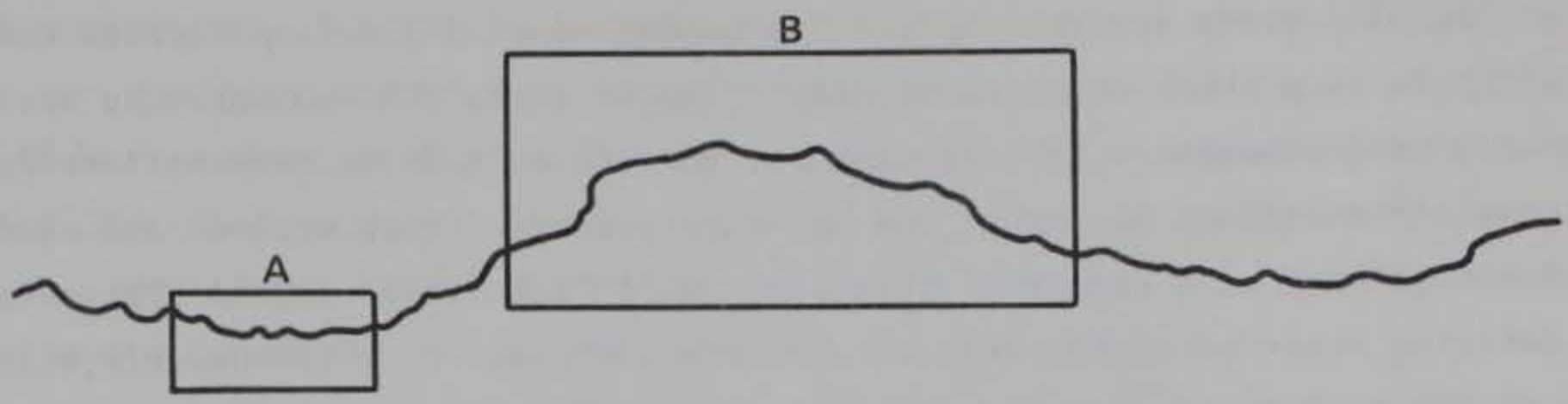

Figure 1. Illustration of specimen size with respect to the relative scale of asperities

strength parameters higher than the total field strength if the large asperity represented only a small portion of the discontinuity. If that were the case, when the discontinuity is mobilized, the stress levels at the large asperity would be very high, resulting in lower shear resistance (Pratt, Black, and Brace, 1974). Specimen B would, however, provide better data if the large asperity were representative of the total discontinuity. Generally, the larger the test specimen, the more reliable the test results.

13. Shear failure may be produced by three basic methods: (a) direct shear, (b) triaxial shear, and (c) torsional shear.

14. The first two years of this study were devoted to the design, construction, and trial testing of two shear devices. The two devices were a direct shear device capable of shearing a 2-ft-square* specimen and a torsional shear device capable of shearing a specimen 1 ft in diameter. For reasons of economy, both devices were designed and constructed so that they could be used either in situ or in the laboratory. Neither device should be thought of as a laboratory shear machine. The objectives for the development of the in situ direct shear device were to provide the CE with a readily available laboratory in situ testing capability, provide a data base for evaluating capabilities of small shear devices, and develop design criteria for the construction of a laboratory shear machine. The large 2-ft by 2-ft

---

* A table of factors for converting U. S. customary units of measurements to metric (SI) units is presented on page 4.

direct shear device will be referred to herein as the in situ direct shear device. A commercial torsional shear device was redesigned to facilitate the comparison with the direct shear test results.

15. In addition to the torsional shear device, other small shear devices were evaluated. They included three direct shear devices capable of testing specimens having a maximum diameter of 6 in.; a 3- by 3-in. direct shear device commonly used for soil testing; and two 2.8-in. (specimen diameter) triaxial devices. All small shear devices evaluated differed in design and construction details and details in the mechanics of load application.

16. Two materials were selected for the testing program. The model material that was developed consisted of a mixture of Ottawa sand, B-11 Hydrostone, loess, and water. After curing, the material looked like a soft sandstone with medium-sized rounded constituent particles. Discontinuities were cast with several symmetrical and nonsymmetrical asperity configurations. The rock selected for laboratory testing was a natural fine-grained jointed sandstone. The sandstone was the lower member of the Castlegate (Mesaverde of the Middle Cretaceous age). Appropriately sized specimens were obtained from a field site near Rangely, Colo. The field site was the location of a previous study by Swolfs (1977) at Terra Tek for the Army Research Office (ARO). As part of this study, large in situ direct shear tests were made along clean discontinuities within the sandstone. Specimens similar to those tested by Terra Tek were selected for testing at U. S. Army Engineer Waterways Experiment Station (WES).

Scope

17. This report briefly discusses the design and development of the in situ direct and torsional shear devices, evaluation of small testing devices, development of the model material, preparation and testing of the specimens, methods of analysis, and test results. The test results are summarized, and suggested techniques for determining the shear strength of discontinuous soft rock are presented.

PART II: A DESCRIPTION OF THE VARIOUS SHEAR TEST DEVICES EVALUATED

In Situ Direct Shear Device

18. In the simplest form of in situ direct shear test, the specimen is subjected to a load perpendicular to and another load parallel to a predetermined failure plane or shear zone. Test specimens are typically cubically shaped blocks in test adits, open pits, or on the natural ground surface that have been isolated on all but the bottom side containing the discontinuity by careful excavation. Usually steel frames are grouted around the specimen to form a rigid reaction member for transmitting the shear load uniformly across the specimen. Normal loads are most often applied by a hydraulic jack that reacts against an anchored beam or test adit ceiling. In some cases, the normal loads are applied by dead weights. Normal loads may be varied or held constant during testing. Lateral movement of the test specimen is permitted by incorporating roller bearings in the normal load system. Shear loads are usually generated by a hydraulic jack acting either horizontally through the shear zone or positioned at an angle to the specimen so that the line of action passes through the centroid of the shear zone.

Equipment design objectives

19. A number of design objectives were established, as follows:

a. Provide for a constant shear displacement rate.

b. Provide for constant normal load.

c. Provide for a portable system minimizing mechanized support in setting up the testing apparatus.

d. Ensure that the test procedures can be duplicated.

e. Ensure a minimum of sample disturbance during specimen preparation.

f. Provide for automatic testing operations and data collection.

Equipment design

20. Constant shear displacement rate. Shear tests are generally either strain (displacement) or stress controlled. In the past, investigators have most often generated in situ shear failure by incremental application of the shear load. By definition these tests were controlled stress tests. Effective stress shear strength parameters are more conveniently obtained from controlled strain-type tests since for saturated or partially saturated

material the magnitude of excess pore pressure is a direct function of the structural deformation generated by shear strains. Controlled strain testing allows convenient monitoring, manipulation, or dissipation of these pore pressures. The in situ test equipment (Figure 2) developed at WES for this study incorporates a controlled strain rate system that permits selection of shear displacement rates. The shear load is generated by two screw jacks developing a total of 60 tons force and having a maximum stroke of 10 in. The jack screws require 36 turns to produce 1 in. of movement and are driven by a variable speed electric motor through two 200:1 gear reducers. Speeds from 0.001 to 0.25 in. per minute can be obtained at the full rated load. A slower displacement rate can be achieved at reduced shear loads. The reduction in shear loads at displacement rates slower than 0.001 in. per minute is caused by a reduction in output torque of the variable speed electric motor at very slow rpm's.

21. Constant normal loads. In situ shear test equipment should provide for a constant initial normal load. Maintaining these constant loads during testing is difficult because the top half of the test specimen tends to ride up or down (dilate or consolidate) according to the general asperity profile of the shear surface. The WES equipment uses a floating deadweight system (Figure 3) which permits the specimen to dilate or consolidate with little change in the initial normal load. A 14-in. diameter (153.94-in.^{2} surface area) flat jack placed between the shear specimen platen and the top platen of the reaction frame provides the normal load. Hydraulic oil is supplied to the flat jack by the deadweight pressure system. Limit switches (Figure 3) allow for repositioning of the piston and deadweight pressure system to accommodate compression or dilation of the specimen while maintaining a constant pressure to the flat jack system.

22. Shear box. The shear box is rigidly constructed of 6- by 2-in. steel channels and 1/4-in. steel plate with inside dimensions of 2 by 2 by 1 ft. A 1/2-in. gap is left between the top and bottom halves of the shear box. Since it is often desirable to inundate the shear zone, a water tank was constructed in which the test specimen can be completely submerged.

23. Reaction frame. Two reaction frames were constructed to facilitate both laboratory and field tests. Components of the completed apparatus are manually portable to permit testing at sites with difficult access and to minimize support requirements.

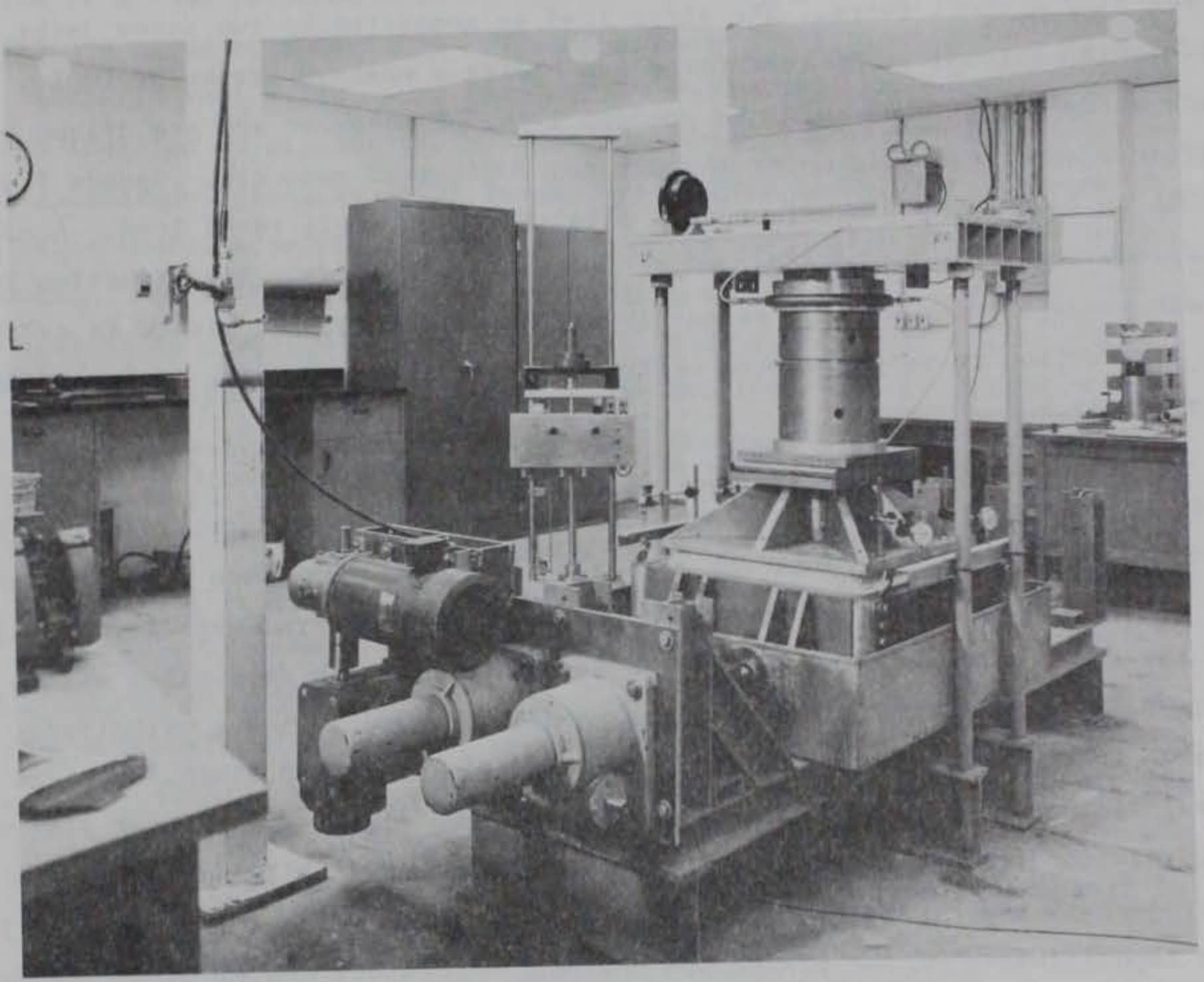

Figure 2. In situ direct shear device set up for laboratory testing

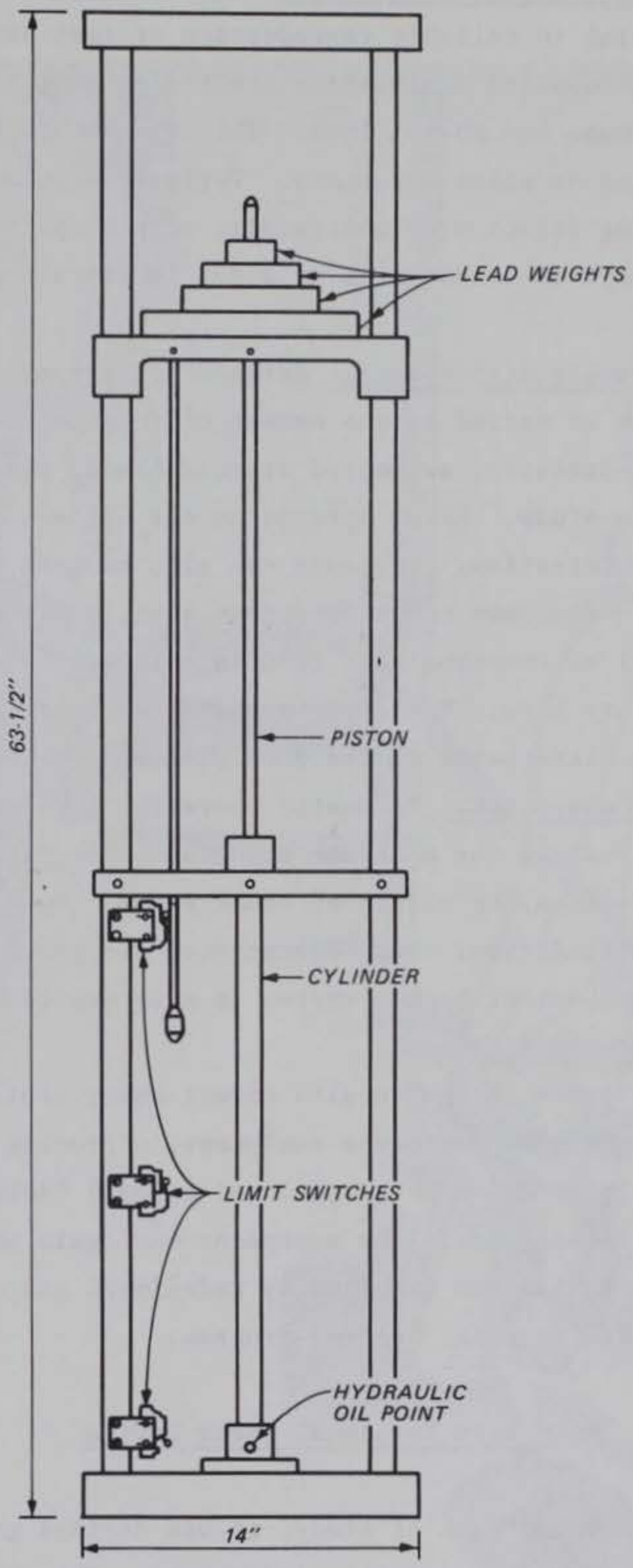

Figure 3. Deadweight normal load system

24. Duplication of test procedures. The ability to duplicate test conditions is essential to reliable reproduction of test data. The most important factors influencing duplication are the ability to control the application of the shear and normal load. The deformation rates can be controlled to within plus or minus 2 percent. Variations in normal loads increase with increasing dilation or compression of the specimen, but in general deformation can be kept to within plus or minus 10 percent of the prescribed load.

25. Minimum sample disturbance. Methods for preparing in situ test specimens are perhaps as varied as the number of in situ tests that have been conducted. A 36-in.-diameter, segmented diamond blade, rock saw (Figure 4) was designed for this study. Water sprayed on the blade aids in removal of cuttings and blade lubrication. Dry cuts can also be made but require a slower cutting rate. Specimen cubes are first sawn from the parent material and then the material surrounding each cube is carefully excavated using picks, shovels, and pry bars. Specimens prepared using this technique appear to have little or no disturbance in the zone of interest (Figures 5 and 6).

26. Automatic operation. Automatic operation is advantageous for two reasons. First, it reduces the manpower required to operate and monitor the tests. Second, it reduces the chance of human error. Once the test has been set up, specimen consolidation, shear operations, and other data are automatically recorded. A mechanical backup system is also provided.

Equipment development

27. The development of the in situ direct shear test equipment was, like the development of most prototype equipment, a process of evolution. The equipment was slightly modified as a result of general "debugging" during its first comprehensive field trial. The equipment was again modified during tests of the model material and was finally redesigned and modified upon completion of the model material testing program.

In Situ Torsional Shear Device

28. Early in this program of study, it was decided to evaluate the in situ torsional shear test as a possible index test. The torsional shear method rotates a cylindrical specimen about an axis normal to the shear zone while controlling the axial load and measuring the torque required to rotate

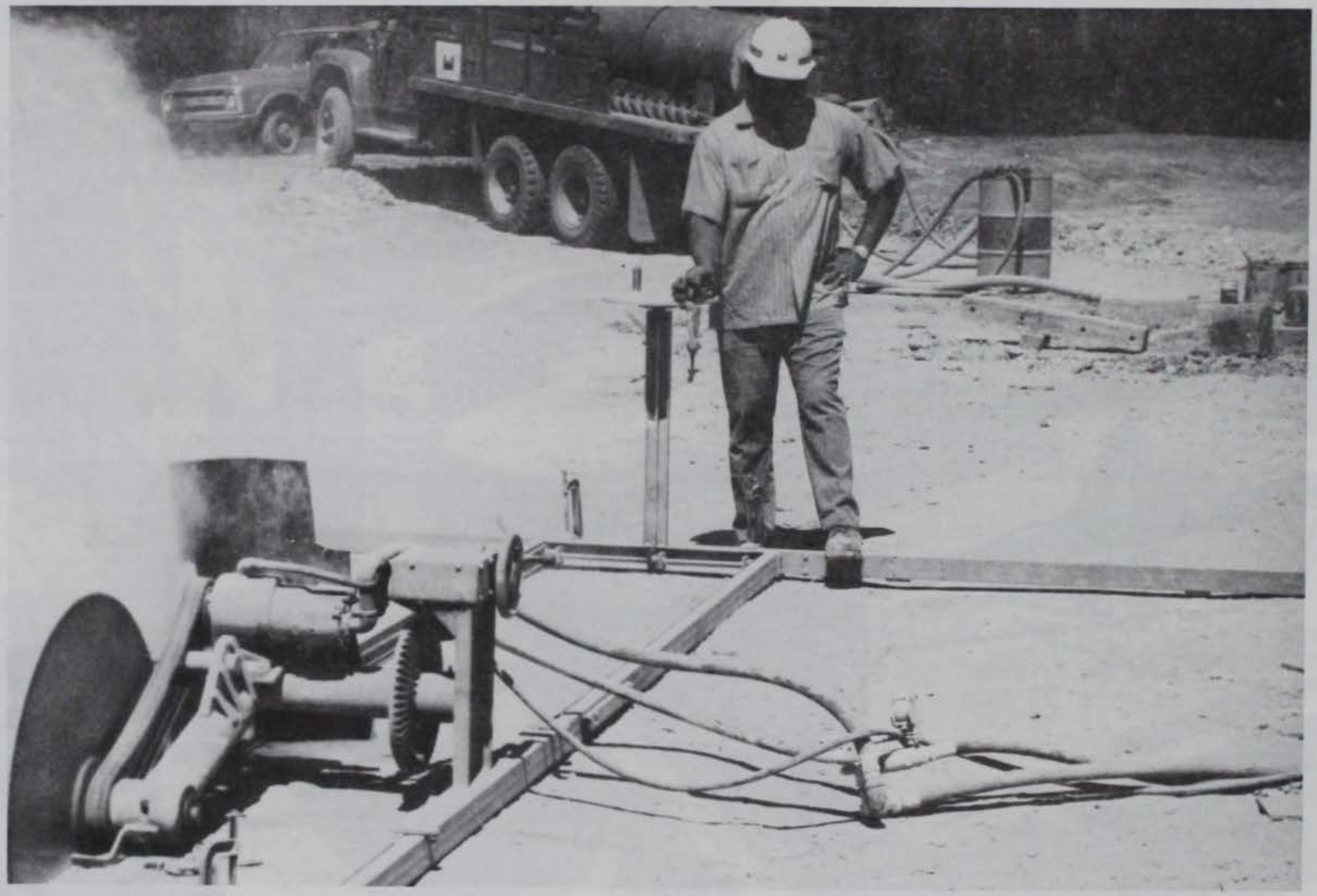

Figure 4. Rock saw

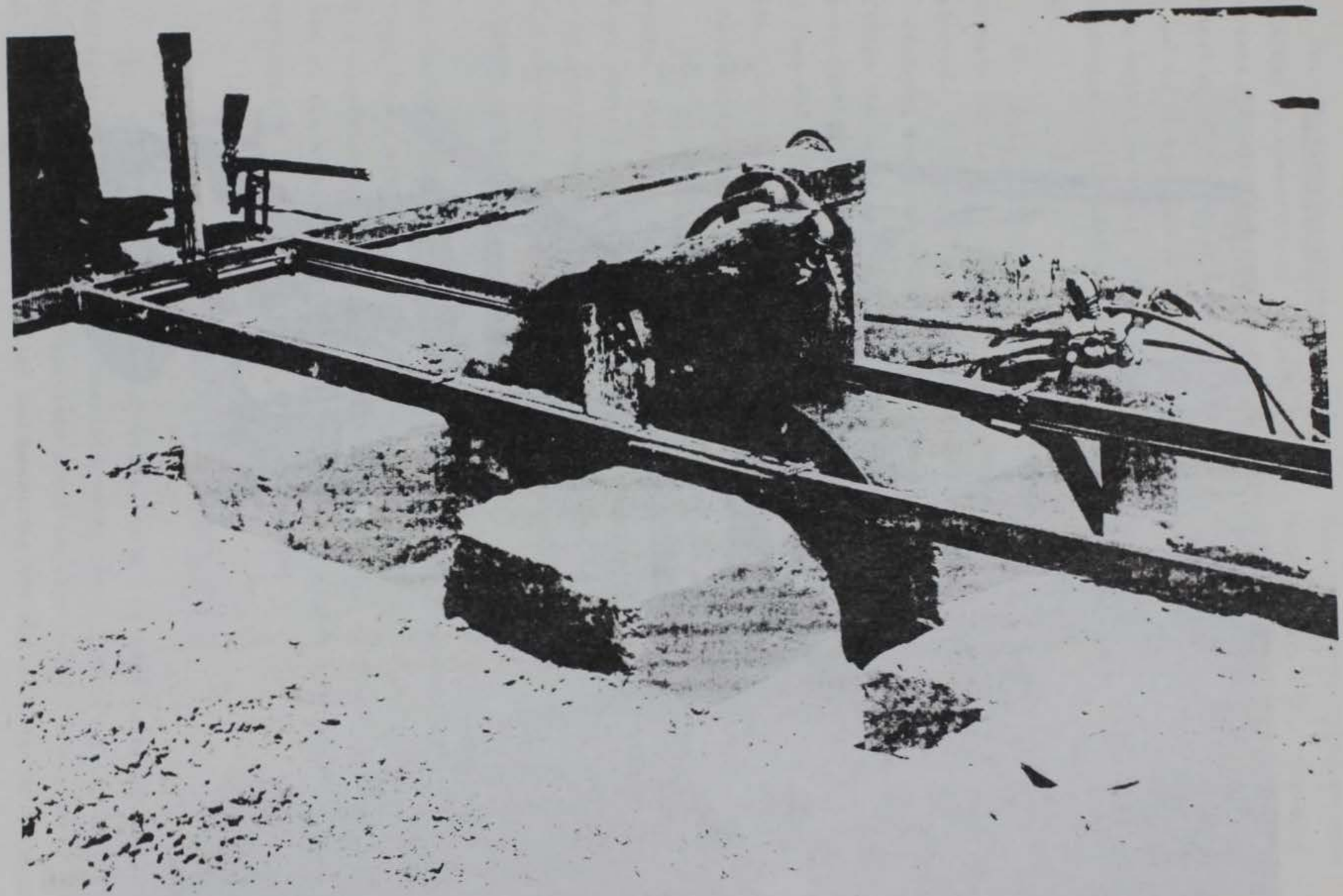

Figure 5. 36-in. rock saw

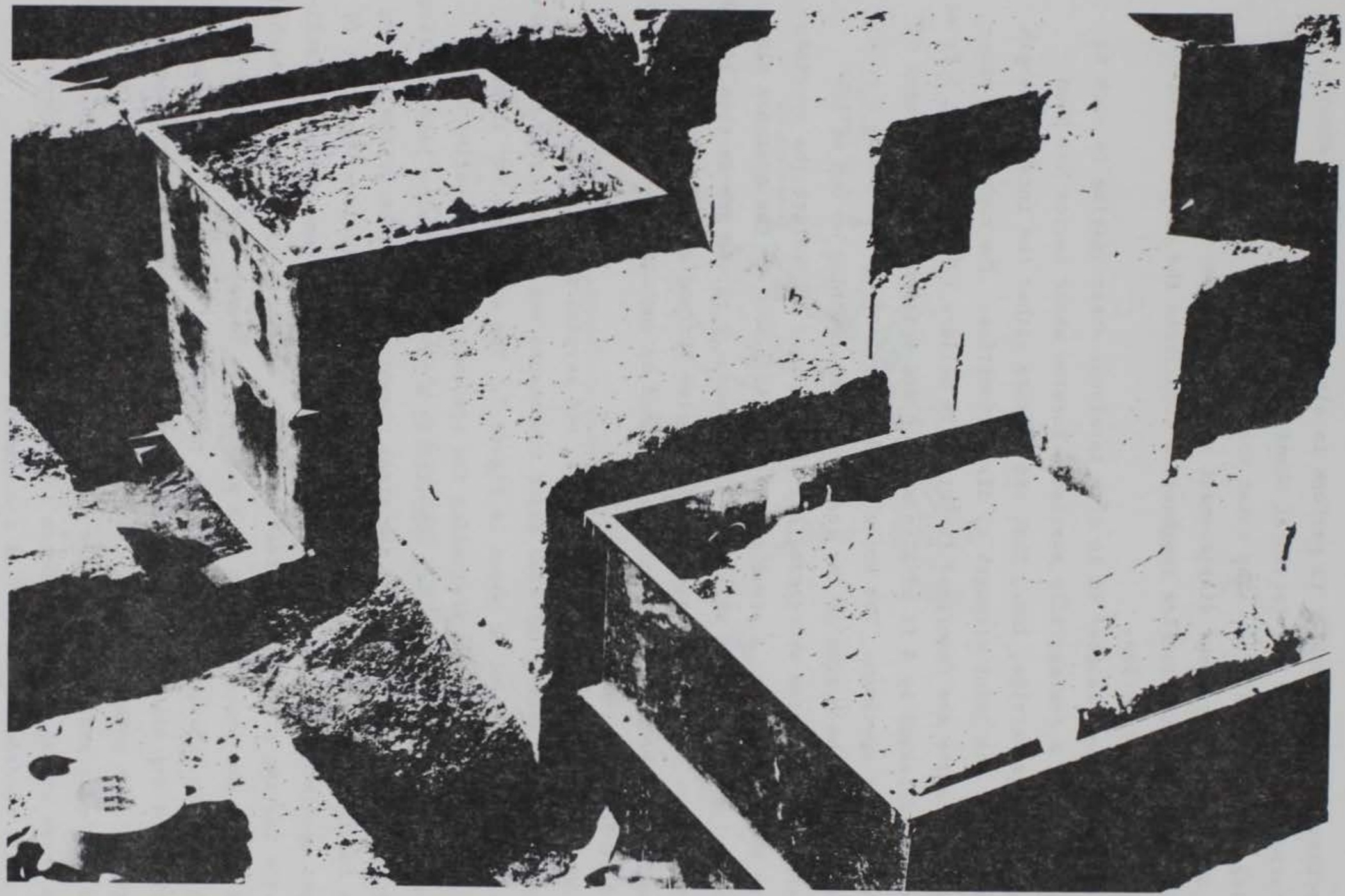

Figure 6. In situ direct shear specimen

the specimen. Although easier to perform in situ than the direct shear test, the rotational motion of the torsional shear test is quite rare in naturally occurring rock mass failures. The shear zone experiences complex phenomena caused by radially dependent displacement rates and stress levels. In addition, linearly trending surface roughnesses complicate the comparison of rotational to linear motion.

29. Literature related to in situ torsional shear testing in rock is sparse. However, a commercially available torsion shear device has been developed by Terrametrics, Inc., that can measure either the intact strength of weak rock or the joint strength of discontinuities. The commercial apparatus and procedure are described in detail by Sellers (1973). First, 5 ft of NX-size hole followed by 5 ft of BX-size hole are drilled into the center of the desired test specimen. The normal load is applied by tensioning a rock bolt anchored to the bottom of the inner hole and reacting on top of the specimen. A 12-in.-diam overcoring bit is then used to isolate the specimen and form the outer wall. A steel torque tube is placed in the overcore slot and cemented to the outside wall of the specimen. A torque arm is then locked on to the torque tube, and torque applied by two hydraulic rams on a common pressure line. The torque reaction is obtained by anchors grouted in the rock a few feet from the test specimen.

30. The equipment, as manufactured, had several undesirable characteristics. Redesign of some major components was accomplished to develop the WES test equipment as shown in Figure 7. The mechanics for transferring torque to the tube and preloading the specimen while overcoring were improved. The normal load is now supplied by a 60-ton hydraulic jack reacting against a frame constructed from two steel channel beams. The bottom bearing plates incorporated thrust bearings to accommodate the rotational movement of the test specimen. A specially modified torque tube was constructed to facilitate the testing of laboratory test specimens. A chain sprocket was attached to the top of the torque tube in such a manner as to permit a continuous 90-deg rotation. Torque was supplied by two 5000-psi hydraulic cylinders. Consolidation and dilation of the test specimen due to shear deformations are measured by four potentiometers. The rotational displacements are obtained from a rack gear assembly driving a 10-turn potentiometer. The normal and torque loads are monitored by 25-ton load cells. All data are recorded on a strip chart recorder. Figure 7 is a schematic of the WES device.

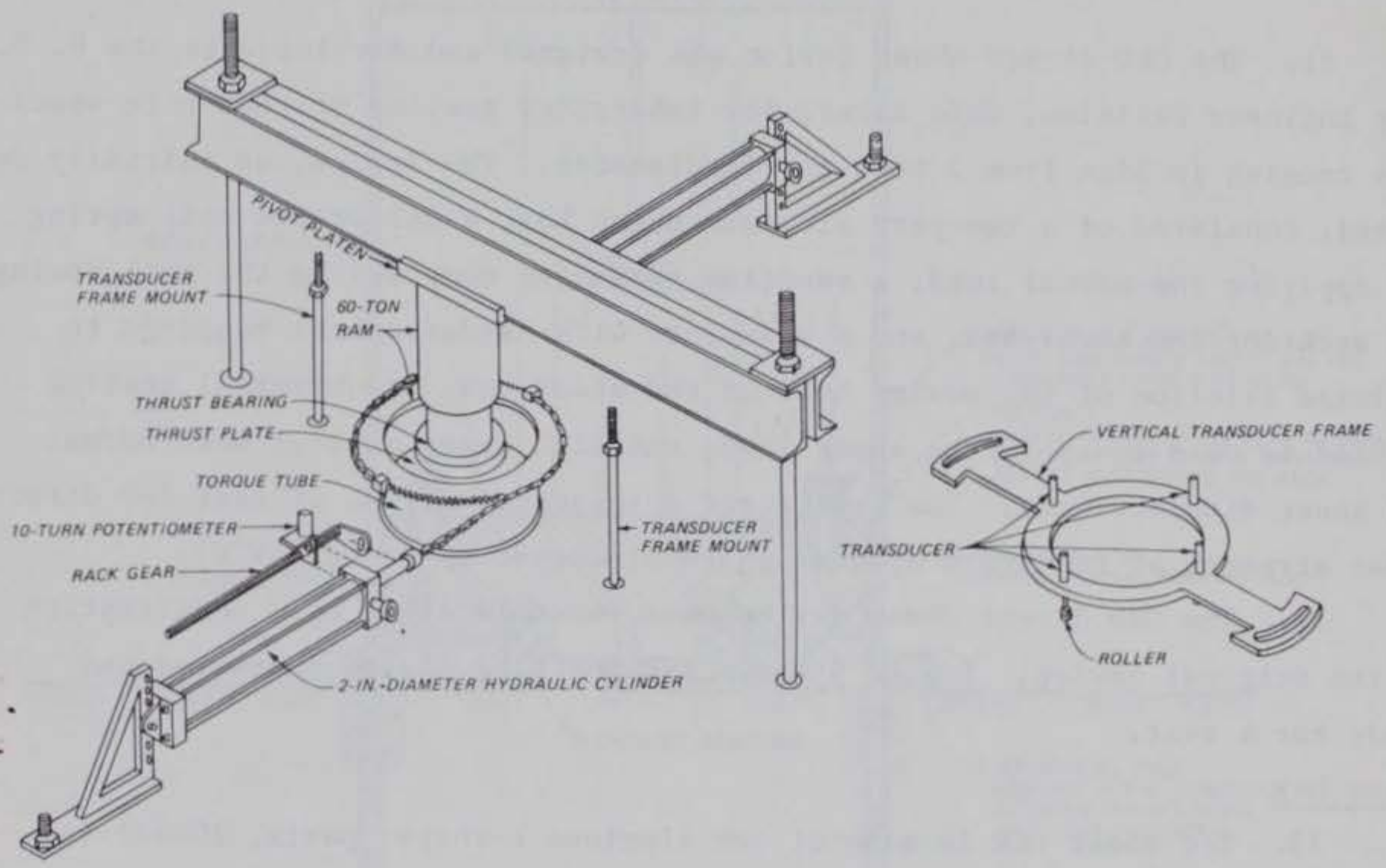

Figure 7. In situ torsional shear device

During sample preparation (overcoring operation), the normal load required to minimize sample disturbance is provided by a WES-designed piston. The piston, riding inside the core barrel, is fitted with several pressure relief valves that maintain a constant pressure (normal load) inside the core barrel as shown in Figure 8.

Ohio River Division Direct Shear Device

31. The ORD direct shear device was designed and developed by the U. S. Army Engineer Division, Ohio River, for laboratory testing of rock core specimens ranging in size from 2 to 6 in. in diameter. The device, as initially designed, consisted of a two-part aluminum shear box, a calibrated coil spring for applying the normal load, a reaction frame for compressing the coil spring and securing the shear box, and a baseplate with hardened ball bearings to minimize friction of the moving half of the shear box. A universal testing machine is used to apply the shear load, and dial gages monitor both normal and shear displacements. The device and a suggested method of test for direct shear strength of rock core specimens are discussed by Kenty (1970).

32. The ORD direct shear device used for this study is a modification of the original device. Figure 9 shows the modified device assembled and ready for a test.

Shear box

33. The shear box is made of two aluminum L-shaped parts, 10-1/2 in. high and 3 in. thick at the specimen receptacle. The specimen receptacle is 7 in. in diameter and will accommodate specimens ranging from 3 to 6 in. in diameter and 4-1/2 to 6 in. in height. The maximum shear displacement for a given shear cycle is 1/2 in.

Normal load system

34. Normal loads were applied by a horizontally mounted hydraulic jack. A constant pressure, variable volume, hydraulic pump supplies hydraulic oil to the jack permitting the jack ram to contract or extend as required for dilation or compression of the specimen during shear. The normal loads were monitored by Bourdon-type pressure gages.

Shear load system

35. Shear loads were applied vertically with a Baldwin Lima 60,000-lb maximum capacity testing machine. The testing machine is equipped with an x-y

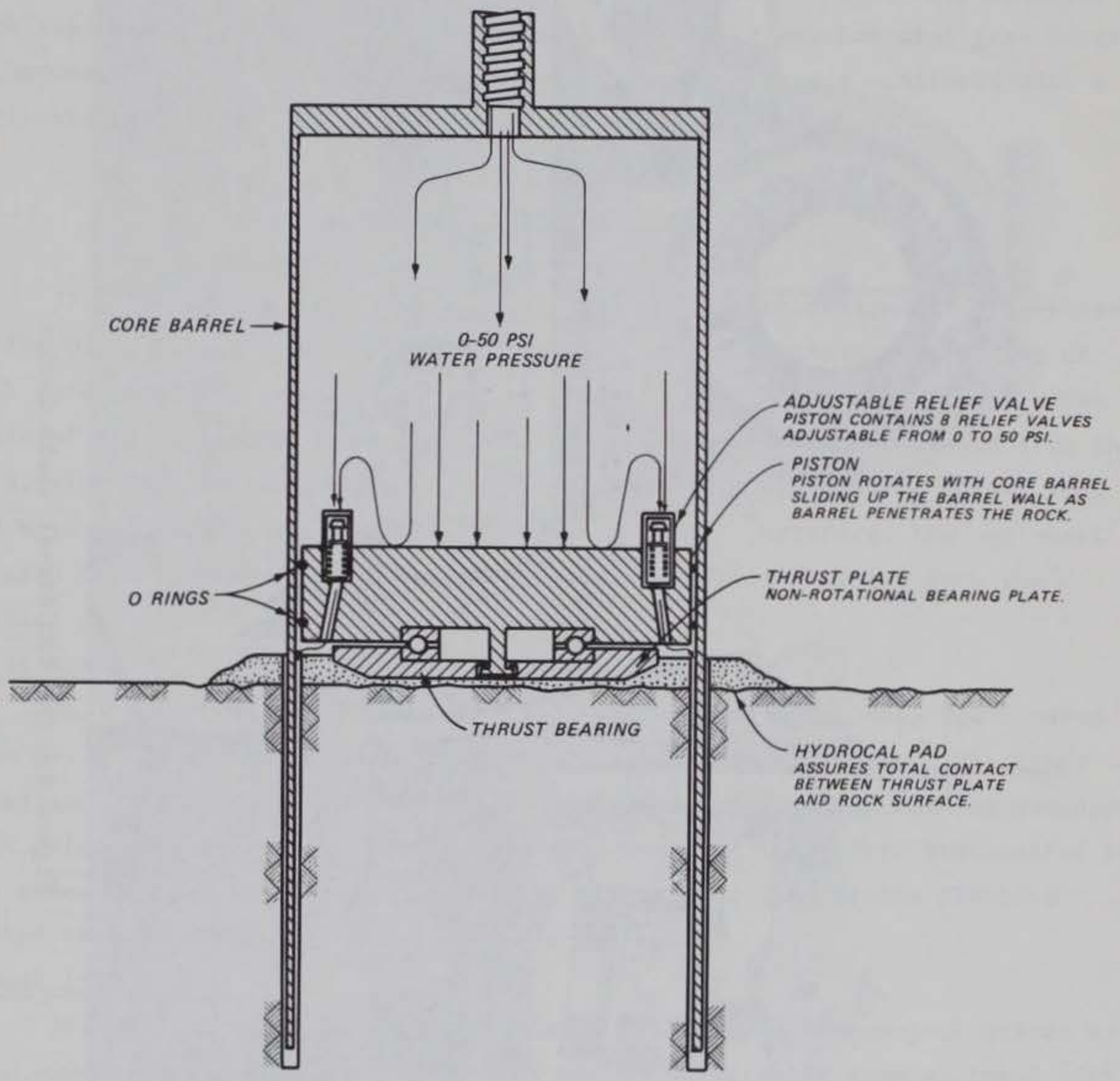

Figure 8. Core barrel assembly used to prepare in situ torsional shear specimens

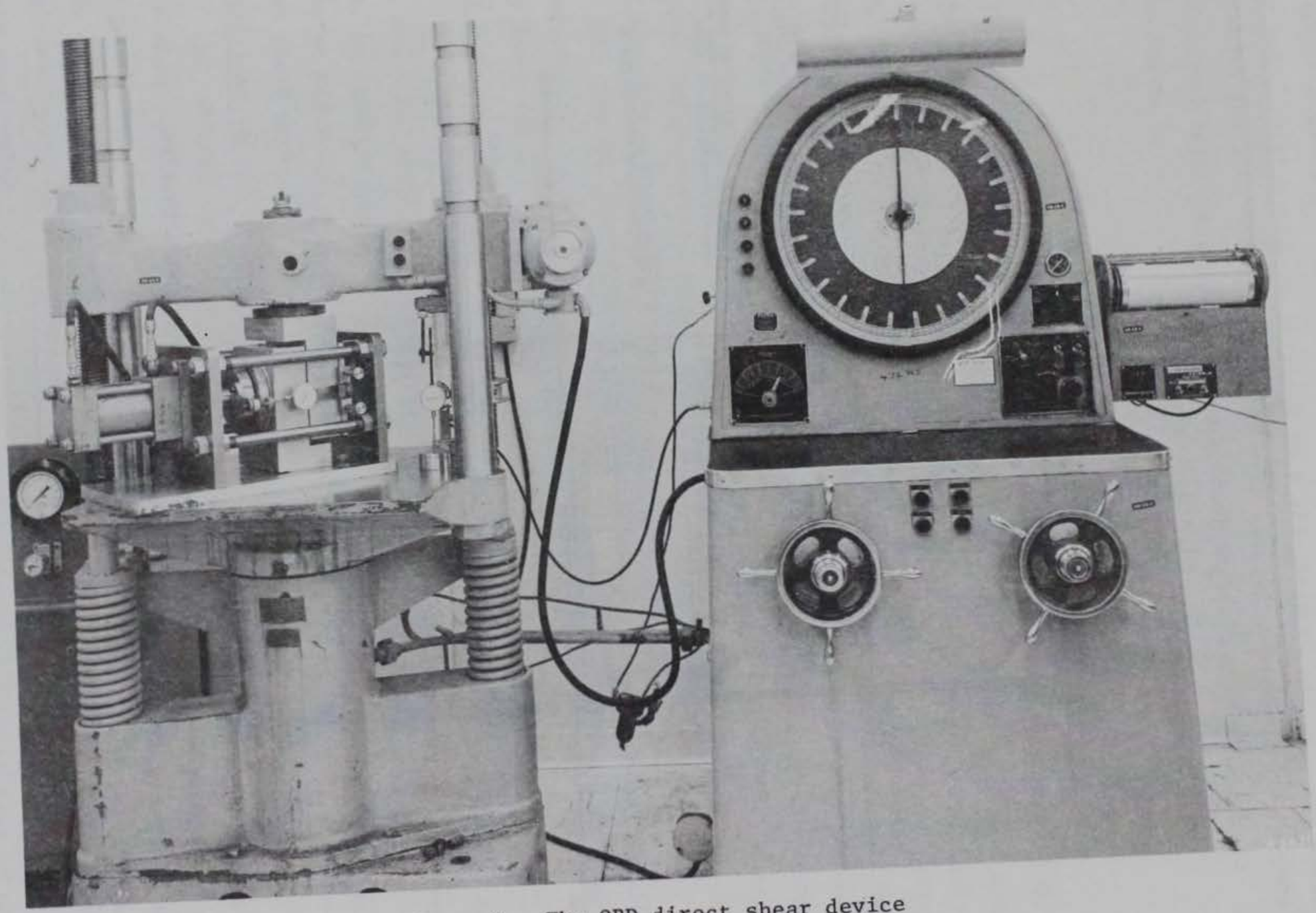

Figure 9. The ORD direct shear device

strip chart recorder that plots load versus shear displacement.

Data acquisition system

36. A linear variable differential transducer (LVDT) mounted between the load platform and stationary head controls the scaled rotation of the strip chart recorder with respect to shear deformation. Shear displacements were also visually monitored by means of a vertically mounted dial gage located between the platform and head. Normal displacements are monitored with a horizontally mounted dial gage between the jack and shear box.

Kansas City Direct Shear Device

37. The Kansas City (KC) direct shear device was designed and developed by the U. S. Army Engineer District, Kansas City, for laboratory testing of rock core specimens from 3 to 6 in. in diameter. Figure 10 presents a schematic of the equipment. The basic equipment components were borrowed from the U. S. Army Engineer District, Omaha, for use in this study. The normal load and data acquisition systems were provided by WES. Therefore, the equipment as used in this study and as shown in Figure 10 varied slightly from the initial design.

Shear box

38. The shear box was made of two square boxes 3 in. deep and tapered from 8-1/2 in. at their widest point to 7-1/2 in. at their base. The taper permitted easy extrusion of the specimen after testing. Each box was equipped with reinforced angle iron ears. Shear and reaction loads were transmitted to the shear box by pinned swivel eyebolts. The center line of the pinholes passed through a plane flush with each shear box.

Normal load system

39. The normal load system consisted of a single 60-ton jack driven by a 10,000-psi maximum capacity, manually operated hydraulic pump equipped with a bleed-off valve. A constant normal load was maintained by carefully monitoring the required load and either applying or relieving hydraulic pressure as needed throughout the test.

Shear load system

40. The shear load system consisted of a loading frame, a screw jack, and a pair of roller bearing platens.

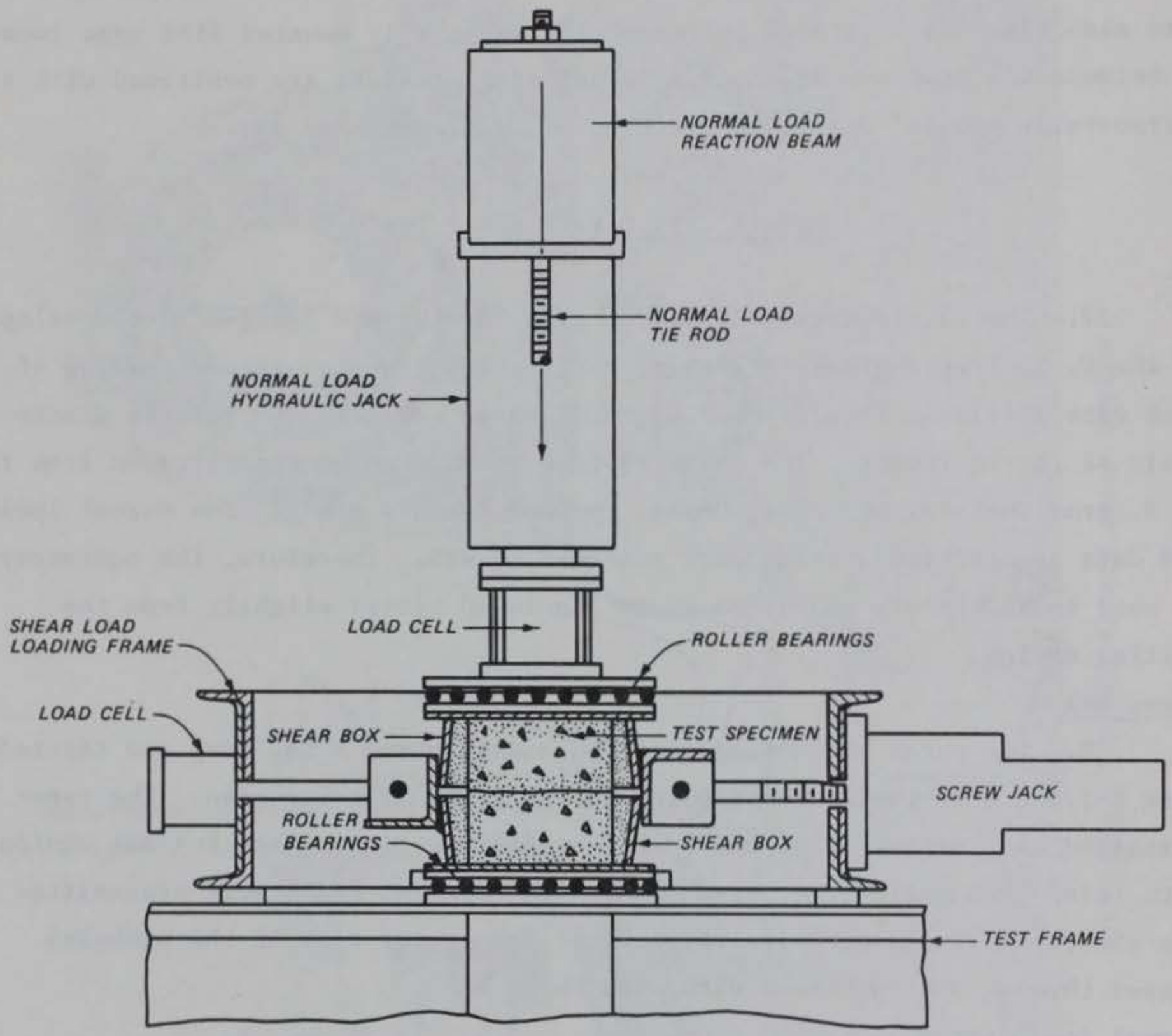

Figure 10. Schematic of KC direct shear device

41. Loading frame. The loading frame was constructed of 8- by 2-1/4-in. steel channels. The inside dimensions of the frame were 1 by 2 ft. The frame provided reaction for both shear and normal loads.

42. Screw jack. The shear loads were generated by a 5-ton maximum capacity screw jack powered by variable speed transmission coupled to a constant velocity electric motor.

Imperial College Direct Shear Device

43. Work conducted at the Imperial College (IC), London, led to the development of a simple shear box device for laboratory or field use. The device shown in Figure 11 is unique in that the shear box, normal load component, and shear load component were constructed as one unit. The shear box was designed to accept rock specimens of up to a 5-in. cube and rock core specimens of up to 4 in. in diameter. Normal and shear loads were applied by 11,000-lb hydraulic rams. An additional ram could be fitted to the shear box to facilitate the reversal of shear direction for the conducting of the residual shear tests if desired. Hydraulic pressures were monitored by Bourdon-type pressure gages, and for the tests conducted at WES, the shear load was also monitored by a 10,000-psi pressure transducer and a strain indicator. Both rams were driven independently by hand-operated hydraulic pumps. An adjustable pressure maintainer incorporated into the normal loading system allowed a constant normal load to be achieved throughout the duration of the test. A dial gage was mounted to the bottom shear box to monitor the lateral shear displacement. Details of the IC shear device are discussed by Brown and Walton (1975).

Soil Testing Direct Shear Device (3 by 3 in.)

44. Figure 12 shows the soil testing direct shear device used in this study. A detailed discussion of the device may be found in the publicaton "Soil Mechanics Testing Facilities at the Waterways Experiment Station" (U. S. Army Engineer Waterways Experiment Station, 1970).

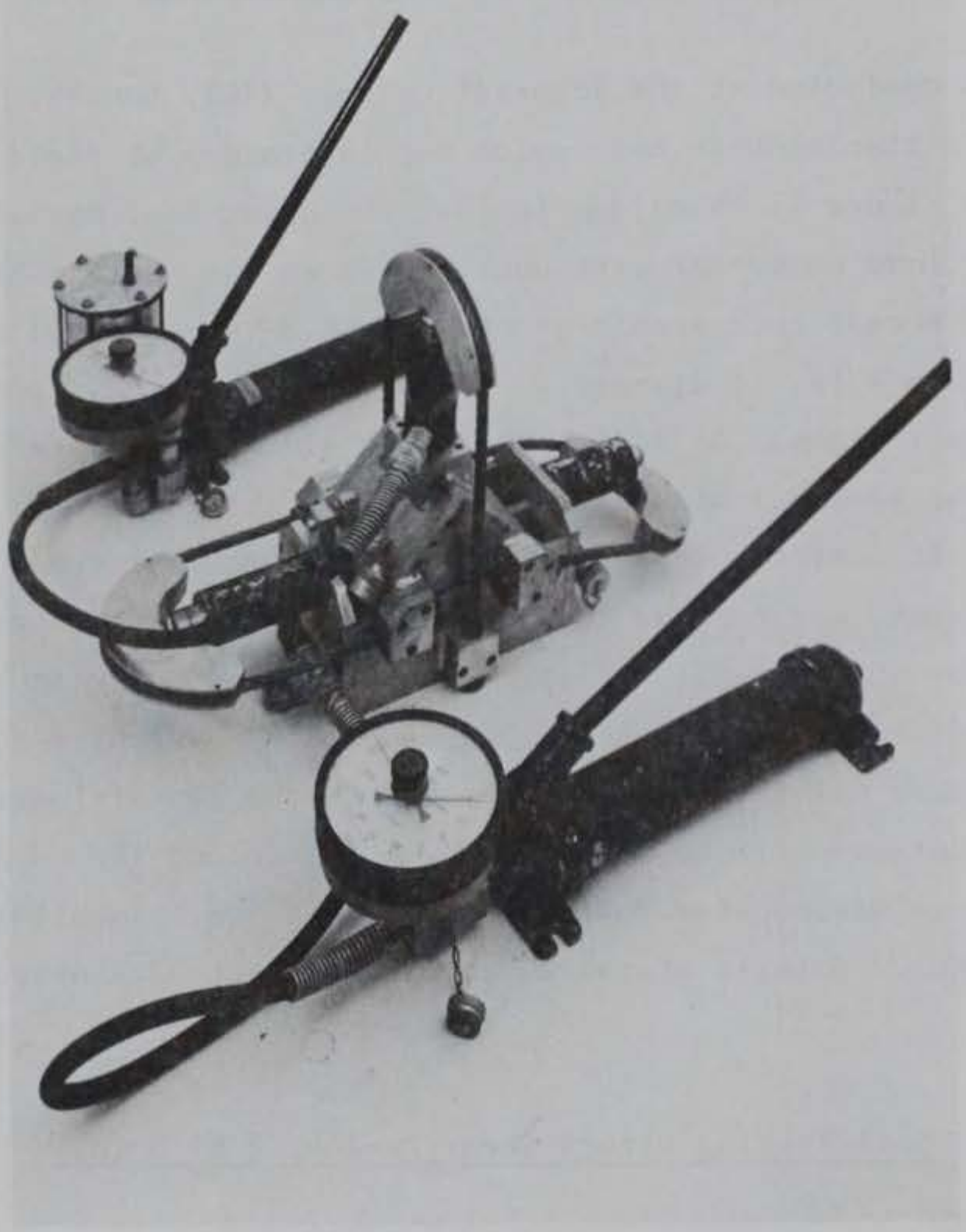

Figure 11. IC direct shear device

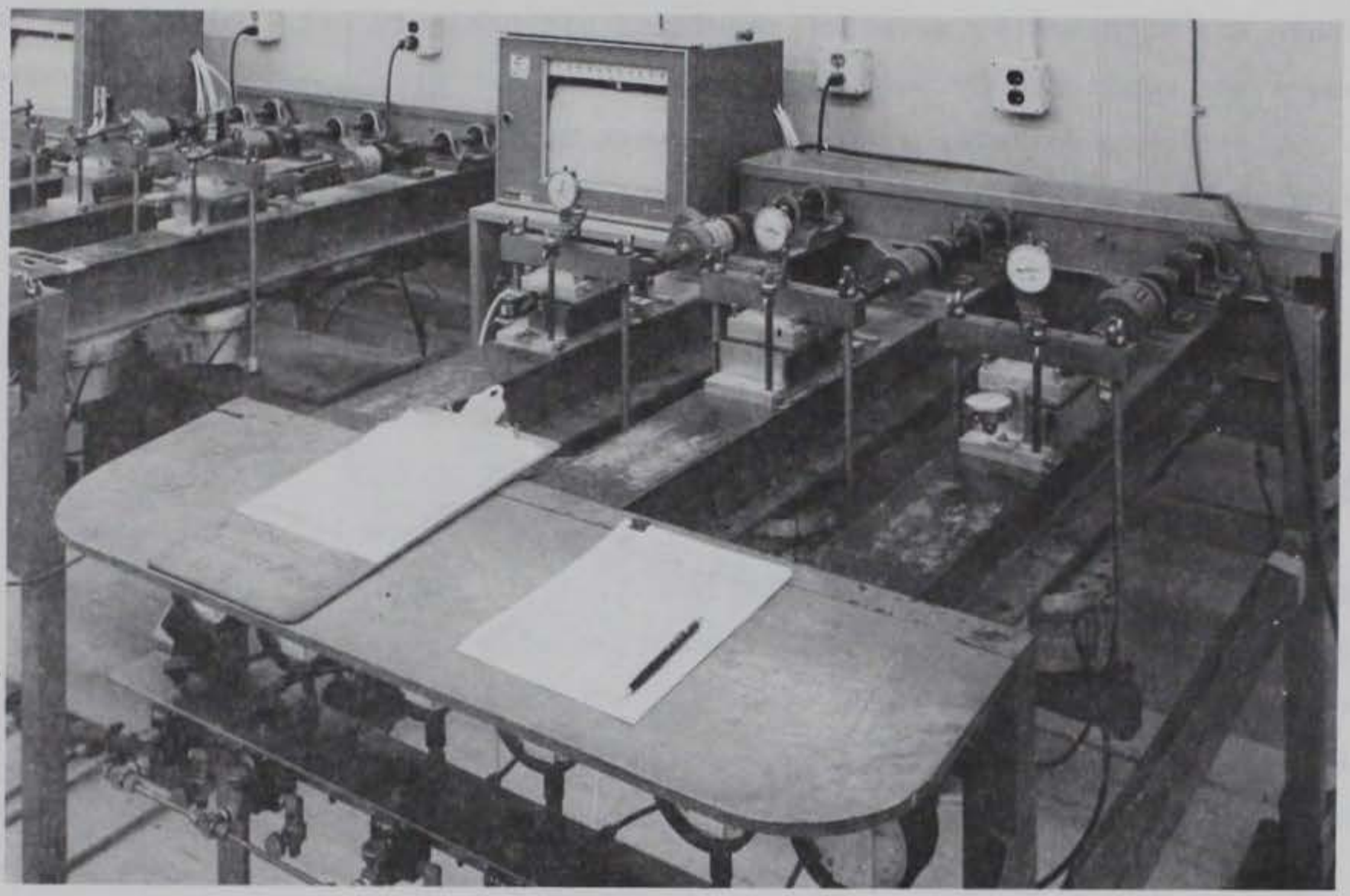

Figure 12. The 3- by 3-in. soil testing direct shear device

Triaxial Shear Devices

45. Two types of triaxial shear devices were used in this study. One was a device normally used at WES for testing soil specimens and the other for testing rock and concrete specimens.

Soil triaxial device

46. The soil triaxial device (Figure 13) was a 200-psi pressure cell capable of testing 2.8-in.-diam by 6-in.-high specimens. The cell's fluid pressure was obtained by means of regulated air pressure over water. The cell pressure was monitored by measuring the driving air pressure with a Bourdon-type air pressure deviator gage. Loads were applied with a 60-kip Universal testing machine equipped with a strip chart recorder. Deviator loads were plotted on the horizontal axis of the strip chart and visually monitored on the load indicator gage of the testing machine. A LVDT mounted between the loading platform and stationary head controlled the scaled rotation of the strip chart recorder with respect to shear deformation.

Rock and concrete triaxial device

47. The rock and concrete triaxial device (Figure 14) was a 4000-psi pressure cell capable of testing specimens 2.8 in. in diam and 6 in. high. Hydraulic oil supplied to the cell with a manually operated hydraulic pump provided the required confining pressure. The cell pressure was visually monitored with a Bourdon-type gage. Axial loads were applied with a 30-kip strain-controlled testing machine and were monitored by visual observation of the machine's load indicator gage. Visual observation of a dial gage mounted between the load table and stationary head was used to monitor axial strains. The device was a closed cell system with no pore pressure control capabilities.

Summary of Equipment Capabilities

48. The pertinent capabilities of each of the shear devices described above are summarized in Table 1.

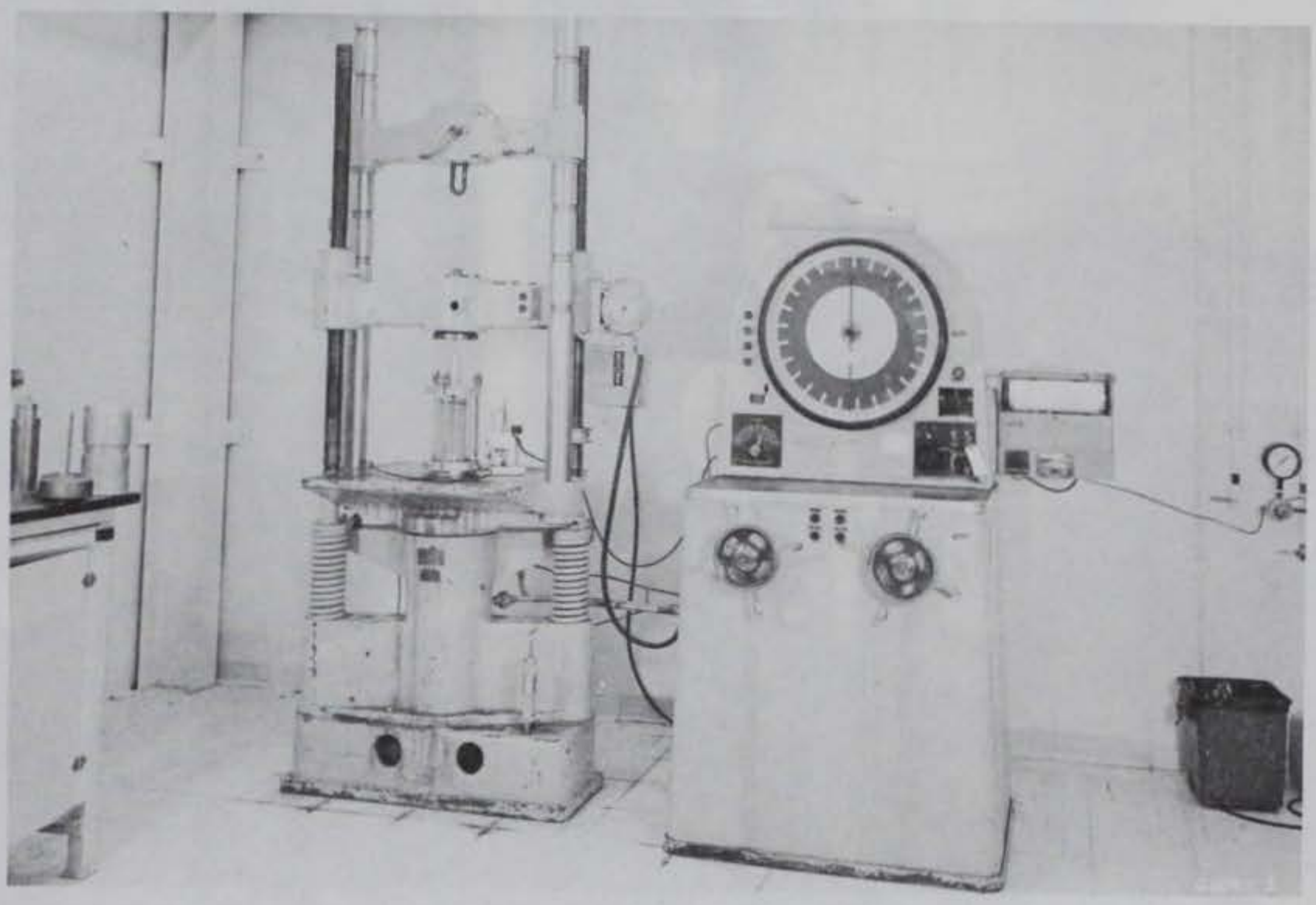

Figure 13. Soil triaxial device

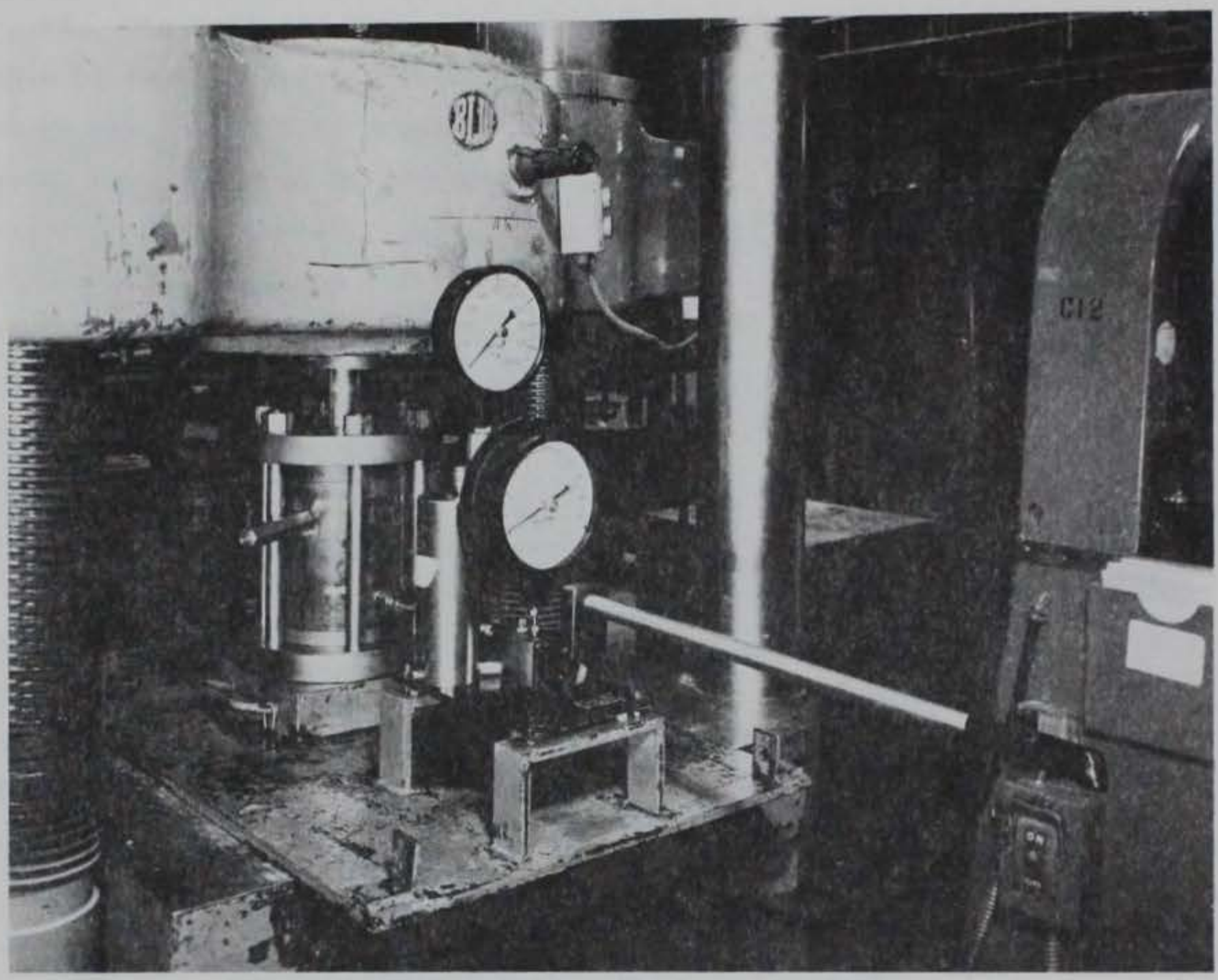

Figure 14. The concrete/rock triaxial device

Table 1

Summary of Equipment Capabilities

Device	Sample Size	Max Shear Load, Axial Load or Torque	Max Normal Load or Cell Pressure	Max Shear Rate	Min Shear Rate	Remarks
In situ direct shear	2 by 2 by 1 ft	120 kips	180 kips	0.25 in./min	0.001 in./min	Tests were strain controlled. Slower strain rates may be achieved with higher gear ratios. Automatic data acquisition
In situ torsional shear	12-in. diam	25 ft-kips	50 kips	0.6 deg/min	0.0014 deg/min	Tests were strain controlled. Automatic data acquisition
ORD direct shear	6-in. diam	60 kips	7 kips	5 in./min	0.0005 in./min	Tests were stress or strain controlled. Normal loads were monitored by hydraulic ram pressure. Automatic data acquisition
KC direct shear	6-in. diam			0.01 in./min	0.0014 in./min	Tests were strain controlled. Strain rates may be varied with different gear ratios. Automatic data acquisition
Soils direct shear	3 by 3 in.	2.5 kips	2.5 kips	0.04 in./min	0.00007 in./min	Tests were strain controlled. Automatic data acquisition
Imperial College direct shear	--	11 kips	11 kips	--	--	Tests were stress or strain controlled, depending on manual operation of hydraulic pumps. Shear and normal loads were monitored by hydraulic ram pressure
Soil triaxial	2.8-in. diam	60 kips	250 psi	5 in./min	0.0005 in./min	Tests were stress or strain controlled. Automatic data acquisition
Rock and concrete triaxial	2.8-in. diam	30 kips	4000 psi	--	--	Tests were stress controlled

PART III: TEST SPECIMENS

Model Material Specimens

49. Difficulties in locating suitable test sites for in situ and laboratory testing of natural discontinuous materials led to the development of a model material as an alternative testing medium. Model material specimens would eliminate the necessity of time-consuming and expensive test pit excavations, would permit control of asperity configurations along discontinuous shear zones, and would permit control of the physical properties. In studies such as this one, where test results from numerous devices are compared, it is necessary to maintain stringent control of the physical properties of each specimen. The physical property control aspect requires each component material to be standardized. Because of the limited capabilities of the shear devices, a relatively weak material would be required in order to shear through intact specimens. A parametric extrapolation based on a Mohr-Coulomb failure criterion indicated a suitable unconfined compressive strength of approximately 43 tsf.

50. Just as important as the strength requirement, the material selected should model rocklike stress-strain behavior. Rosenblad (1971) investigated the rocklike behavior of various rock model materials and selected a mix of river sand, hydrocal B-11, and water. The material simulated a schistose gneiss in many of its properties and had an average unconfined compressive (UC) strength of 43.9 tsf. Because of its desirable characteristics Rosenblad's model material was duplicated insofar as was possible for this study.

Mix Design

Materials

51. The components for the model material used in this study were hydrocal B-11, Ottawa sand, loess (a windblown soil), and water.

52. Hydrocal B-11. Hydrocal B-11 (specific gravity, 2.77) is a commercially available, high early strength gypsum cement capable of producing models of uniform and stable dimensions with a final maximum expansion factor of 0.08 percent for all hydrocal and water mixes. The rate of strength gain

is very rapid after the initial setting action begins (vicat set time of 25 to 35 min). Since slight strength differences are possible between production batches of any cementing agent, a quantity of B-11 sufficient to complete the testing program was purchased from a single production run. The B-11 arrived in moisture-proof bags and was stored in a temperature-controlled (heated and cooled) room.

53. Ottawa sand. Ottawa sand (specific gravity, 2.65) was selected as the primary filler or aggregate because of its universal availability and standardized characteristics. A 20-40 grain size distribution was used to simulate a medium to fine grain constituent material.

54. Loess. Loess (specific gravity, 2.69) was used as a secondary filler to hold the hydrocal in suspension as will be discussed below. The loess came from a road cut at WES and was free of vegetation and other organic matter.

Trial batches

55. The development of the design mix for the model material was basically a trial and error procedure of preparing numerous hand-mixed batches of 0.7 cu ft each. The strength of each trial batch was based on the 6-day average UC strength of 3- by 6-in. cylinders. The UC specimens were vibrated for approximately 5 min on a vibrating table immediately after molding the cylinder.

56. Initial trial batches were made by varying the percentages, by weight, of hydrocal, sand, and tap water. A mix that appeared to meet the requirements of 40 to 50 tsf UC strength contained 75 percent sand, 12.5 percent hydrocal, and 12.5 percent water. However, a close visual inspection revealed that a thin hard shell or crust approximately 1/3 in. thick had formed on the bottom surfaces of the specimens. The crust was apparently caused by hydrocal settling out of the mix (hydrocal specific gravity, 2.77, versus sand specific gravity, 2.65). Various other mixes of hydrocal, sand, and water were tried, but to no avail. The problem was attributed to the lack of fine material to sufficiently fill the voids, thus allowing the heavier hydrocal particles to settle.

57. A new series of trial batches was made with various percentages, by weight, of hydrocal, sand, water, and loess (loess was used as a fine filler). The mix finally selected for the model material consisted of 9.33 percent hydrocal B-11, 70.23 percent Ottawa sand, 8.74 percent loess, and

11.70 percent tap water, by weight. The average 6-day UC strength was 41.1 tsf with a standard deviation of 5.5 tsf.

Rangely Sandstone Specimens

Geology of specimen location

58. The area from which the test specimens were taken (T.2N; R.103W; Sec. 4) is located on the northern flank of the Rangely anticline in northwestern Colorado. This west-northwest trending structure is a simple, elongate, plunging monoclinal flexure with surface dips varying from 2 to 4 deg on the northern flank to 15 to 40 deg on the southern flank. In this area, the exposed Castlegate sandstone is the lowest member of the Price River formation (Mesaverde group) and overlies the Mancos shale.

Specimen properties

59. The Castlegate sandstone specimens were a gray-orange, yellowish-brown weathered, limey, friable, and very fine-grained littoral marine sediment. Constituent grain size averaged 0.05 mm with an intact density of 123 pcf. The average UC strength was 118.8 tsf.

PART IV: SPECIMEN PREPARATION

Model Material

In situ direct and torsional shear molds

60. Eight asperity plates, one matching pair for each of the asperity configurations shown in Figure 15, were fabricated from 1-in.-thick aluminum plates. Side frames for the in situ direct shear specimens were constructed of 6- by 6-in. steel channels bolted together to allow easy stripping of the mold. The torsional shear side frames were constructed from 11-in. inside diameter steel pipes split down the side with provisions made to bolt each half of the two molds together for easy stripping. Asperity plates were designed to fit slightly recessed into the bottom of each mold and were held securely in place by tightening the bolts holding the side frames together.

Index test molds

61. Unconfined compression test molds were 3-in.-diam by 6-in.-high cylindrical cardboard molds. Intact 6-in.-diam direct shear specimens were also formed in cardboard molds.

Triaxial test molds

62. Triaxial test molds were 2.8- by 6-in. split steel molds. The smooth discontinuous specimens were formed by casting against a 2.8-in.-diam, wedge-shaped (truncated), solid cylinder placed in the bottom of the mold. The wedge (predetermined failure plane) was inclined 30 deg with respect to the vertical axis.

Model material batch

63. A batch of sufficient quantity to form a complete in situ direct shear specimen, a torsional shear specimen, and various index specimens (6-in.-diam direct shear, UC, and triaxial) required 6.0 cu ft of material. A 7.0-cu-ft-capacity concrete mixer was used to mechanically mix the materials. The correct quantities of hydrocal B-11, Ottawa sand, and loess were weighed and placed in the mixer and dry mixed for 10 min to ensure a uniform distribution of materials. The correct quantity of water was then added to the dry mix, and the batch was mixed for an additional 5 min.

Forming the specimen

64. Test specimens, which were formed directly from molds, included the

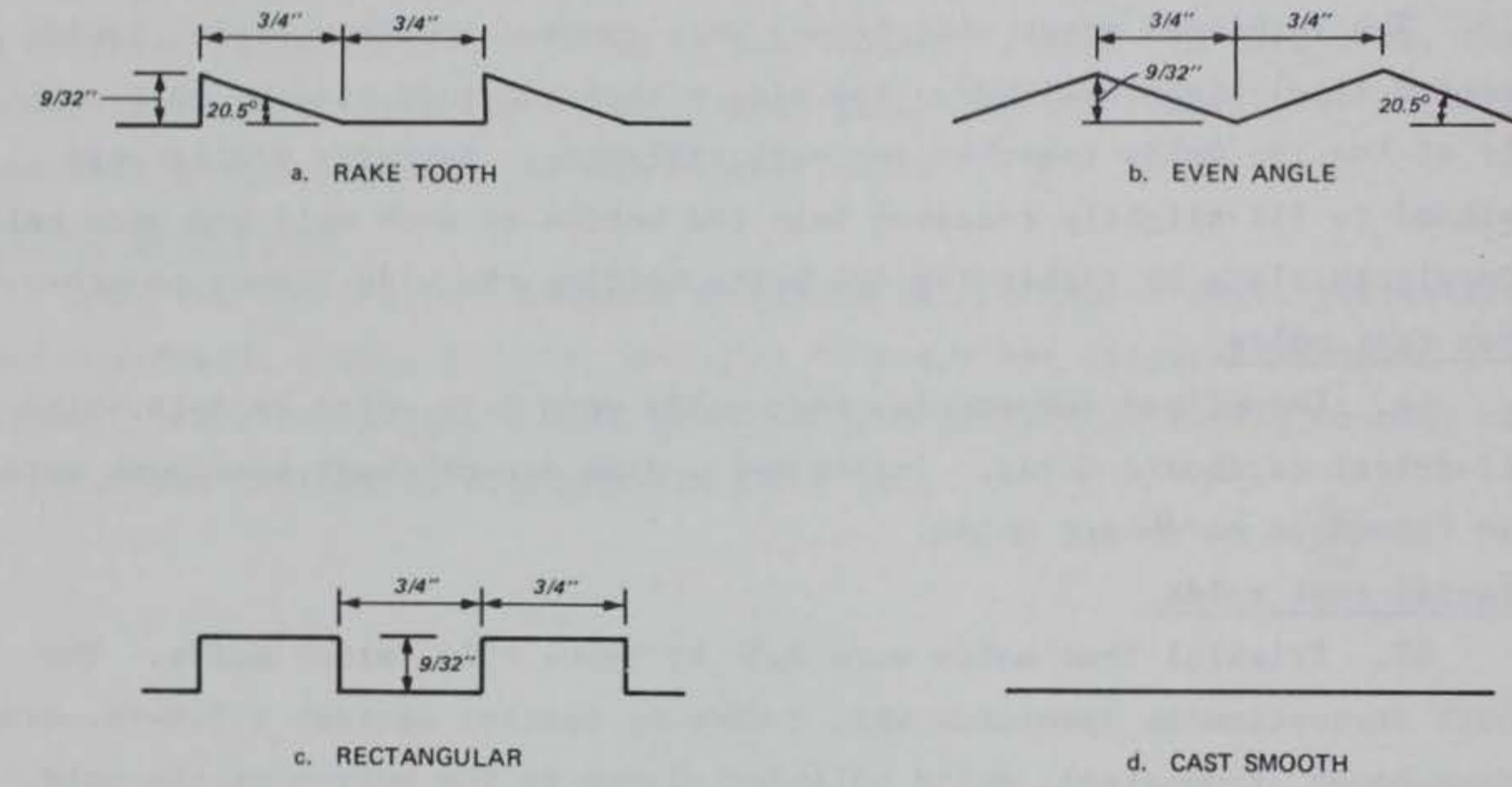

Figure 15. Schematic of asperity configurations

in situ direct shear, torsional shear, intact and smooth cast 6-in.-diam direct shear (ORD, KC, and IC devices), UC, and triaxial. Direct shear specimens (6-in.-diam) with asperities and soils direct shear specimens (3 by 3 in.) were prepared by coring and sawing from in situ direct shear and 6-in.-diam direct shear specimens, respectively.

65. Maintaining asperity integrity was recognized as a problem early in the program because of problems associated with bonding of the model material to the molds. The technique that provided the best bond brake involved painting the asperity plates with a thin coat of lacquer, and after the lacquer had dried, spraying the plates with Fluoroglide, a dry film lubricant and anti-stick fluorocarbon agent. Additionally, just before placing the model material in the molds, the side frames and asperity plates were sprayed with a light coat of silicone lubricant.

66. Because of the short set time (approximately 35 min), specimen preparation required the use of two vibrating tables. In situ direct and torsional shear molds were clamped to the vibrating tables with C-clamps. Slurry model material was placed into the molds in three 2-in. layers, with each layer being vibrated 5 min before the placing of the next layer. After the final layer had been placed and vibrated, the specimens were removed from the vibrating tables, screeded, and allowed to set up.

67. The rectangular asperity specimens were deleted from the testing program because specimens with intact asperities could not be made. Even with the extremely low expansion characteristics of hydrocal, sufficient expansion occurred to cause wedging of the asperities in the molds. The wedging action was sufficient to cause some or all of the cast asperities to shear off during the mold stripping process.

Discontinuous 6-in.-diam direct shear specimens with asperities

68. Discontinuous 6-in.-diam direct shear specimens with asperities were prepared from in situ direct shear specimens. Matching halves of in situ direct shear specimens were placed face to face and cored with a 6-in.-diam diamond bit core barrel. Cuttings were removed with air. A maximum of nine 6-in.-diam specimens could be prepared from each in situ direct shear specimen.

Direct shear specimens

69. The 3- by 3-in. direct shear specimens were prepared by trimming 6-in.-diam intact specimens with a dry-cut diamond blade. Specimens were

trimmed slightly larger than the shear boxes. Final trimming was accomplished by lightly sanding the specimen sides with sandpaper.

Curing the specimens

70. All cementing agents that undergo hydration require more water to make a sand plaster mix fluid (workable) than is needed for hydration. As the material sets up, the extra water becomes free or uncombined. The rate (curing time) at which moisture is driven from a specimen depends upon the manner or conditions under which it is cured and upon the specimen's size and shape.

71. Standardized procedures for testing and curing mortar cubes are presented in "Handbook for Concrete and Cement," CRD-C 227-78 (U. S. Army Engineer Waterways Experiment Station, 1949). In the specification, the term mortar applies to both portland and gypsum cement bases. Briefly, the specification states that the mortar cube specimens will be cured in a moist (fog) room for 20 to 24 hours.

72. Rosenblad (1971) accelerated the removal of free water by curing specimens in a 115°F temperature-controlled oven. He also noted that after a specimen reaches the zero free moisture condition and is stored at normal room conditions, it does not absorb moisture from the atmosphere. Thus, there was no limitation on length of exposure of the specimen to normal room conditions.

73. Specimens for this study were cured both in a fog room and a 115°F temperature-controlled walk-in oven. After the material had achieved initial set (1 to 1.5 hours), the specimens were placed in the fog room for one day (20 to 24 hours) in conformance with CRD-C 227-78 specifications. At the end of the first day, the molds were stripped and the specimens placed in the oven for three days. On the fourth day, the specimens were removed from the oven and stored at room temperature until tested. All specimens were tested on the fifth, sixth, seventh, or eighth day.

74. Curing time in the oven was based on UC test results and free water loss (total weight lost) of UC test specimens. Both weight loss and strength had stabilized after three days in the oven. No UC tests or weight loss measurements were made before the third day in the oven. The rate of free water loss is proportional to the specimen's total surface area per unit volume. Table 2 presents a summary of surface area per unit volume for each size and shape of specimen prepared. For a given curing process, the larger the surface area per unit volume, the shorter the required curing time.

Scales of sufficient capacity and sensitivity were not available to monitor weight losses of the in situ direct and torsional shear specimens. Even though supportive data are not available for the model material presented herein, the assumption that all the specimens had reached the zero free water state is reasonable in view of the relatively small differences in the surface area per unit volume ratios as indicated in Table 2. Rosenblad (1971) found that for a natural and portland cement base mortar with a 20 percent initial water content, two specimens with surface area per unit volume ratios of 4.14 and 2.35 required 4 and 6 days, respectively, to reach the zero free moisture status.

Table 2

Summary of Cast Specimens' Surface Area Per Unit Volume

Type of Specimen	Shape of Cross Section	Dimensions	Surface Area Per Unit Volume
In situ direct shear	Square	2 ft by 2 ft by 6 in.	0.79
Torsional shear	Circular	4.5 in. by 11 in.	0.81
UC and triaxial	Circular	3 in. by 6 in.	1.67
Index direct shear*	Circular	6 in. by 6 in.	1.00

* Intact and smooth cast failure surface specimens only.

Rangely Sandstone

In situ direct shear specimens

75. The surface of the otherwise massive sandstone unit at the Rangely site was crisscrossed with numerous fractures. The fractures can be divided into three distinct sets running predominantly N35°W, N55°E, and N85°E. The first two sets contain rather inconspicuous, hairline fractures spaced 2 to 3 ft apart. The third and most conspicuous set, striking east-west, contains

long fractures spaced about 6 ft apart. The last set of fractures appears to be a stress-relief feature, and the discontinuities therein were selected for in situ tests by Terra Tek.

76. The specimens selected for testing at WES consisted of three discontinuous specimens with approximate dimensions of 2 by 2 by 1 ft thick. Prospective failure zones were centered on a conspicuous fracture visually similar to the discontinuity tested by Terra Tek. The pit excavation technique was used to remove the specimens. This technique involved sawing (using the rock saw discussed in paragraph 25) a cleft 2 ft deep, parallel and 6 in. to either side of the fracture. Cuts perpendicular to the fracture, and spaced 2 ft apart, established the final specimen dimensions. A peripheral cut approximately 1 ft from the outer edge of each specimen was made around each specimen. Cuttings from all saw cuts were removed with air. Pry bars, sledgehammers, and wedges were used to excavate the material around the specimens to minimize disturbance along the discontinuities. The specimen cubes were clamped together before shearing the base of the specimen away from the parent material. A visual examination of the specimens upon removal from the excavation pit indicated that the fracture did not extend all the way through the specimen; the bottom 4 to 6 in. was still intact. Except for the top 1 in. (more or less), the fracture was tight and clean. The top 1 in. of the fracture contained varying amounts of surface debris. In the in situ state, the specimens felt dry to the touch.

77. Final preparation of the specimens was made at WES. Bottoms of the specimens were sawed smooth with a 36-in.-diam diamond blade rock saw. Since the specimens were dry in the in situ state, no special care was taken to prevent moisture loss or absorption. Just prior to testing, the joint in each specimen was extended through to the bottom of the specimen by prying the specimen halves apart (tensile failure).

Core specimens

78. Core samples 6 in. in diam were taken adjacent to the excavation pit and along the same fracture line as the in situ direct shear specimens. Three core samples (each 2 ft long) were recovered over the top 2 ft of the fracture zone using a thin-wall diamond bit core barrel. As with the in situ direct shear specimens, the fracture extended down to the bottom 4 to 6 in. of the samples. Upon recovery, the samples were clamped together with circular

water hose clamps and packed in sawdust. Six discontinuous and two intact specimens were prepared from the samples by sawing the samples into 6-in. lengths. The specimens were stored in the laboratory until tested.

PART V: TEST PROCEDURES

79. Some of the unique characteristics of each shear device used in this study were discussed in Part II. Methods for applying the shear and normal loads, methods for monitoring the shear and normal deformations, and the technique of securing the specimens within the shear boxes were discussed. Such characteristics are device operational characteristics and are related to procedures only in their ability to perform a certain task or function.

80. In any testing program where test results from several shear devices are compared, precautions in the form of standardized procedures should be taken to ensure compatibility among tests. A suggested method for direct shear tests is given in "Rock Testing Handbook" (U. S. Army Engineer Waterways Experiment Station, 1980) and in "Suggested Methods for Determining Shear Strength" (International Society for Rock Mechanics, 1974). The latter publication also suggests procedures for torsional shear tests. The test procedures presented herein were adapted to meet the particular requirements of this study, using the above-suggested procedures as guidelines. Triaxial and unconfined compression tests were performed according to the standards presented in "Rock Testing Handbook."

Type of Test

81. Conventionally, a shear test may be unconsolidated undrained, consolidated undrained (with or without pore water pressure measurements), or consolidated drained. The discontinuities are clean and normal stresses are below the level required to cause constituent particle-to-particle compression. However, for convention's sake, the tests conducted for this report may be classified as consolidated drained or S tests since pore water pressures are essentially zero (dry specimens).

Direct and Torsional Shear Test Procedures

Consolidation

82. The consolidation stage of testing allows pore water pressures in the rock and in filling materials adjacent to the shear plane to dissipate under the full normal stress before the shear load is applied. Since all

specimens tested during this study were at an air dry state, pore water pressure dissipation was not considered a problem. The consolidation period was to allow stabilization of any elastic deformation and to permit any redistribution of normal stresses caused by grain or asperity crushing along the discontinuities. For all tests presented herein, the specimens were allowed to consolidate for a minimum of 30 min or until the rate of normal deformation was 0.0005 in. per min, whichever occurred last.

Shear rate

83. Shear rate is the rate at which shear deformation occurs, in the case of strain-controlled tests, or the rate at which the shear load is applied, in the case of stress-controlled tests. The in situ, ORD, KC, 3- by 3-in., and the torsional shear tests were strain controlled. The IC direct shear tests were stress controlled. Table 3 presents a summary of the various shear rates for the direct and torsional shear tests.

84. In undrained tests, the control of shear rates is important to the extent that adequate time must be given to the redistribution of shearing stresses during the application of the shear load. To investigate the effects of shear rate, a staged shear test was conducted in the in situ direct shear device on a model material smooth cast surface. For a 6-tsf normal load, no change in shear load up to peak strength was observed for shear rates below 0.01 in. per min. Table 3 indicates a variation in the shear rates of the various test devices (due primarily to differences in operational characteristics). However, all shear rates were considerably less than the indicated 0.01 in. per min.

Shear gap

85. Shear gap refers to the space between the shear boxes through which the shear plane develops. In an ideal direct shear test, the failure or shear plane develops perpendicular to the normal stress and parallel to the shear stress. The ideal plane is referred to as the theoretical shear plane. The larger the gap, the greater the chance that the shear plane will develop at some angle skewed to the direction of the normal and shear stresses. The shear plane with the greatest deviation from the ideal theoretical plane would be a plane passing diagonally across the shear gap. Any plane through which the shear plane actually develops may be referred to as the observed shear plane. If the difference between the theoretical shear plane and the observed shear plane is 5 deg or less, the angle of internal friction computed from

Table 3

Summary of Shear Rates for Direct and Torsional Shear Tests

Type of Shear Device	Average Shear Rate	Deviation in Shear Rate	Remarks
In situ direct	0.001 in./min	±0.0005 in./min	Screw jacks, gear box, and variable speed electric motor allowed good control of shear rate
ORD direct	0.004 in./min	±0.003 in./min	Deviation in shear rate caused by inability to accurately duplicate shear rates from one test to another with the Universal Testing Machine
KC direct	0.007 in./min	See Remarks	Constant speed electric motor and gear box arrangement maintained constant shear rate. Shear rate dictated by available gear ratio
KC direct*	0.004 in./min	See Remarks	Constant speed electric motor and gear box arrangement maintained constant shear rates
3 by 3 in.	0.001 in./min	±0.0004 in./min	Zero-maximum device allowed good control of shear rates
IC direct	50-lb per shear load increment	See Remarks	Each load increment was held constant for 1 min or for 0.001 in./min (or less) of shear deformation
Torsional	0.007 rad/min	±0.0015 rad/min	Deviation in shear rate caused by hydraulic fluid leak-by in constant displacement pump

* KC direct shear tests on Rangely sandstone were conducted at MRD Laboratory.

Mohr-Coulomb failure criterion, assuming a perfect theoretical shear plane, will be in error by no more than 2.5 deg. Consideration of differences in the theoretical and observed shear planes is especially critical when testing intact specimens where shear planes are permitted to develop along any plane within the shear gap.

86. The shear gaps for all tests except the 3- by 3-in. soils direct shear tests and the in situ direct shear tests on Rangely sandstone were 1/2 in. The 1/2-in. gap was sufficient to accommodate model material specimens with asperities and yet small enough so that the maximum observed shear plane would be less than 5 deg with respect to the theoretical shear plane.

87. The shear gap for the 3- by 3-in. soils direct shear tests was maintained at 1/8 in. Because of the 1/8-in. shear gap, only intact specimens and specimens with smooth cast discontinuous surfaces were tested in this device. The 1/2-in. shear gap used in the other tests would have resulted in a maximum possible deviation in theoretical and observed shear planes of 9.46 deg. The 3- by 3-in. device was designed so that the line of action of the shear load passes through the center of a 1/16-in. shear gap. A 1/2-in. shear gap would have resulted in an excessive moment within the specimen.

88. Shear gaps for the in situ direct shear tests on Rangely sandstone specimens were 3/4 in. The 3/4-in. gaps were necessary to accommodate the full height of the natural asperities within the joint.

Direction of shear

89. The direction of shear with respect to asperity orientation is summarized in Table 4.

Securing of specimens within shear boxes

90. The specimens were secured within the various shear boxes using two methods. In the first method, defined as a loose fit, the shear boxes were placed directly around the specimen. In the second method, defined as a rigid fit, the specimens were either grouted or epoxyed to the shear boxes. The primary difference between the two categories is that in a loose fit case the shear box does not act as an integral unit with the specimen; whereas in the rigid case, both the shear box and specimen act as a single unit. Specimens requiring grout or epoxy as a cementing agent were painted (excluding discontinuities) with a moistureproof coating (Protexo-Cote) sealant to prevent the

Table 4

Summary of the Direction of Shear
with Respect to Asperity Orientation

Type of Test	Specimen Material	Asperity Shape	Direction of Shear
Direct shear	Model	Even angle	Perpendicular to asperity axis
		Rake tooth	Perpendicular to asperity axis and against vertical face of the asperities
		Smooth cast	May be in any direction along the discontinuity
	Rangely sandstone	Natural	Parallel to joint as situated in the field
Torsional shear	Model	Even angle	Rotational
		Rake tooth	Rotational
		Smooth cast	Rotational

specimen from absorbing moisture or epoxy. Table 5 presents a summary of how the test specimens were secured.

91. The IC direct shear device was designed to accommodate core specimens up to 4 in. in diameter. The unique diagonally opposed design of the shear boxes required special shaping of the 6-in.-diam specimens in order to fit the boxes. Figure 16 illustrates half of an even angle discontinuous IC direct shear specimen shaped for testing. Specimens were shaped with a band saw and a specially designed jig to ensure reliable duplication of specimens. Unlike other shear devices, which use grout for securing the specimens, the IC device specimens were first grouted into a plexiglass mold of the same dimensions as the shear boxes. The grout acted as a filler to provide a snug fit between the specimen and shear box. After the grout set up, the specimen was removed from the mold and placed into the shear box for testing.

General procedures

92. The general procedures for all tests were basically the same. The procedural sequences are listed in order of occurrence:

a. All load cells, pressure transducers, pressure gages, and displacement transducers were calibrated before use.

b. Specimens were secured within the appropriate shear boxes, taking care to ensure the proper orientation of asperities with respect to the direction of shear and maintaining the appropriate shear gap.

c. The shear boxes (or torque tubes) were assembled within their reaction frames.

d. Normal and shear displacement monitoring devices (dial gage or displacement transducers) were mounted to the shear boxes (or torque tubes).

e. Shear load applicators (hydraulic rams, screw jacks, or loading table of test machines) were secured or brought into contact with the shear boxes (or torque tubes).

f. Normal load hydraulic rams or flat jacks were brought into contact with the shear boxes (or torque tube). The appropriate normal stress was applied for the consolidation cycle. Normal deformations were monitored during the consolidation cycle.

g. After the consolidation cycle, the specimens were sheared at appropriate shear rates. In all tests, both shear loads and shear deformations were monitored. For most tests, normal deformations were also monitored during the shear cycle.

h. All tests, except the in situ direct shear tests on Rangely sandstone specimens, were single-point tests. All specimens were sheared to failure (peak shear load). Most specimens were sheared until shear loads appeared to stabilize. The in situ

Table 5

Methods for Securing Test Specimens in Direct and Torsional Shear Devices

Type of Shear Device	Specimen Material	Type of Grout	Remarks
In situ direct	Model	None	Classified as loose fit. Component parts of shear box were bolted around specimen
In situ direct	Rangely sandstone	Hydrocal	Classified as rigid fit. Specimen was placed in shear box in proper position and shear gap filled with modeling clay. Grout was then poured around specimen and rodded. When grout set up, clay was removed from shear gap
ORD direct	Model	Hydrocal	Classified as rigid fit. Specimen was placed in shear box in proper position and shear gap filled with split rubber gaskets. Grout was then poured around specimen and rodded. When grout set up, gaskets were removed
KC direct	Model and Rangely sandstone	Hydrocal	See ORD direct shear device remarks
3- by 3-in. direct	Model	None	Classified as loose fit. Specimen was trimmed to fit shear box. Shear box was then pressed around specimen
IC direct	Model	Hydrocal	See paragraph 91
Torsional	Model	Epoxy	Hydrocal did not provide sufficient bond strength between torque tubes and specimen; therefore, epoxy was used. Specimen was placed in the proper position in the top torque tube and then epoxy was poured around specimen. When top epoxy set up, a premeasured volume of epoxy was poured into the bottom torque tube. The bottom half of specimen was then pressed into epoxy causing epoxy to displace around specimen

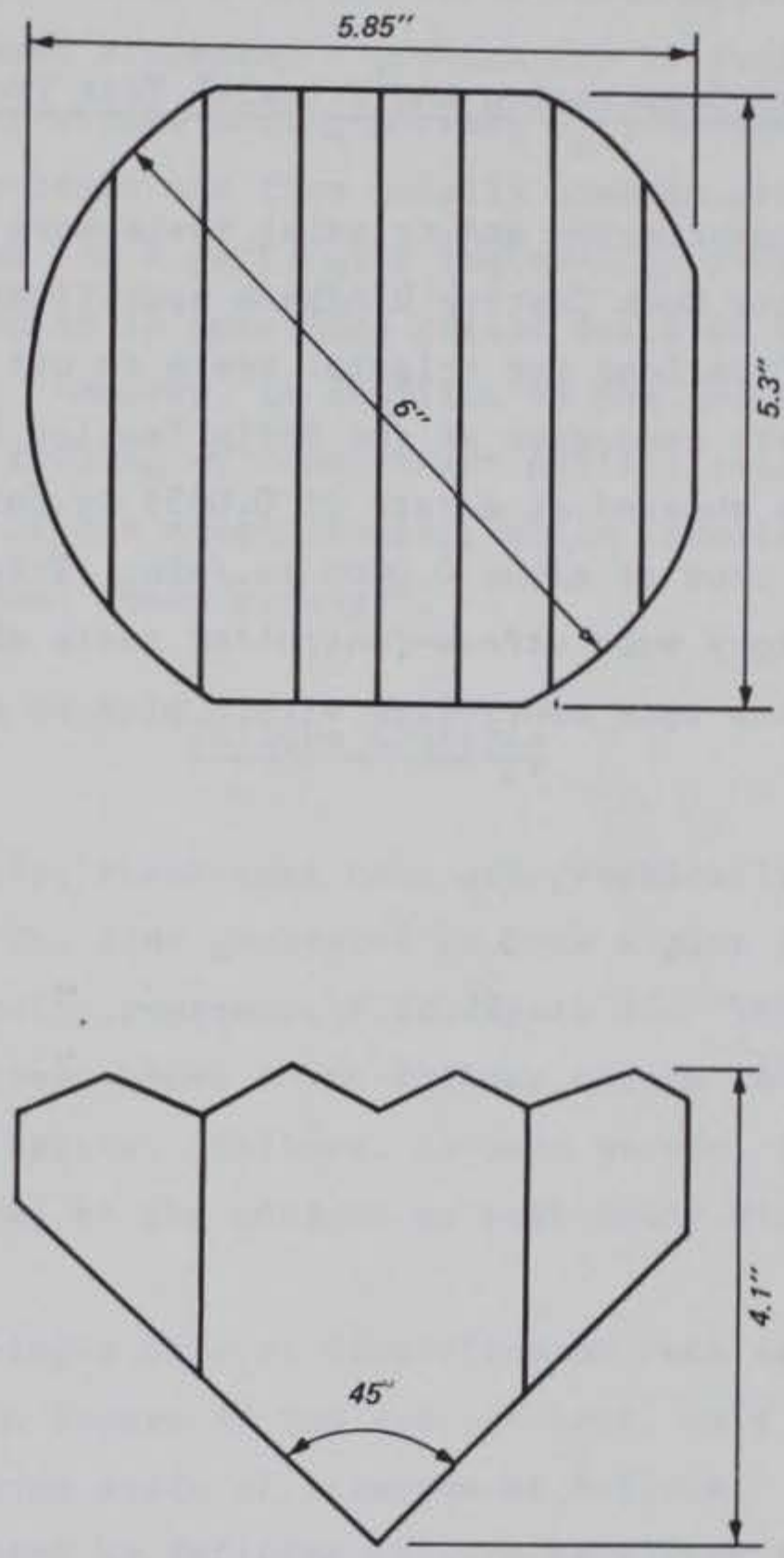

Figure 16. Shape of IC direct shear specimen

direct shear tests on Rangely sandstone specimens were multi-stage tests. Three natural asperity profiles were made along lines parallel to the direction of shear and located at third points along the shear surface before each shear cycle. At the conclusion of each shear cycle, the top half of the specimen was removed and any loose debris brushed off before commencing a new test cycle.

Unconfined Compression and Triaxial Test Procedures

93. Unconfined compression and triaxial tests were conducted in accordance with the appropriate Rock Testing Handbook specifications. The Rock Testing Handbook specifications for triaxial tests do not specify shear rates.

94. Triaxial tests conducted at the Soils Testing Laboratory were strain-controlled tests sheared at a rate of 0.0055 in./min. Strain rates were controlled within plus or minus 0.0005 in./min. Triaxial tests conducted at the Concrete Laboratory were stress-controlled tests sheared at a rate of 50 psi/min. Stress rates were controlled within plus or minus 5 psi/min.

PART VI: METHODS OF ANALYSIS

95. Before discussing the results of this study, perhaps it is appropriate to briefly review the various analytical methods available for analyzing shear test data. The usual objective of a shear test is to predict the magnitude of maximum shear stresses, τ , which can be resisted along a discontinuity for a particular stress acting normal, σ_n , to the discontinuity. The data obtained from such tests are then usually used to predict the shear strength characteristics for a particular engineering problem. The shear strength of a discontinuity is sometimes called friction because it is normally stress dependent. However, in addition to the joint surface friction, wedging, rotation, and rolling of constituent particles can contribute to the total shear resistance of the discontinuity, while cementation and interlocking can develop additional shear strength.

Failure Criteria

96. Conventionally, shear test data are graphically presented by plotting τ versus σ_n . The line generated by such a plot is called the failure envelope, as hypothetically represented in Figure 17. The failure envelope defines the level of stress above which failure occurs and below which a stable state of stress exists. Failure, as used herein, is defined in terms of the stresses developed at the maximum or peak shear strength taken from the stress-strain curves.

97. Failure envelopes of most discontinuous rock are generally curvilinear as illustrated in Figure 17 and are, at best, only good approximations representative of the true state of stresses at failure. Prototype design procedures are facilitated by defining failure envelopes in terms of mathematical formulae. Numerous formulae based on theoretical and empirical relationships affecting the shear strength of discontinuous rock are currently in use today.

Mohr-Coulomb failure criterion

98. The Mohr-Coulomb failure criterion is the most widely used and perhaps most controversial failure criterion in soil and rock mechanics. The acceptance of the criterion is a simple consequence of the way c and $\emptyset$ are defined and the ease by which the criterion can be adapted to prototype design

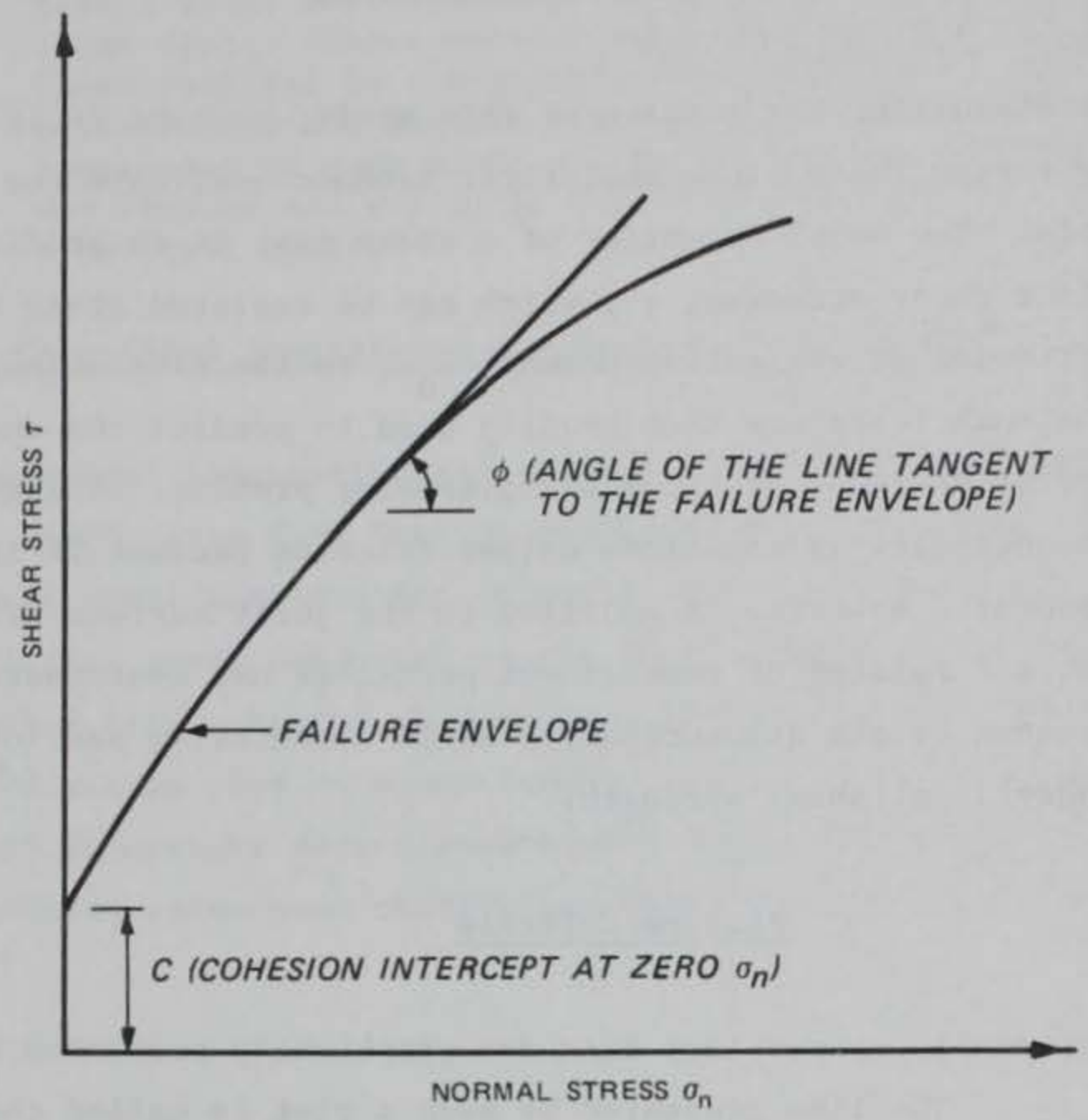

Figure 17. Hypothetical failure envelope

procedures. Basically, the failure envelope is defined by a line tangent to a family of Mohr's circles and described mathematically by Coulomb's equation:

$$\tau = c + \sigma \tan \phi \tag{1}$$

99. The Mohr-Coulomb failure criterion is directly applicable only to triaxial tests where both the major and minor principal stresses are known. With a few basic assumptions, the criterion is also applicable to direct and torsional shear tests.

100. The theoretical development of the Mohr-Coulomb failure criterion will not be discussed in detail. The reader is referred to the many textbooks on strength of materials. However, it is important to briefly review some of the pertinent applications of the criterion as it directly applies to the analysis of the shear tests presented herein.

101. Triaxial tests. Predicting the shear stress, τ, for any given stress, σ, normal to the shear plane requires the determination of the shear strength components c and ϕ. Values of c and ϕ may be found by two methods from a series of triaxial tests. First, one may draw the Mohr circles for each test and draw the Mohr-Coulomb failure envelope best fitting the tangent to all circles. Second, one can plot the apex points of each circle on a plot of $(\sigma_1 + \sigma_3)/2$ versus $(\sigma_1 - \sigma_3)/2$ (known as a p-q diagram) and draw a line through these points (referred to herein as the p-q line) and then compute c and ϕ from trigonometric relationships. The choice between these two methods is largely one of personal preference. However, when there are many tests in a test series, it will usually be less confusing to plot the results on a p-q diagram, and further, it will be easier to fit a best-fit line through a series of data points than to attempt to pass a line tangent to many circles. For these reasons, this report will follow the practice of plotting the results of triaxial tests on a p-q diagram.

102. Figure 18 shows the relationship between the Mohr-Coulomb failure criterion and p-q diagram. Equations 2 and 3 in Figure 18 are used to convert the major and minor principal stresses to p-q points. A line of least-squares best fit (Equation 6) is then established for all p-q points from which the a and α parameters shown on Figure 18 are determined directly. Equations 4 and 5 are then used to determine the c and ϕ shear strength parameters.

103. The shear strength parameters c and ϕ as determined from Equations 4 and 5, respectively, assume that the theoretical failure plane and the actual (observed) failure planes are the same (see Figure 18). For cases where the observed failure plane and theoretical failure plane are not the same, such as the precast failure plane specimens presented in this report, Equations 4 and 5 are not valid since they compute c and ϕ based on the state of stress at points tangent with the failure envelope and Mohr circles. Figure 19 shows the relationship between a failure envelope compatible with an observed failure plane other than the theoretical plane $(\beta_o \neq 45 + \frac{\phi}{2})$ and the p-q diagram. In this case, Equations 7 and 8 are used to compute c and ϕ, respectively. As can be seen, the failure envelope intercepts each Mohr's circle twice. However, there can be only one state of stress compatible with the inclination of the observed failure plane β_o.

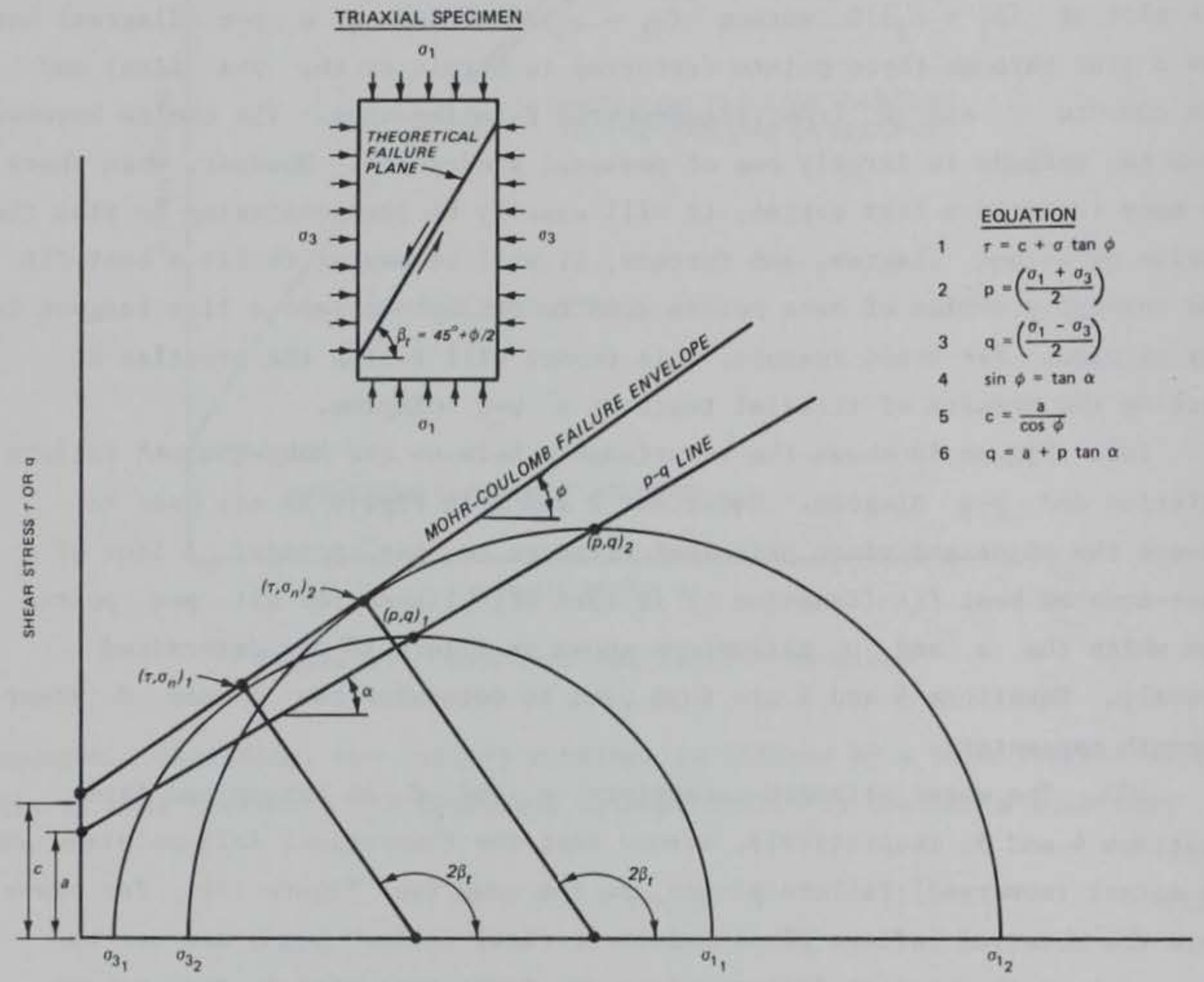

Figure 18. Relationship of Mohr-Coulomb failure criterion and p-q diagram

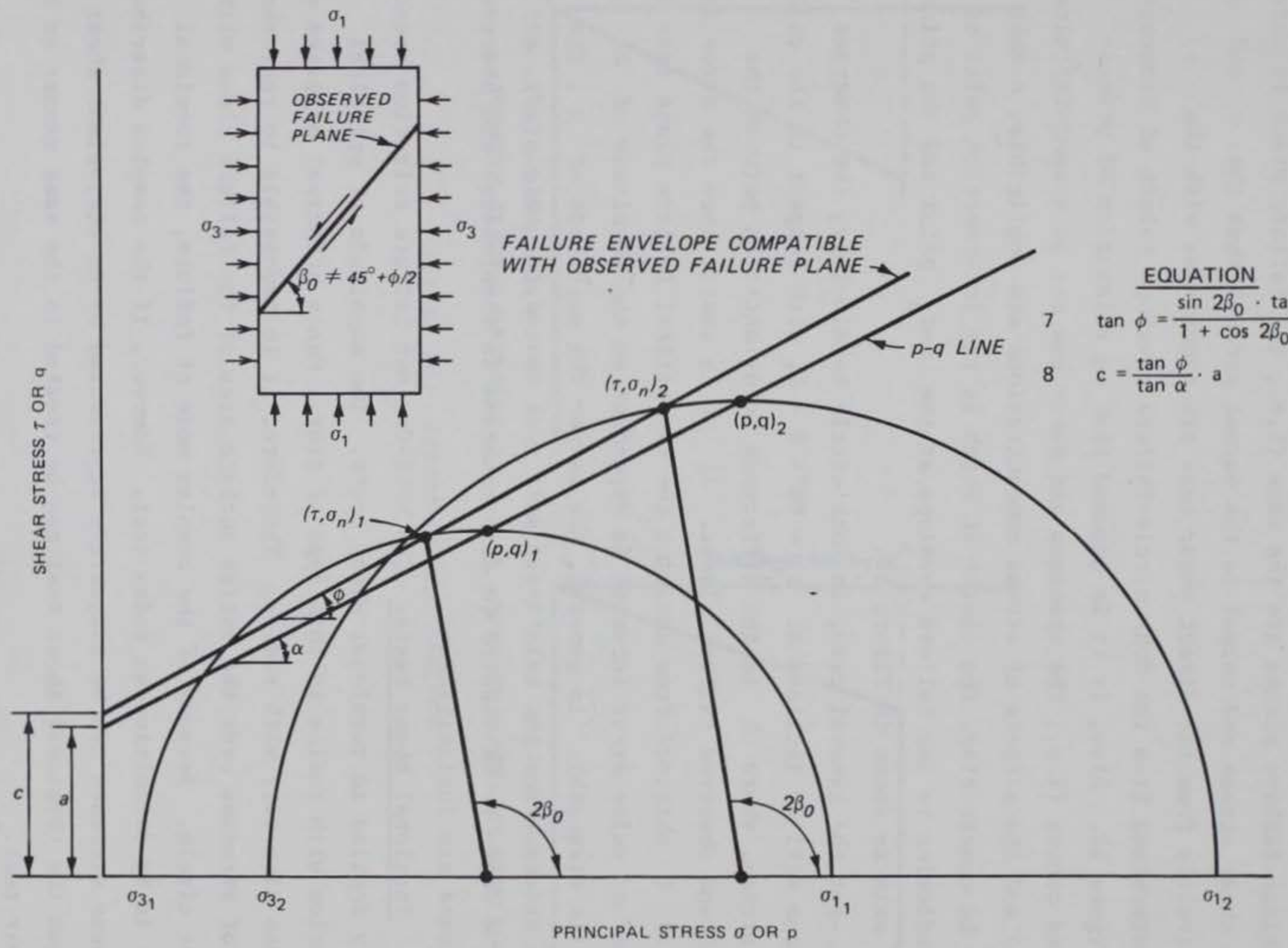

	EQUATION
7	$\tan \phi = \dfrac{\sin 2\beta_0 \cdot \tan \alpha}{1 + \cos 2\beta_0 \tan \alpha}$
8	$c = \dfrac{\tan \phi}{\tan \alpha} \cdot a$

Figure 19. Relationship of failure envelope compatible with observed failure plane other than the theoretical failure plane and p-q diagram

104. Direct shear tests. In the direct shear test, only the average normal stress and average shear stresses on a single plane are known. Hence, from the test results alone, it is not possible to draw the Mohr circle giving the state of stresses. However, if one makes the assumption that the observed and theoretical failure planes are the same (i.e., the failure plane is parallel to the shear stress and normal to the normal stress) then the τ and σ_n obtained directly from the direct shear test are synonymous with the τ and σ_n determined from the Mohr circle-failure envelope points of tangency shown in Figure 18. Also, if it is assumed that no relaxation of principal stresses occurs (i.e., the specimen and shear box act as a semi-infinite half space) and the effects of stress concentrations are negligible, a Mohr circle may be constructed, the center of which is the intersection point of a line perpendicular to the failure envelope at the τ-σ_n point and the principal stress axis as shown in Figure 18.

105. For the general case, in Mohr circle terminology, the observed failure plane will be inclined at $\beta_o = 90° + \phi - \delta$, with respect to the major principal stress, where δ is the difference in orientation between the theoretical and observed failure planes. If δ is small, then the error in the value of ϕ obtained from assuming the theoretical failure plane case is small. The c value error incurred is dependent on the magnitude of c (also tensile strength). In general, the larger the magnitude of c, the larger the errors. For the relatively soft rock tested for this study, any errors in c and ϕ attributed to discrepancies in theoretical and observed failure planes are insignificant.

106. Torsional shear tests. The Mohr-Coulomb failure criterion cannot be directly applied to torsional shear tests. The magnitude of principal strains varies with radius in this type of test. Hence principal stresses and shear stress also vary with radius. Therefore, it is impossible to represent the state of stresses over the entire surface area of the failure plane with a single Mohr circle. Because of the complex mode of failure, the torsional shear test is by definition an index test. However, if the complex distribution of shear stresses can be adequately represented by an equivalent shear stress, then the torsional shear test can be treated in the same manner as the direct shear test.

107. If the specimen is assumed to behave as a perfectly elastic or elastic-plastic material as illustrated in Figure 20a and 20b, respectively,

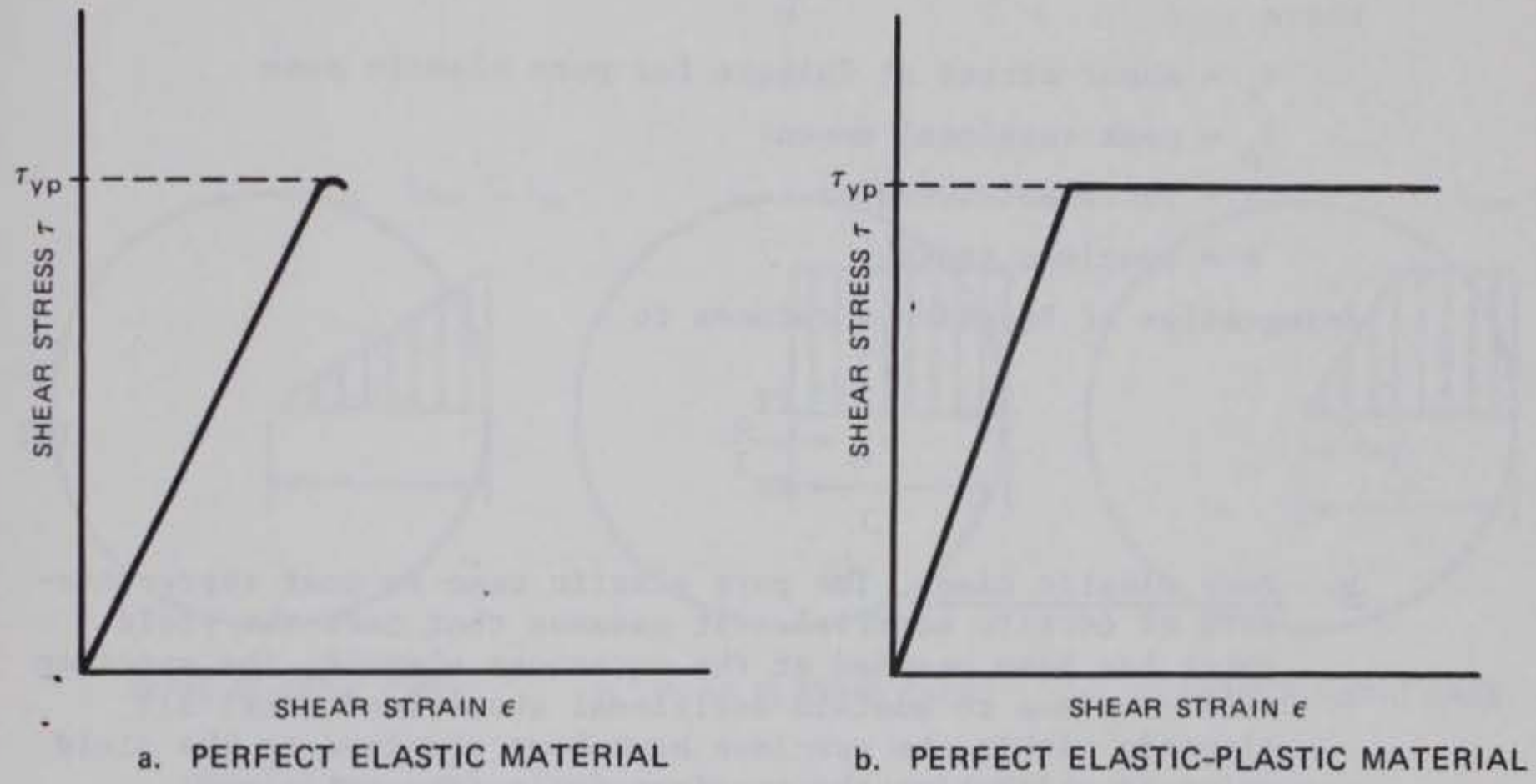

Figure 20. Stress-strain diagram

three possible alternate shear-stress distributions may occur as illustrated in Figure 21.

a. Pure elastic case. The pure elastic case is most closely representative of brittle material. It assumes that once the yield point has been reached at the outermost element, the material cannot sustain any additional shear load at which time the specimen fails. The shear stress at failure for this case can be determined by the general equation

$$\tau_e = \frac{T_p}{\frac{2\pi}{r}\int_0^r \rho^3 d\rho} \tag{9}$$

where

τ_e = shear stress at failure for pure elastic case

T_p = peak torsional moment

ρ = incremental radius

r = specimen radius

Integration of Equation 9 reduces to

$$\tau_e = \frac{2T_p}{\pi r^3} \tag{10}$$

b. Pure elastic case. The pure elastic case is most representative of ductile material. It assumes that once the yield point has been reached at the outermost element, the specimen will continue to sustain additional shear load until all elements within the specimen have been strained to the yield point at which time the specimen fails (unconstrained deformation). The peak shear stress at failure for this case can be determined by the general equation

$$\tau_p = \frac{T_p}{2\pi\int_0^r \rho^2 d\rho} \tag{11}$$

where

τ_p = shear stress at failure for pure elastic case.

By integration, Equation 11 reduces to

$$\tau_p = \frac{3T_p}{2\pi r^3} \tag{12}$$

c. Elastic-plastic case. The elastic-plastic case assumes that once the yield point has been reached at the outermost element, the specimen will temporarily continue to sustain shear load until all elements within specific limits of the specimen

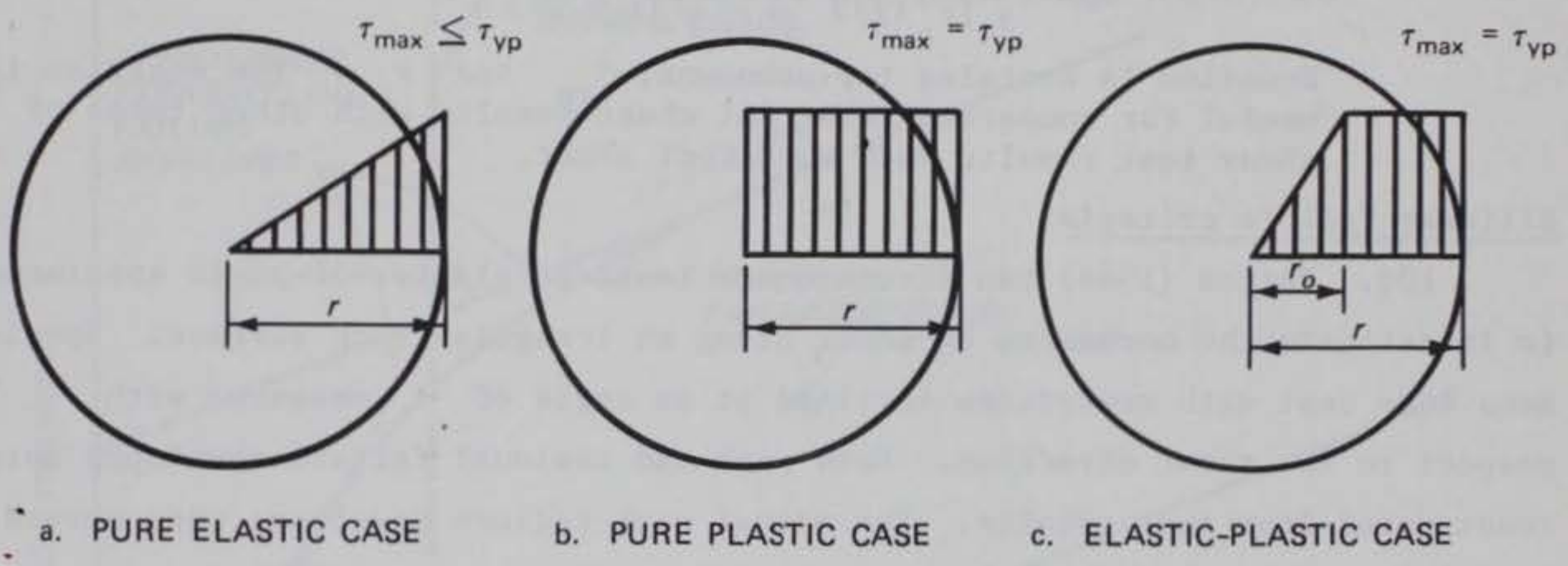

Figure 21. Shear stress distribution (r = specimen radius, r_o = elastic limit radius)

defined by $r-r_o$ (Figure 21) have been strained to the yield point at which time the specimen cannot sustain any additional shear load and the specimen fails. The peak shear stress at failure for this case can be determined by the general equation

$$\tau_{ep} = \frac{T_p}{\frac{2\pi}{r}\int_o^{r_o} \rho^3 d\rho + 2\pi \int_{r_o}^{r} \rho^2 d\rho} \tag{13}$$

where

τ_{ep} = shear stress at failure for elastic-plastic case

r_o = radius of elastic limit

By integration, Equation 13 reduces to

$$\tau_{ep} = \frac{T_p}{\pi \left[r_o^3 (1/2 \frac{r_o}{r} - 2/3) + 2/3\ r^3\right]} \tag{14}$$

Equation 14 contains two unknowns, τ_{ep} and r_o. The equation is useful for comparing torsional shear results with other types of shear test results such as direct shear.

Bilinear failure criteria

108. Patton (1966) ran direct shear tests on plaster-of-paris specimens to investigate the mechanism of shear along an irregular rock surface. Specimens were cast with asperities inclined at an angle of i measured with respect to the shear direction. Both peak and residual failure envelopes were constructed from test results. The actual peak failure envelopes were curves as illustrated in Figure 22 but were approximated by two straight lines. Line OAB in Figure 22 is a typical peak failure envelope (Deere et al., 1967).

109. Shear failure at low normal loads (line OA, Figure 22) is associated with vertical displacements produced by the upper block sliding up the inclined surfaces. Line OA is defined by Equation 15:

$$\tau = \sigma_n \tan (\phi_u + i) \tag{15}$$

where

ϕ_u = angle of sliding resistance along smooth plaster surfaces

i = asperity inclination angle in direction of shear

At high normal loads, the failure mode changes. The vertical displacements are small with the teeth sheared off at or near their base as approximated by line AB in Figure 22. The change in failure mode occurs at some stress level

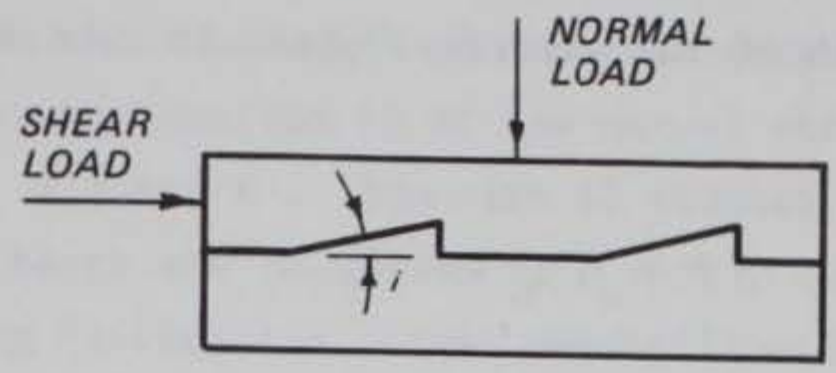

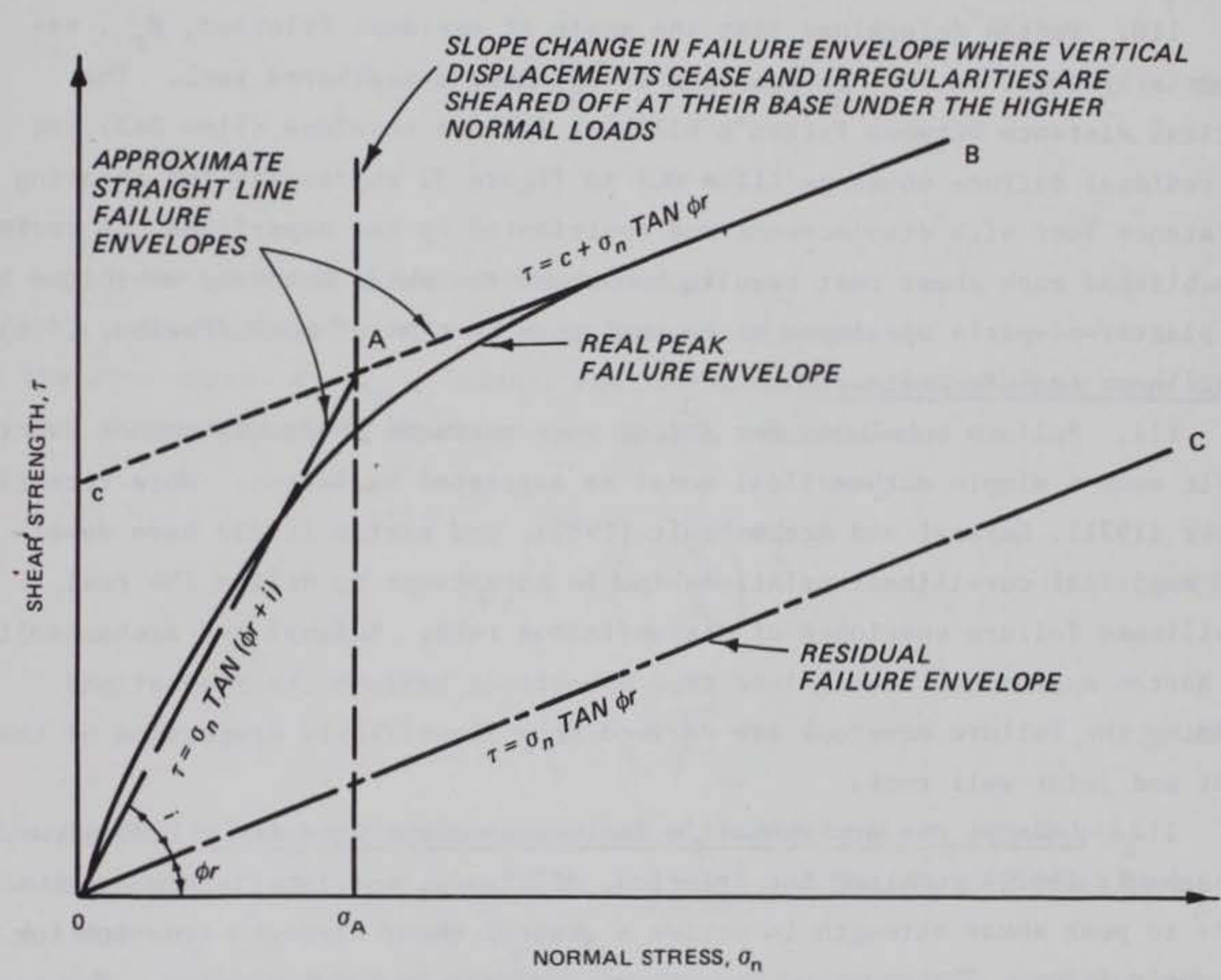

Figure 22. Maximum and residual strength failure envelope from tests of discontinuities (after Deere et al., 1967)

(approximated by σ_A in Figure 22), where less energy is required to shear the asperities than to override asperities. The level of stress, σ_A, is dependent upon the asperity inclination angle i, the size of the asperity, and the intact shear strength of the asperity. Line AB is defined by Equation 16:

$$\tau = c + \sigma_n \tan \phi_r \tag{16}$$

where

ϕ_r = the angle of residual sliding resistance

110. Patton determined that the angle of residual friction, ϕ_r, was essentially equal to ϕ_u in Equation 15 for most unweathered rock. The vertical distance between Patton's bilinear failure envelope (line OAB) and the residual failure envelope (line OC) in Figure 22 represents the shearing resistance lost with displacement and contributed by the asperities. A review of published rock shear test results has shown the shear behavior exhibited by the plaster-of-paris specimens to be analogous to that of rock (Patton, 1966).

Curvilinear failure criterion

111. Failure envelopes for actual rock surfaces obviously cannot exactly fit such a simple mathematical model as suggested by Patton. More recently, Jaeger (1971), Ladanyi and Archambault (1980), and Barton (1973) have developed empirical curvilinear relationships in an attempt to define the real curvilinear failure envelopes of discontinuous rock. Ladanyi and Archambault, and Barton approaches have gained some acceptance because their equations defining the failure envelope are derived from identifiable properties of the joint and joint wall rock.

112. Ladanyi and Archambualt's failure envelope equation. Ladanyi and Archambault (1970) combined the friction, dilatancy, and interlock contributions to peak shear strength to derive a general shear strength equation for discontinuities. The equation has proved accurate in model studies. The peak shear strength is defined by Equation 17:

$$\tau = \frac{\sigma_n (1 - a_s)(V + \tan \phi_u) + a_s \cdot S_R}{1 - (1 - a_s) \cdot V \cdot \tan \phi_u} \tag{17}$$

where

a_s = the proportion of joint area sheared through the asperities

V = the dilation rate at the peak shear stress

S_R = the peak shear strength of the rock composing the asperities

Equation 17 reduces to Equation 15 at low normal stresses ($\sigma_n < \sigma_A$, Figure 22) when $a_s = 0$ and $V = \tan i$. Equation 17 reduces to $\tau = S_R$ at very high σ_n where all the teeth are sheared off, $a_s = 1$, and $V = 0$. Ladanyi suggested substituting Fairhurst's (1964) parabolic criterion for S_R, as defined by Equation 18, for the case when $\sigma_n \geq q_u$:

$$S_R = q_u \frac{1 + n - 1}{n} (1 + n\,\sigma/q_u)^{1/2} \tag{18}$$

where

q_u = the unconfined compressive strength

n = the ratio of compressive to tensile strength

For the case where $\sigma_n < q_u$, Ladanyi and Archambault suggested power laws for a_s and V as defined by Equations 19 and 20, respectively:

$$a_s = 1 - \left(1 - \frac{\sigma_n}{q_u}\right)^{K_1} \tag{19}$$

$$V = \left(1 - \frac{\sigma_o}{q_u}\right)^{K_2} \tan i \tag{20}$$

The suggested values of the exponents are $K_1 = 1.5$ and $K_2 = 4.0$; a_s increases from 0 at $\sigma_n = 0$ to 1 at $\sigma_n = q_u$, while V decreases from $\tan i$ when $\sigma_n = 0$ to 0 at $\sigma_n = q_u$.

113. Barton's failure envelope equation. Barton (1973) proposed and later (1976) modified an empirical shear strength failure criterion defined by Equation 21 for clean discontinuities accounting for the variation of dilatancy with normal stress and the strength of the asperities:

$$\tau = \sigma_n \tan \left[JRC \log_{10} \left(\frac{JCS}{\sigma_n} \right) + \phi_r \right] \tag{21}$$

where

JRC = the joint roughness coefficient

JCS = the joint wall unconfined compressive strength

Equation 21 is applicable for normal stress levels up to the unconfined compressive strength of the joint wall rock (approximately equal to σ_A in Figure 22). The term JRC is an assigned coefficient which expresses the influence of joint roughness, varying linearly from 0 to 20 over the range from perfectly smooth to very rough.

Relationship between discontinuous and intact rock behavior

114. Failure mechanics associated with discontinuous and intact rock are distinctly different. However, failure envelopes for discontinuous and intact rock share several common characteristics. Figure 23 illustrates typical failure envelopes for an unweathered discontinuous and intact limestone. Both envelopes are curvilinear and intersect each other at point T corresponding to a principal stress of σ_T. In fracture mechanics of intact rock point T is referred to as the transition stress between brittle and ductile behavior. In friction mechanics of discontinuous rock point T is associated with the transition stress between asperity override and asperity shear. With increasing principal stress past σ_T, both discontinuous and intact rock increase in shear strength until at some principal stress level both materials reach a zero τ/σ gradient.

115. Barton (1976) demonstrated that for most intact rock the point of zero τ/σ gradient occurs at the intersection of a line inclined at 26.7 deg and the Mohr's failure envelope for intact rock as shown by point C in Figure 23. Barton (1976) defined the line (line AC in Figure 23) as the critical state line and the point of zero gradient as the critical state for intact rock (point c in Figure 23). The Mohr's stress circle (circle 2 in Figure 23) whose apex defines the critical state corresponds to a failure condition where the major principal stress is three times the minor principal stress.

116. A similar critical state stress for discontinuous rock has not been defined. Opinions differ as to whether discontinuous and intact rock failure envelopes track each other past the transition stress σ_T or form separate envelopes as shown in Figure 23. In some ways it is difficult to imagine that discontinuous rock could be stronger than intact rock at higher

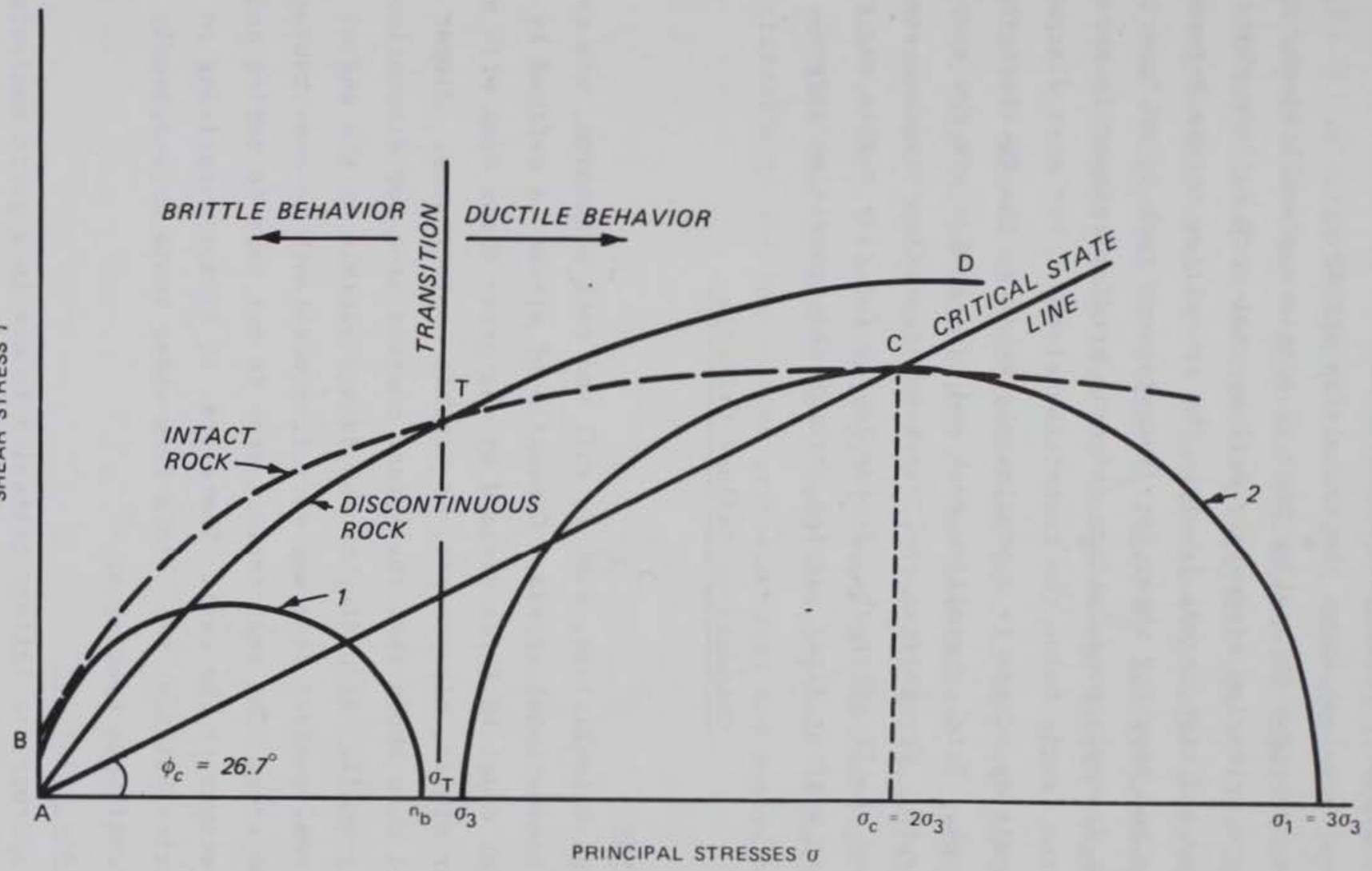

Figure 23. Discontinuous and intact rock failure envelope characteristics typical of unweathered limestone

stress levels. Mogi (1974) suggested that there may be two distinct types of behavior for discontinuous rocks, which he termed A-type and B-type, depending on whether they followed the fracture envelope (intact rock envelope) or a separate frictional envelope above the transition stress.

117. It is important to realize that no single current bilinear or curvilinear failure criterion adequately defines real rock failure characteristics at both low and high stress levels. The transition stress between asperity override and asperity shear for discontinuous rock is an important concept. Current discontinuous failure criteria predict reasonable shear behavior for stress levels below the transition stress. For most discontinuous rock the transition stress is approximately equal to the UC strength of the joint wall rock. Hard crystalline rock and clay shales are the exception to this general rule. Crystalline rock can have transition stresses several times greater than the UC strength. Stress levels for clay shales may reach the critical state without first passing through the transition stress.

Comments on Failure Criteria

Conventional stress

118. Design calculations, both in soil and rock mechanics, are carried out in terms of conventional stress. Conventional stress is defined by a given stress level equal to force divided by the gross shear area with no consideration for atomic, microscopic, or visible contact area. Jaeger (1971) and Barton (1971) have shown that the actual contact area for discontinuous rock is extremely small. According to the damage visible at the end of a shear test, the real contact area may vary from one-tenth to one-thousandth or less of the gross area. The real contact area is not easy to define and will vary from one specimen to the next. Therefore, it is not surprising to find considerable scatter between τ-σ plots from shear tests on supposedly similar natural discontinuous specimens.

Appropriate failure criterion

119. The appropriate failure criterion to use in a given analysis is dependent upon the intended use of the analysis. Conventional design procedures require use of linear or bilinear failure criterion. Curvilinear failure criterion will perhaps better define all levels of stress at failure but will require complex techniques for design purposes.

120. Curvilinear criteria currently available do not account for a possible cohesion intercept at zero normal stress. These criteria will fit the majority of naturally occurring joints. However, if the asperity inclination angle i is large enough ($i > 90° - \phi_u$), less work will be required to shear the asperities than to override the asperities regardless of confining stress. In such cases, a cohesion intercept will occur. For some design cases it may be desirable to fit a failure envelope with a curvilinear criterion and then extrapolate effective c_d and ϕ_d design parameters from a best-fit linear relationship over the design normal stress range as shown in Figure 24.

121. The Mohr-Coulomb criterion was used to compare the test results presented in Part VII of this report. The Mohr-Coulomb criterion was selected for three reasons. First, most of the data can fit a linear failure envelope. Second, the c and ϕ shear strength parameters obtained from a Mohr-Coulomb failure envelope are convenient for comparison purposes. Finally, the Mohr-Coulomb criterion is the most common criterion used for analyzing shear data.

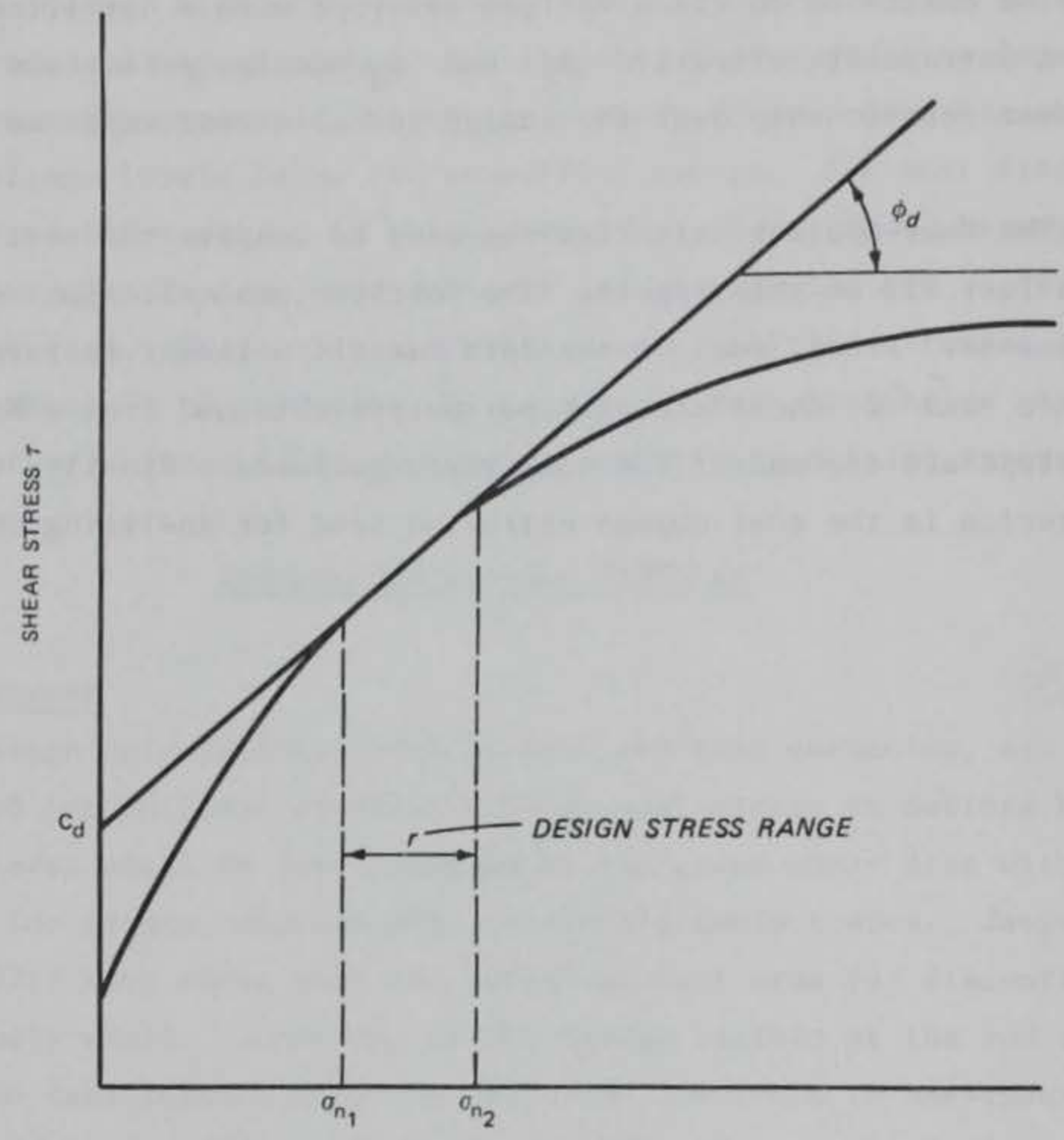

Figure 24. Extrapolation of effective design parameters from curvilinear failure envelope

PART VII: TEST RESULTS

Summary of Tests

122. Table 6 is a summary of the types and number of tests for each type of specimen. A total of 114 unconfined compression tests and 221 shear tests were made on model material specimens. Twenty-nine shear tests were made on the Rangely sandstone. Generally, at least six shear tests were made for each type of test and specimen investigated to establish failure envelope trends over a range of normal stresses or cell pressures from 2 to 8 tsf. Where plotted $\tau - \sigma$ scatter was excessive for a given series of tests, additional tests were made.

Model Material Specimens

UC tests

123. The UC tests were made to ensure strength uniformity between model material batches. At least two tests were made on either 4- or 6-day-old specimens from each batch. Table 7 is a summary of the UC test results. Figure 25 is a plot of mean UC strength and standard deviation versus specimen age. Figure 25 indicates a uniform strength between the 4- and 6-day-old specimens, with a slight increase in strength (approximately 7 percent) for 8- to 10-day-old specimens. Specimens 11 days old increased in strength by approximately 21 percent with respect to the 4-day-old specimens. Because of the trend for increasing strength with age, all shear tests on model material were made on the fifth, sixth, seventh, or eighth day after casting. The trend for increasing strength does not support Rosenblad's findings that strength was independent of shelf life.

124. The standard deviation for UC tests on rock, no matter what precautions are taken in preparing the specimens, is often high. Three factors contribute to test scatter: stress distribution at the specimen ends, size of the specimen, and microfissures within the specimen.

125. Adequate precautions may be taken to minimize adverse stress distribution effects by using specimens with length-to-diameter ratios of 2 to 3 and ensuring that the specimen ends are smooth and perpendicular to the direction of the applied load.

Table 6

Summary of Type and Number of Tests for Each Type of Specimen

Type of Test	Model Material: Smooth Cast	Model Material: Even Angle	Model Material: Rake Tooth	Model Material: Intact	Rangely Sandstone: Natural	Rangely Sandstone: Sawn	Rangely Sandstone: Intact	Total Number of Tests
Unconfined compression (UC)				40 - 4 days* 35 - 6 days 21 - 8 days 5 - 10 days 13 - 11 days				114
Direct shear in situ	8	7	7		6			28
Torsional shear	6	5	9					20
Direct shear ORD	20	8	10	17				55
Direct shear KC	13	8	10	8	6		2	47
Direct shear IC	14	13	9	8				43
Direct shear 3- by 3-in.	9			9		6	9	33
Triaxial GL**	6			6				12
Triaxial SL**				12				12

* The 4, 6, 8, 10, and 11 days refer to the age of the model material.

** GL designates Geotechnical Laboratory; SL designates Structures Laboratory.

Table 7

Summary of UC Test Results

	Specimen Age When Tested				
	4 days	6 days	8 days	10 days	11 days
No. of batches tested	22	19	12	3	7
Total No. of tests	40	35	21	5	13
Mean UC strength M , tsf	41.5	41.1	44.5	44.2	50.3
Std deviation S , tsf	6.3	5.5	6.8	7.3	11.0

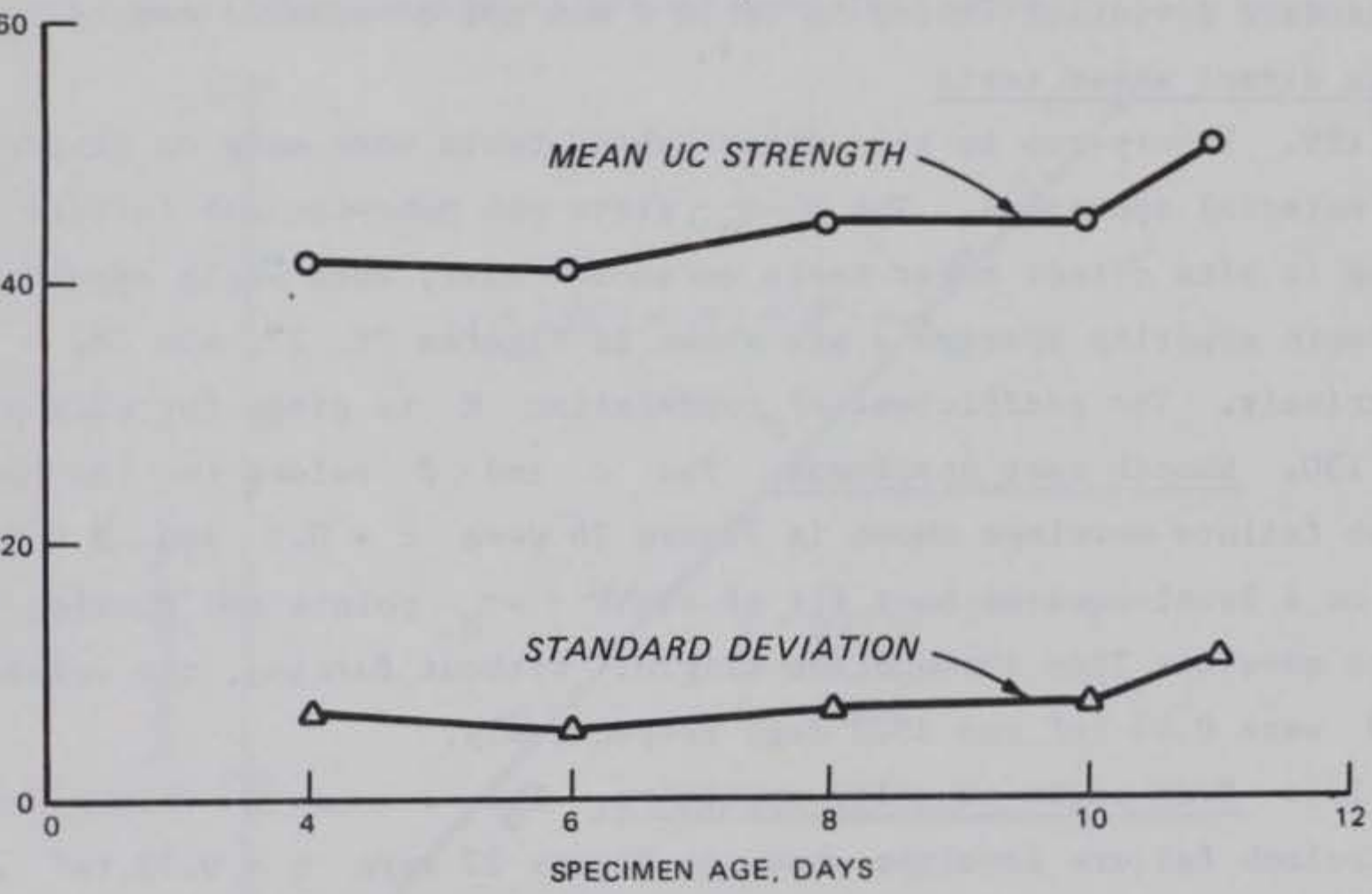

Figure 25. Specimen age versus UC strength and standard deviation

126. Theories explain that a large test sample can be thought of as being the sum of several smaller samples and that the average strength of the larger sample does not depend on the average strength of the smaller samples but on the lowest strength of any of the small samples. Therefore, the average UC strength tends to decrease as the specimen size increases.

127. Bernaix (1966) demonstrated that there is an obvious correlation between the ratio of the standard deviation to the mean strength (S/M) and the degree of fissuration. The denser the fissures, the greater the dispersion of the test results. There is no such correlation between the degree of fissuration and the absolute value of the rock strength. Bernaix found that a biotite gneiss with an average number of microfissures had a typical S/M ratio of 0.22.

128. The model material test results listed in Table 7 had fourth, sixth, eighth, tenth, and eleventh day S/M ratios of 0.15, 0.13, 0.15, 0.16, and 0.21, respectively. Considering the various factors affecting UC strength, the standard deviation listed in Table 7 was not considered excessive.

In situ direct shear tests

129. Twenty-two in situ direct shear tests were made on discontinuous model material specimens. The $\tau - \sigma_n$ plots and Mohr-Coulomb failure envelopes for the in situ direct shear tests on smooth cast, even angle asperity, and rake tooth asperity specimens are shown in Figures 26, 27, and 28, respectively. The coefficient of correlation R is given for each plot.

130. Smooth cast specimens. The c and ϕ values for the Mohr-Coulomb failure envelope shown in Figure 26 were $c = 0.0$ and $\phi = 38.5$ deg, based on a least-squares best fit of eight $\tau - \sigma_n$ points and forcing the failure envelope line through the origin. Without forcing, the values for c and ϕ were 0.05 tsf and 38.2 deg, respectively.

131. Even angle asperity specimens. The c and ϕ values for the Mohr-Coulomb failure envelope shown in Figure 27 were $c = 0.72$ tsf and $\phi = 47.8$ deg based on a least-squares best fit of seven $\tau - \sigma_n$ points. Observation of all shear surfaces after testing showed all asperities had sheared at their bases.

132. Rake tooth asperity specimens. The c and ϕ values for the Mohr-Coulomb failure envelope shown in Figure 28 were $c = 1.91$ tsf and $\phi = 39.8$ deg based on a least-squares best fit of seven $\tau - \sigma_n$ points.

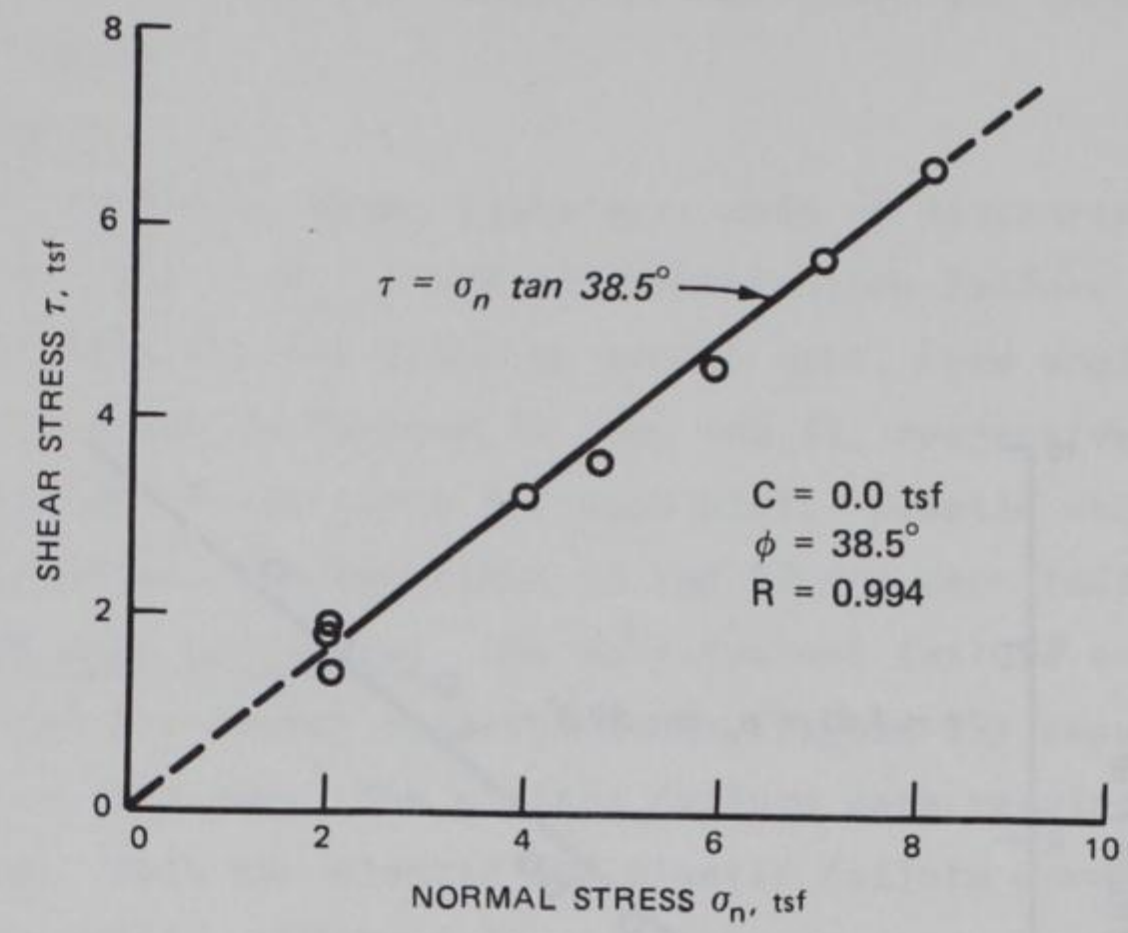

Figure 26. In situ direct shear test results for model material smooth cast specimens

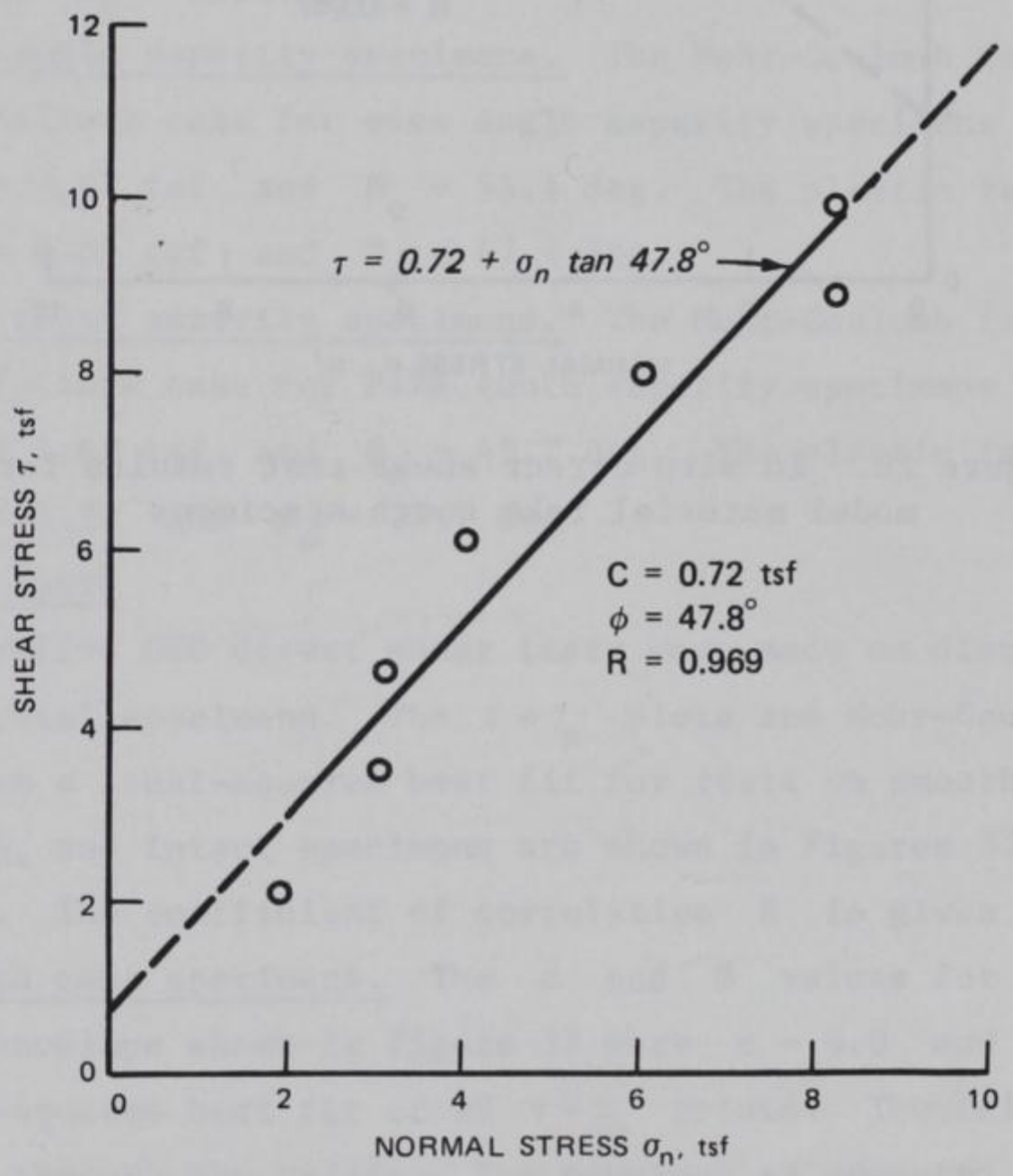

Figure 27. In situ direct shear test results for model material even angle asperity specimens

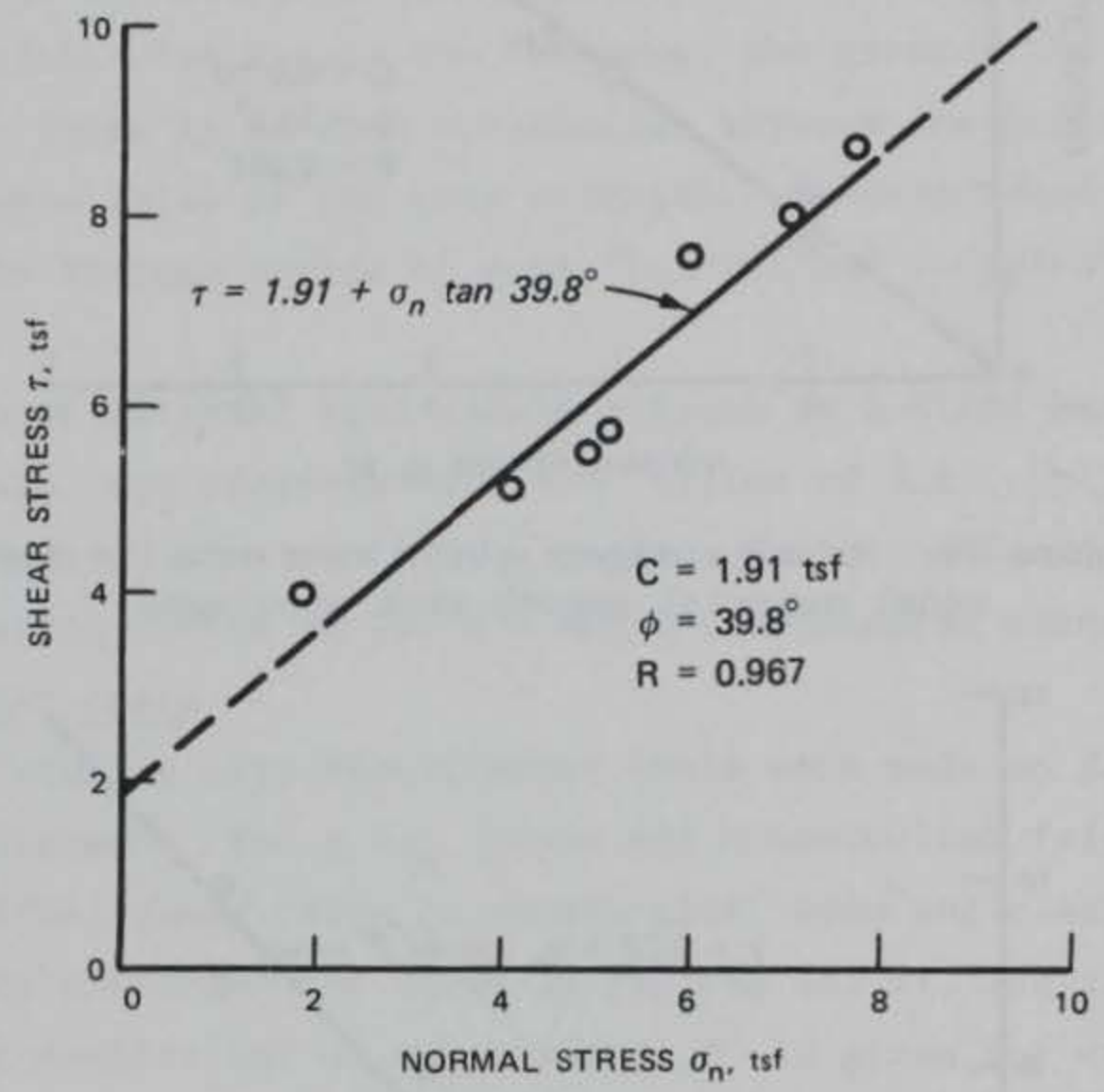

Figure 28. In situ direct shear test results for model material rake tooth specimens

Observation of all shear surfaces after testing showed all asperities had sheared at their bases.

Torsional shear tests

133. Twenty torsional shear tests were made on discontinuous model material specimens. The $\tau - \sigma_n$ plots and Mohr-Coulomb failure envelopes based on a least-squares best fit for tests on smooth cast, even angle, and rake tooth specimens are shown in Figures 29, 30, and 31, respectively. The coefficient of correlation R is given for each plot. Elastic and plastic shear stresses were calculated from Equations 10 and 12 for each individual test.

134. Smooth cast specimens. The Mohr-Coulomb failure envelope for the elastic failure case for smooth cast specimens (Figure 29) resulted in $c_e = 0.0$ and $\phi_e = 35.9$ deg. The plastic failure case resulted in $c_p = 0.0$ and $\phi_p = 28.4$ deg. Both the elastic and plastic failure envelopes were forced through the origin. Without forcing, the c and ϕ values were as follows: elastic case $c_e = 0.06$ tsf and $\phi_e = 35.5$ deg; plastic case $c_p = 0.05$ tsf and $\phi_p = 28.2$ deg.

135. Even angle asperity specimens. The Mohr-Coulomb failure envelope for the elastic failure case for even angle asperity specimens (Figure 30) resulted in $c_e = 0.12$ tsf and $\phi_e = 55.4$ deg. The plastic failure case resulted in $c_p = 0.09$ tsf and $\phi_p = 47.4$ deg.

136. Rake tooth asperity specimens. The Mohr-Coulomb failure envelope for the elastic failure case for rake tooth asperity specimens (Figure 31) resulted in $c_e = 1.63$ tsf and $\phi_e = 45.2$ deg. The plastic failure case resulted in $c_p = 1.22$ and $\phi_p = 37.1$ deg.

ORD direct shear tests

137. Fifty-five ORD direct shear tests were made on discontinuous and intact model material specimens. The $\tau - \sigma_n$ plots and Mohr-Coulomb failure envelopes based on a least-squares best fit for tests on smooth cast, even angle, rake tooth, and intact specimens are shown in Figures 32, 33, 34, and 35, respectively. The coefficient of correlation R is given for each plot.

138. Smooth cast specimens. The c and ϕ values for the Mohr-Coulomb failure envelope shown in Figure 32 were $c = 0.0$ and $\phi = 28.2$ deg based on a least-squares best fit of 20 $\tau - \sigma_n$ points. The failure envelope shown was forced through the origin. The envelope as computed for all points had a cohesion intercept of 0.28 tsf and a friction angle of 26.3 deg.

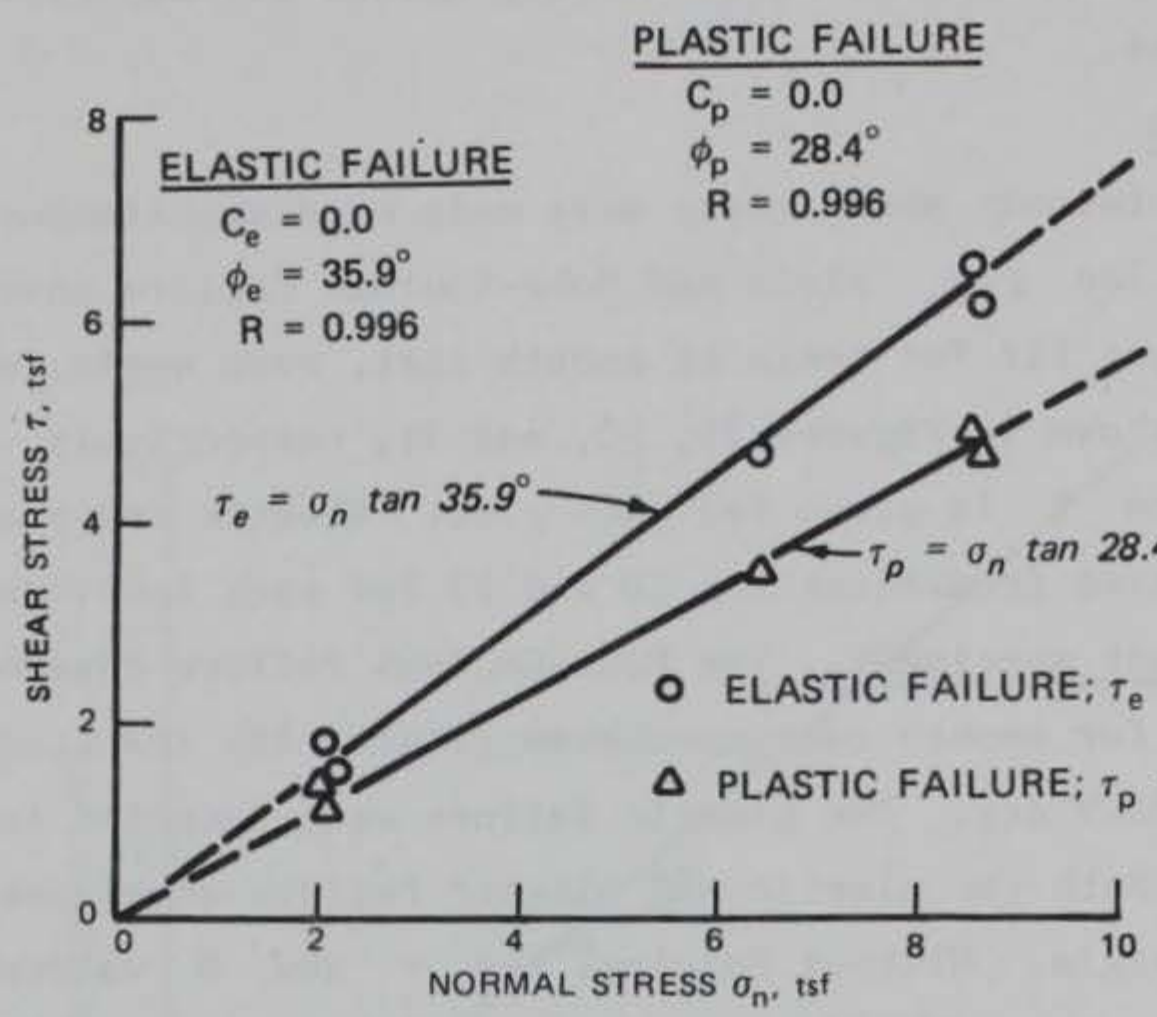

Figure 29. Torsional shear test results for model material smooth cast specimens

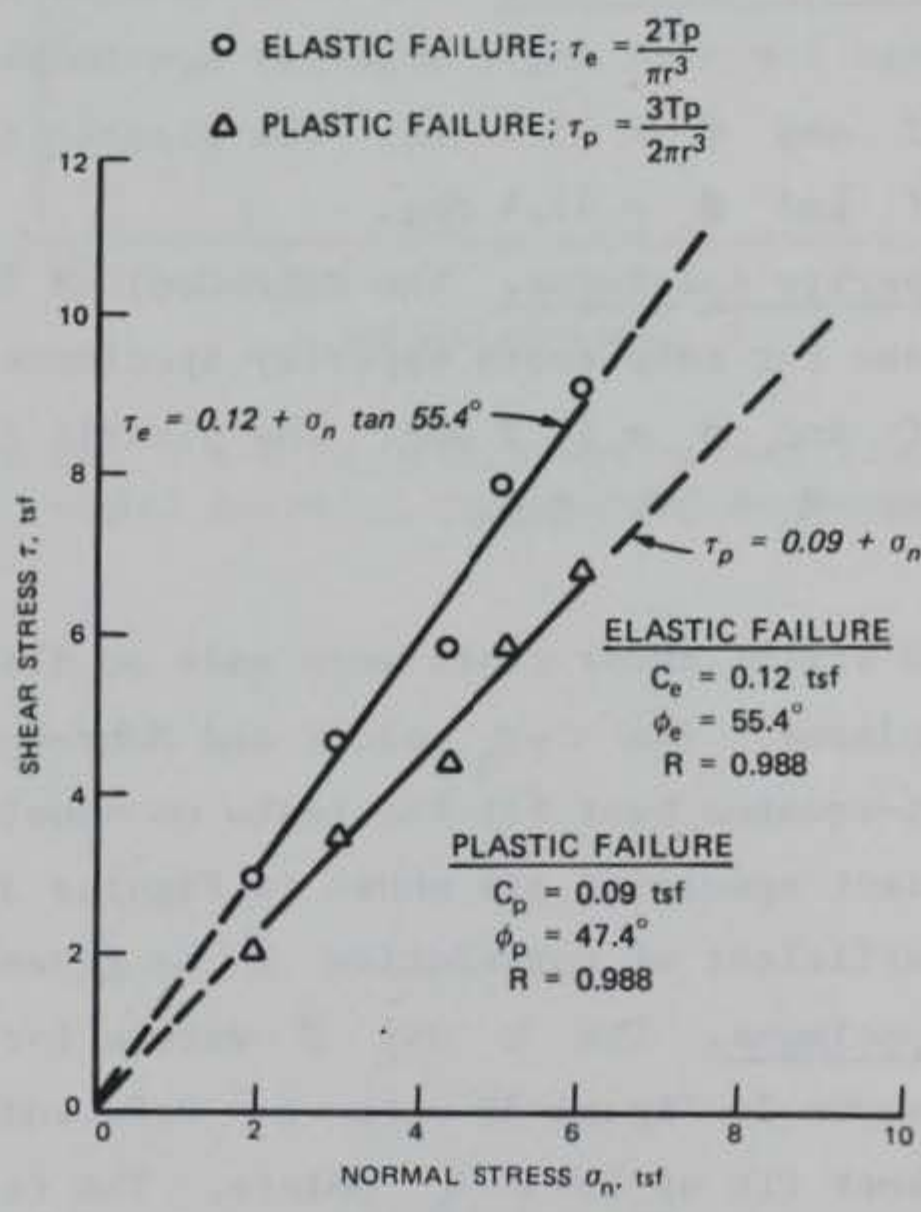

Figure 30. Torsional shear test results for model material even angle asperity specimens

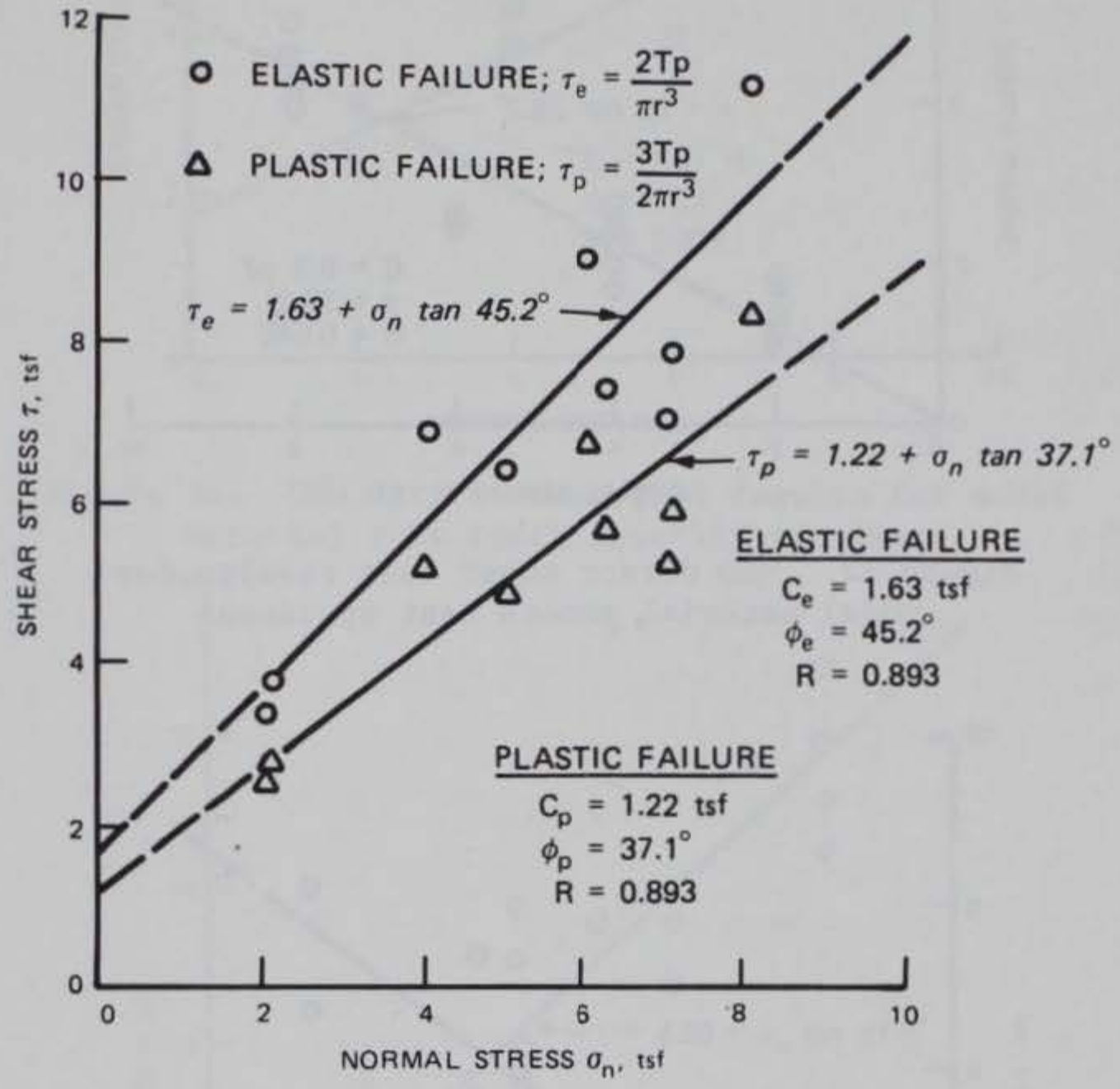

Figure 31. Torsional shear test results for model material rake tooth asperity specimens

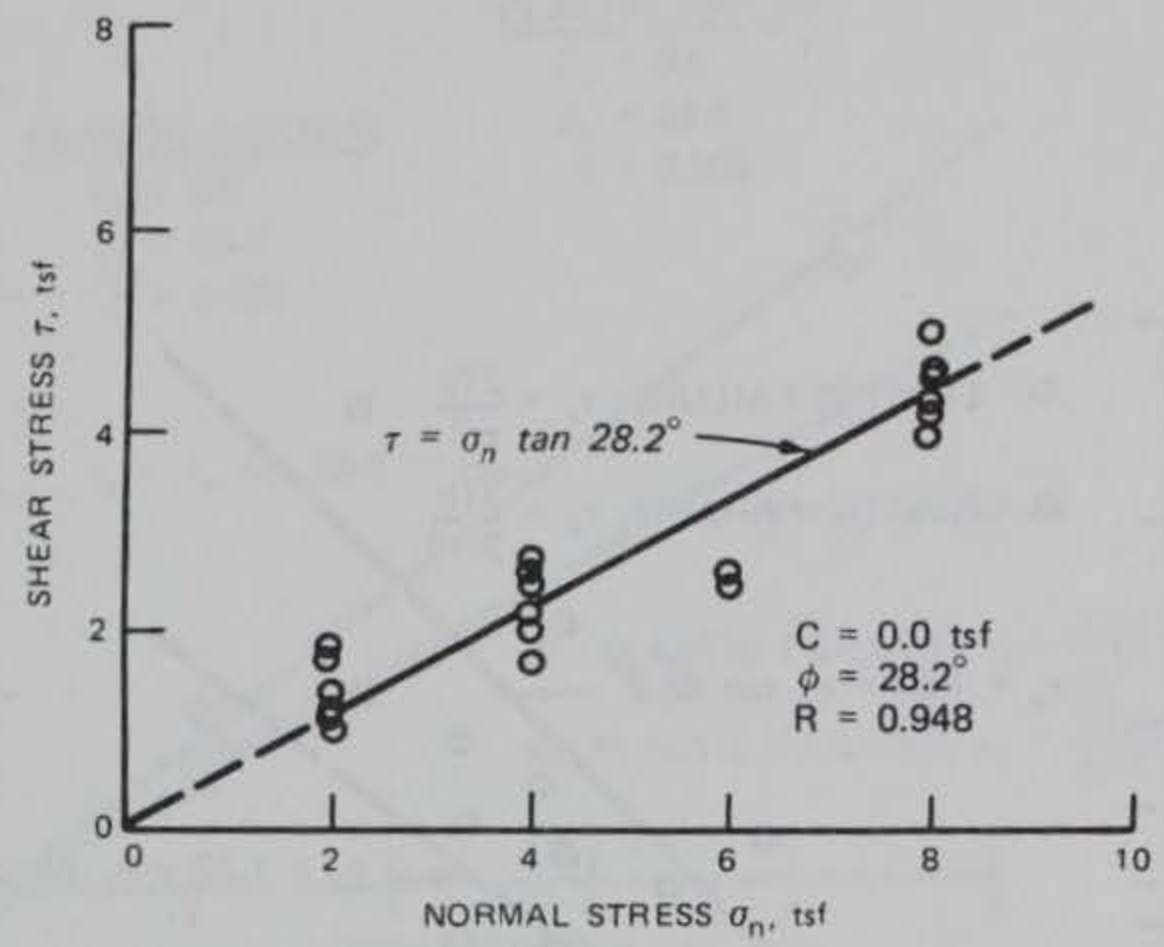

Figure 32. ORD direct shear test results for model material smooth cast specimens

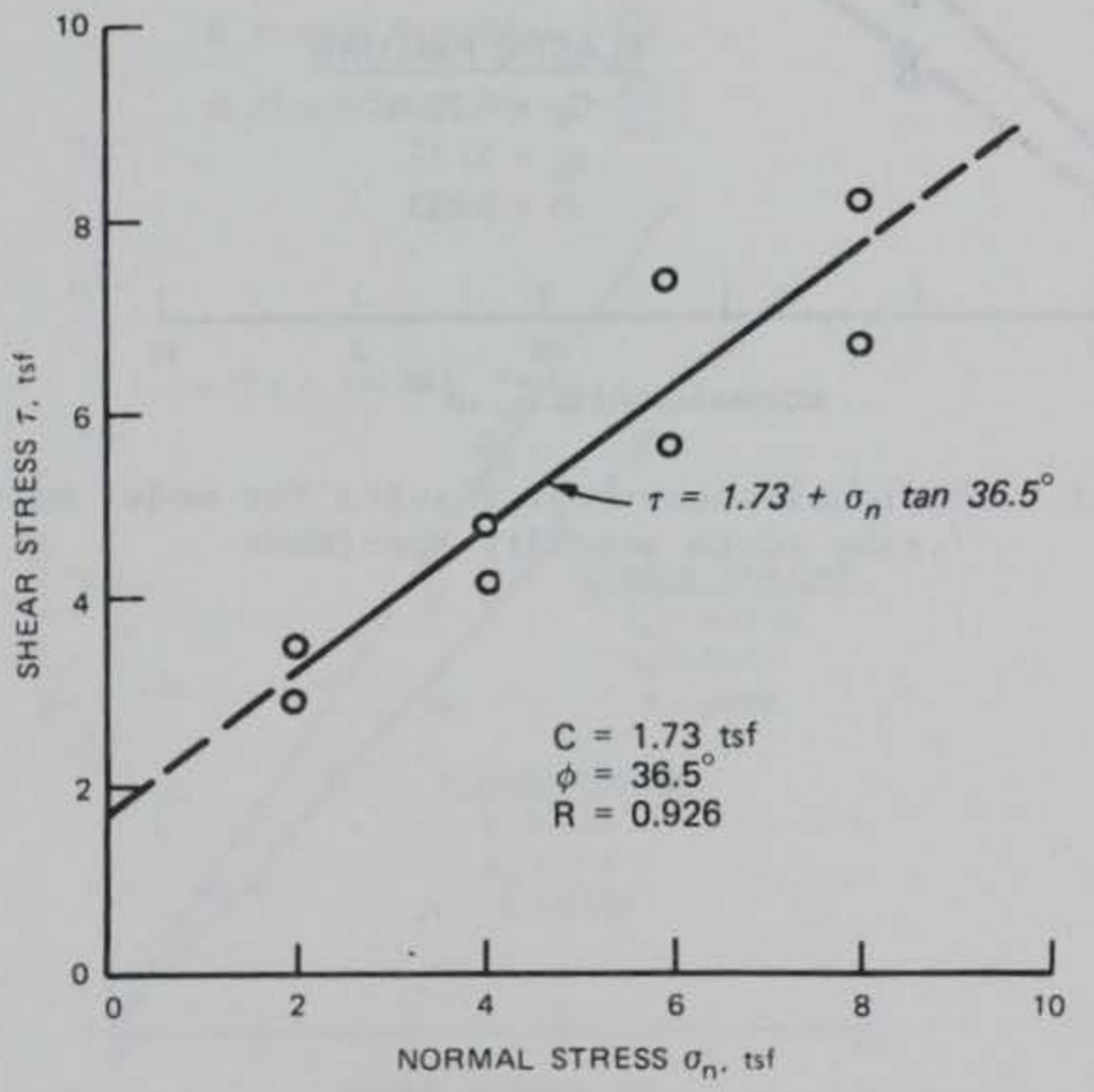

Figure 33. ORD direct shear test results for model material even angle asperity specimens

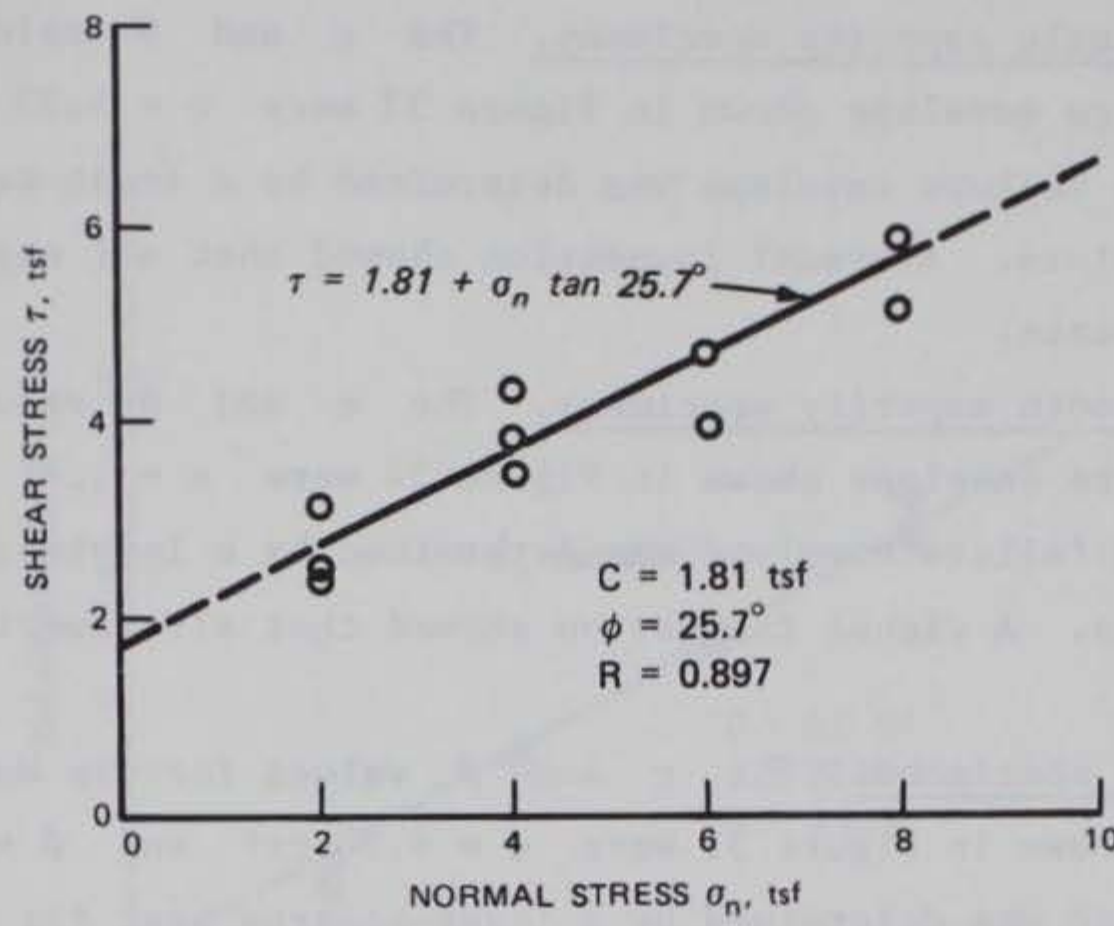

Figure 34. ORD direct shear test results for model material rake tooth asperity specimens

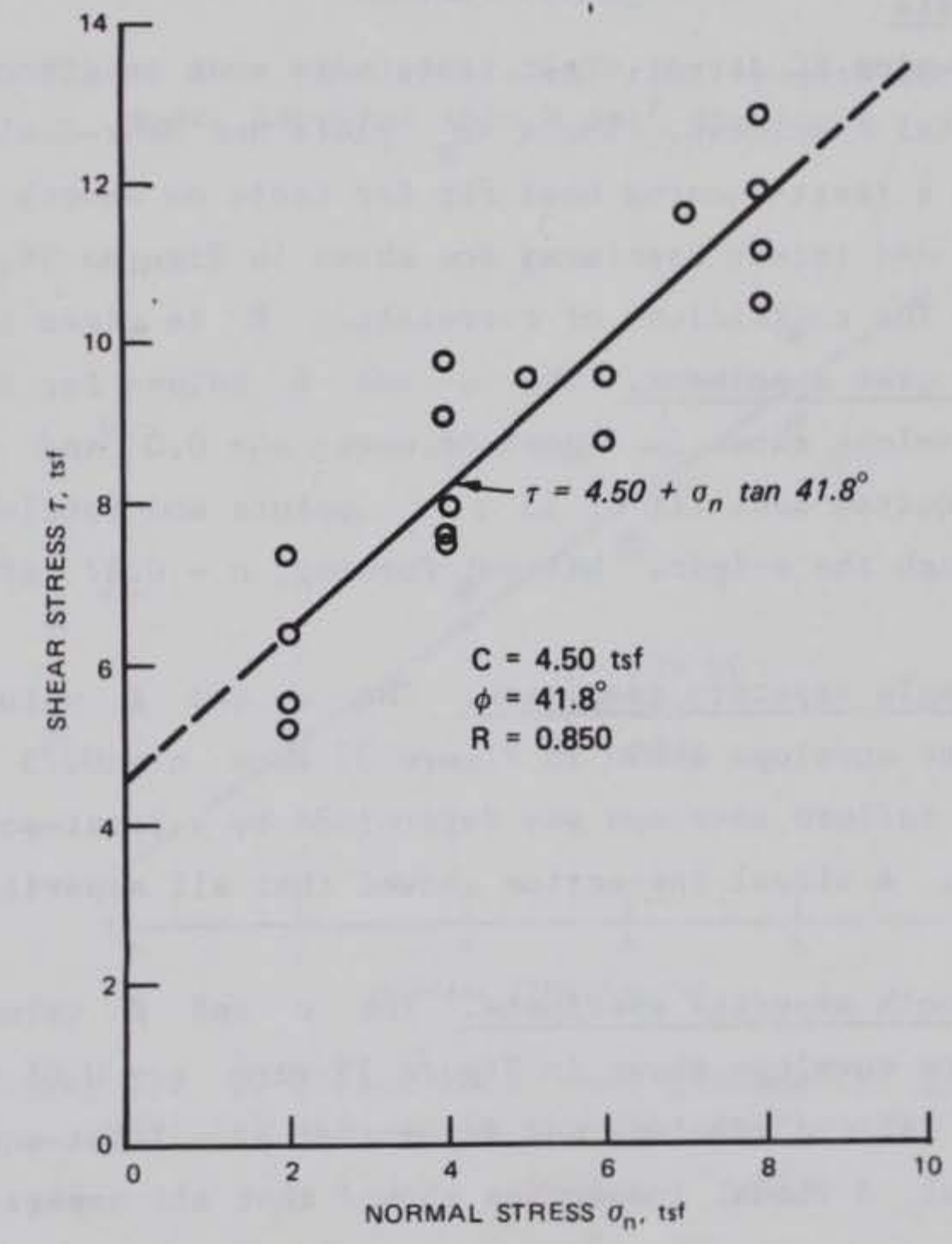

Figure 35. ORD direct shear test results for model material intact specimens

139. Even angle asperity specimens. The c and ϕ values for the Mohr-Coulomb failure envelope shown in Figure 33 were c = 1.73 tsf and ϕ = 36.5 deg. The failure envelope was determined by a least-squares best fit of eight $\tau - \sigma_n$ points. A visual inspection showed that all asperities sheared at their bases.

140. Rake tooth asperity specimens. The c and ϕ values for the Mohr-Coulomb failure envelope shown in Figure 34 were c = 1.81 tsf and ϕ = 25.7 deg. The failure envelope was determined by a least-squares best fit of 10 $\tau - \sigma_n$ points. A visual inspection showed that all asperities sheared at their bases.

141. Intact specimens. The c and ϕ values for the Mohr-Coulomb failure envelope shown in Figure 35 were c = 4.50 tsf and ϕ = 41.8 deg. The failure envelope was determined by a least-squares best fit of 17 $\tau - \sigma_n$ points.

KC direct shear tests

142. Thirty-nine KC direct shear tests were made on discontinuous and intact model material specimens. The $\tau - \sigma_n$ plots and Mohr-Coulomb failure envelopes based on a least-squares best fit for tests on smooth cast, even angle, rake tooth, and intact specimens are shown in Figures 36, 37, 38, and 39, respectively. The coefficient of correlation R is given for each plot.

143. Smooth cast specimens. The c and ϕ values for the Mohr-Coulomb failure envelope shown in Figure 36 were c = 0.0 and ϕ = 29.0 deg based on a least-squares best fit of 13 $\tau - \sigma_n$ points and forcing the failure envelope line through the origin. Without forcing, c = 0.37 tsf and ϕ = 30.2 deg.

144. Even angle asperity specimens. The c and ϕ values for the Mohr-Coulomb failure envelope shown in Figure 37 were c = 0.73 tsf and ϕ = 35.2 deg. The failure envelope was determined by a least-squares best fit of 8 $\tau - \sigma_n$ points. A visual inspection showed that all asperities sheared at their bases.

145. Rake tooth asperity specimens. The c and ϕ values for the Mohr-Coulomb failure envelope shown in Figure 38 were c = 0.61 tsf and ϕ = 31.6 deg. The failure envelope was determined by a least-squares best fit of 10 $\tau - \sigma_n$ points. A visual inspection showed that all asperities sheared at their bases.

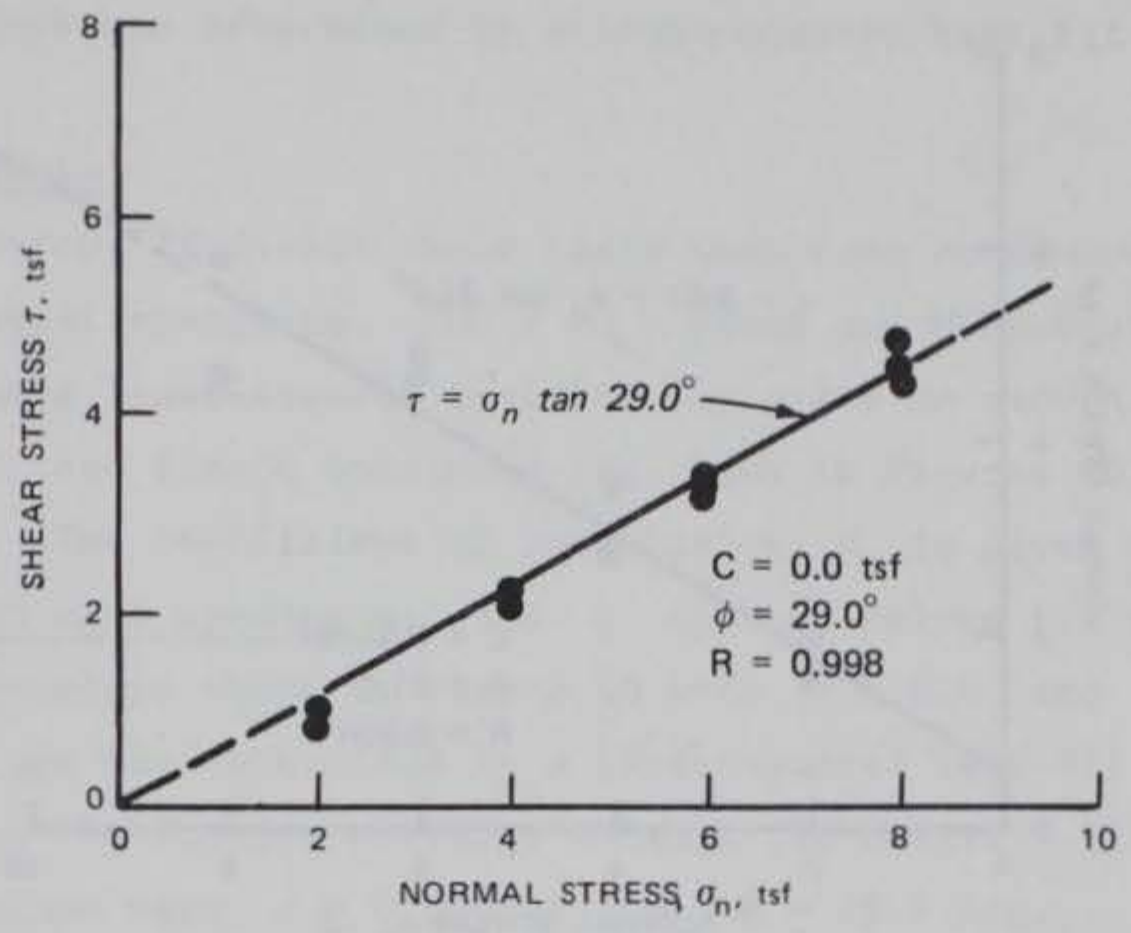

Figure 36. KC direct shear test results for model material smooth cast specimens

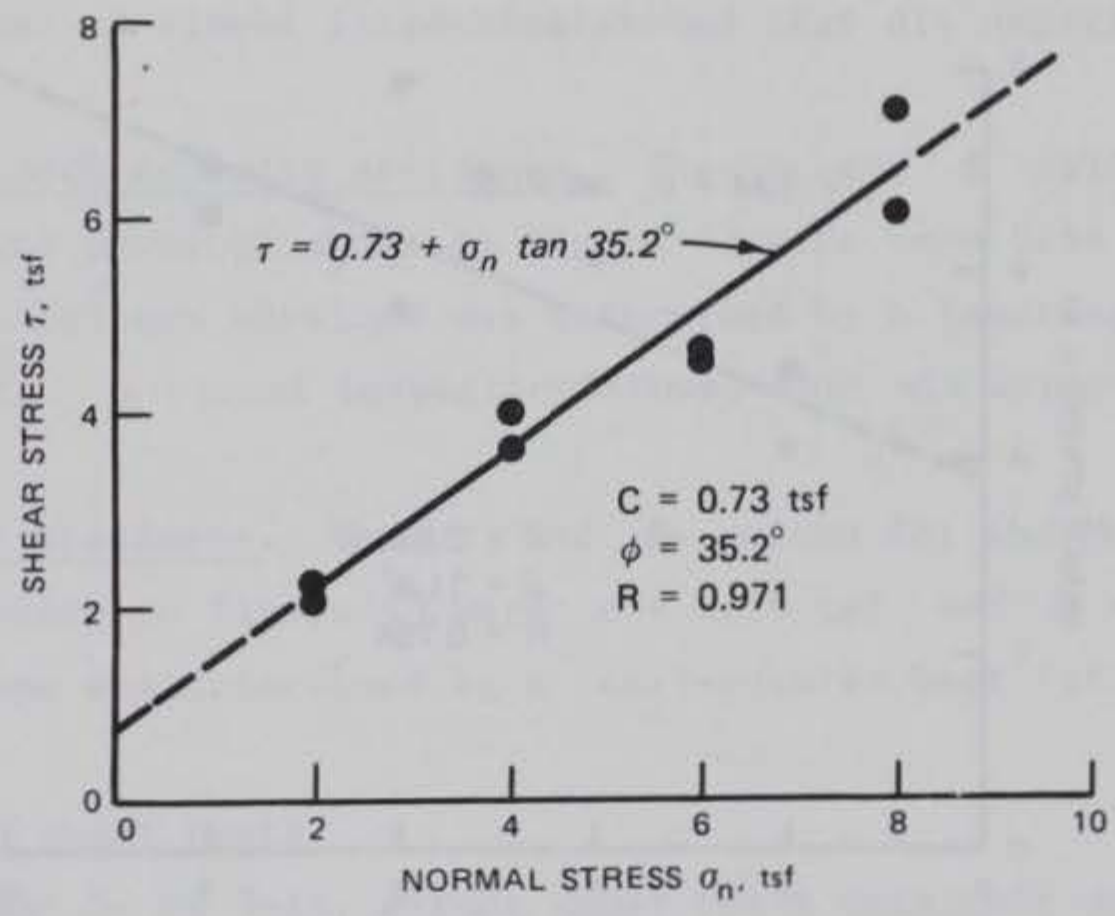

Figure 37. KC direct shear test results for model material even angle asperity specimens

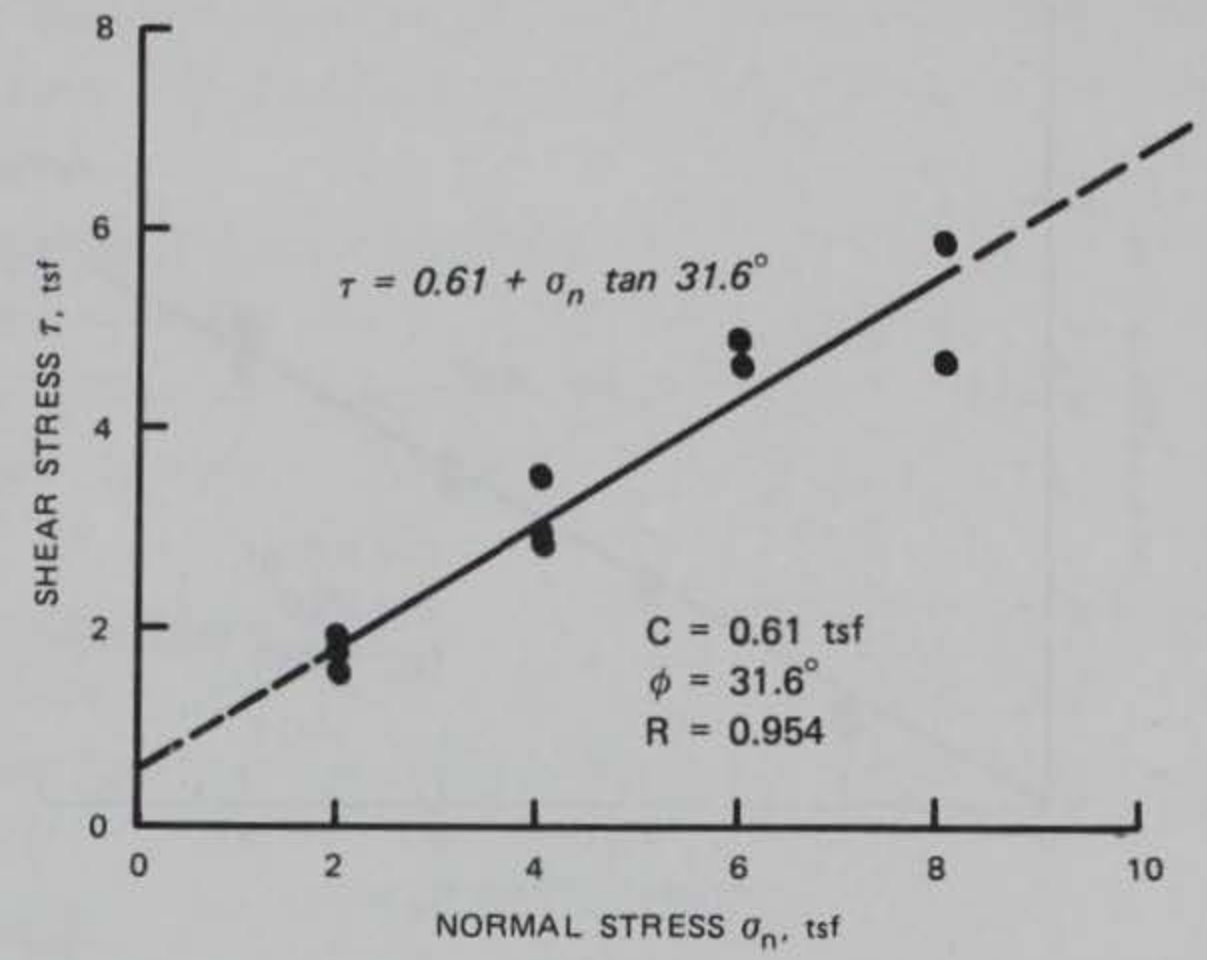

Figure 38. KC direct shear test results for model material rake tooth asperity specimens

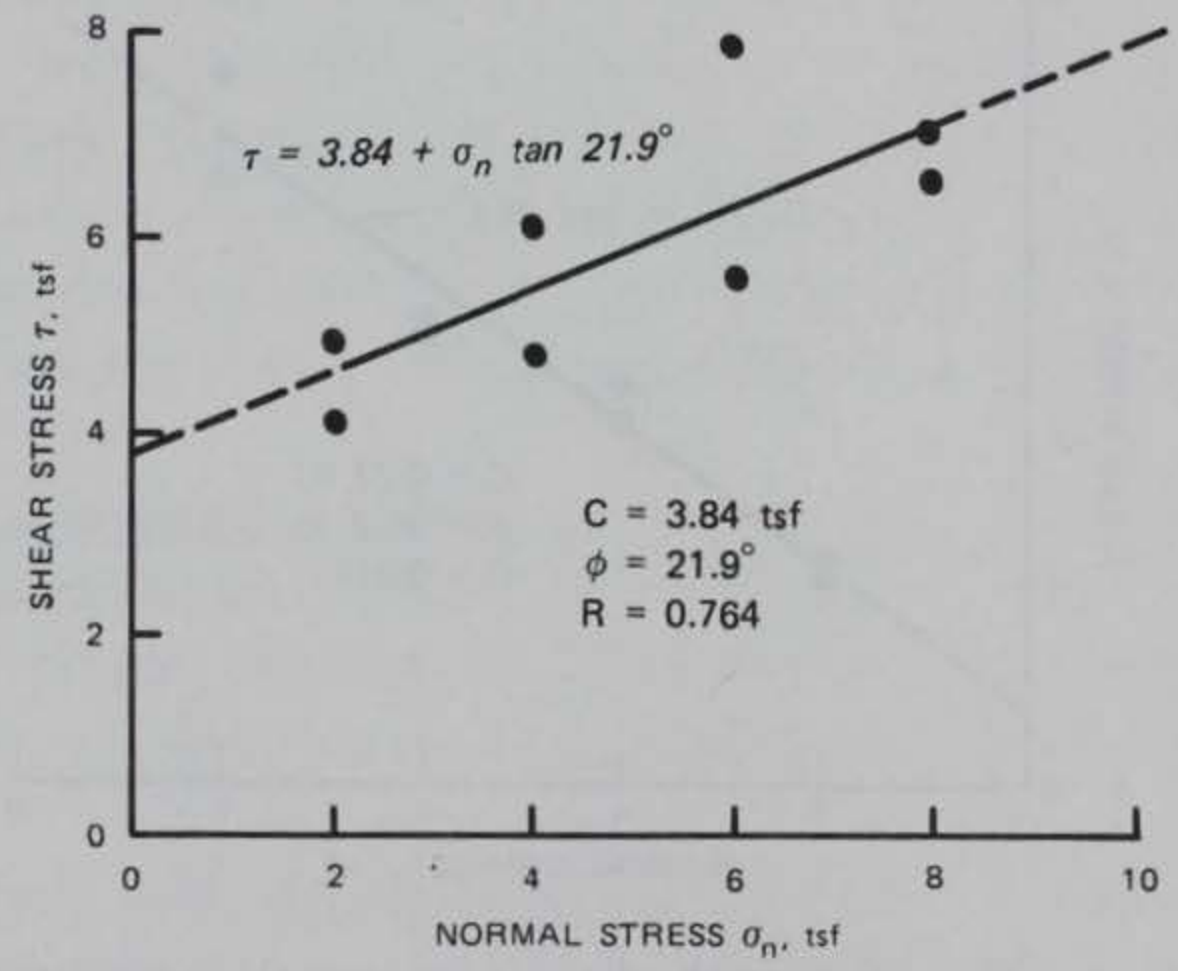

Figure 39. KC direct shear test results for model material intact specimens

146. Intact specimens. The c and $\emptyset$ values for the Mohr-Coulomb failure envelope shown in Figure 39 were c = 3.84 tsf and $\emptyset$ = 21.9 deg. The failure envelope was determined by a least-squares best fit of 8 $\tau - \sigma_n$ points.

IC direct shear tests

147. Forty-four IC direct shear tests were made on discontinuous and intact model material specimens. The $\tau - \sigma_n$ plots and Mohr-Coulomb failure envelopes based on a least-squares best fit for tests on smooth cast, even angle, rake tooth, and intact specimens are shown in Figures 40, 41, 42, and 43, respectively. The coefficient of correlation R is given for each plot.

148. Smooth cast specimens. The c and $\emptyset$ values for the Mohr-Coulomb failure envelope shown in Figure 40 were c = 0.0 and $\emptyset$ = 31.4 deg. The failure envelope was determined by a least-squares best fit of 14 $\tau - \sigma_n$ points and forcing the failure envelope through the origin. Without forcing, the c and $\emptyset$ values were c = 0.31 tsf and $\emptyset$ = 29.4 deg.

149. Even angle asperity specimens. The c and $\emptyset$ values for the Mohr-Coulomb failure envelope shown in Figure 41 were c = 2.10 tsf and $\emptyset$ = 30.8 deg. The failure envelope was determined by a least-squares best fit of 13 $\tau - \sigma_n$ points. A visual inspection showed that all asperities shear at their bases.

150. Rake tooth asperity specimens. The c and $\emptyset$ values for the Mohr-Coulomb failure envelope shown in Figure 42 were c = 0.54 tsf and $\emptyset$ = 29.4 deg. The failure envelope was determined by a least-squares best fit of 9 $\tau - \sigma_n$ points. A visual inspection showed that all asperities shear at their bases.

151. Intact specimens. The c and $\emptyset$ values for the Mohr-Coulomb failure envelope shown in Figure 43 were c = 2.79 tsf and $\emptyset$ = 25.3 deg. The failure envelope was determined by a least-squares best fit of 8 $\tau - \sigma_n$ points.

3- by 3-in. direct shear tests

152. Eighteen 3- by 3-in. direct shear tests were made on smooth cast discontinuous and intact model material specimens. The $\tau - \sigma_n$ plots and Mohr-Coulomb failure envelopes based on a least-squares best fit for tests on the smooth cast and intact specimens are shown in Figures 44 and 45, respectively. The coefficient of correlation R is given for both plots.

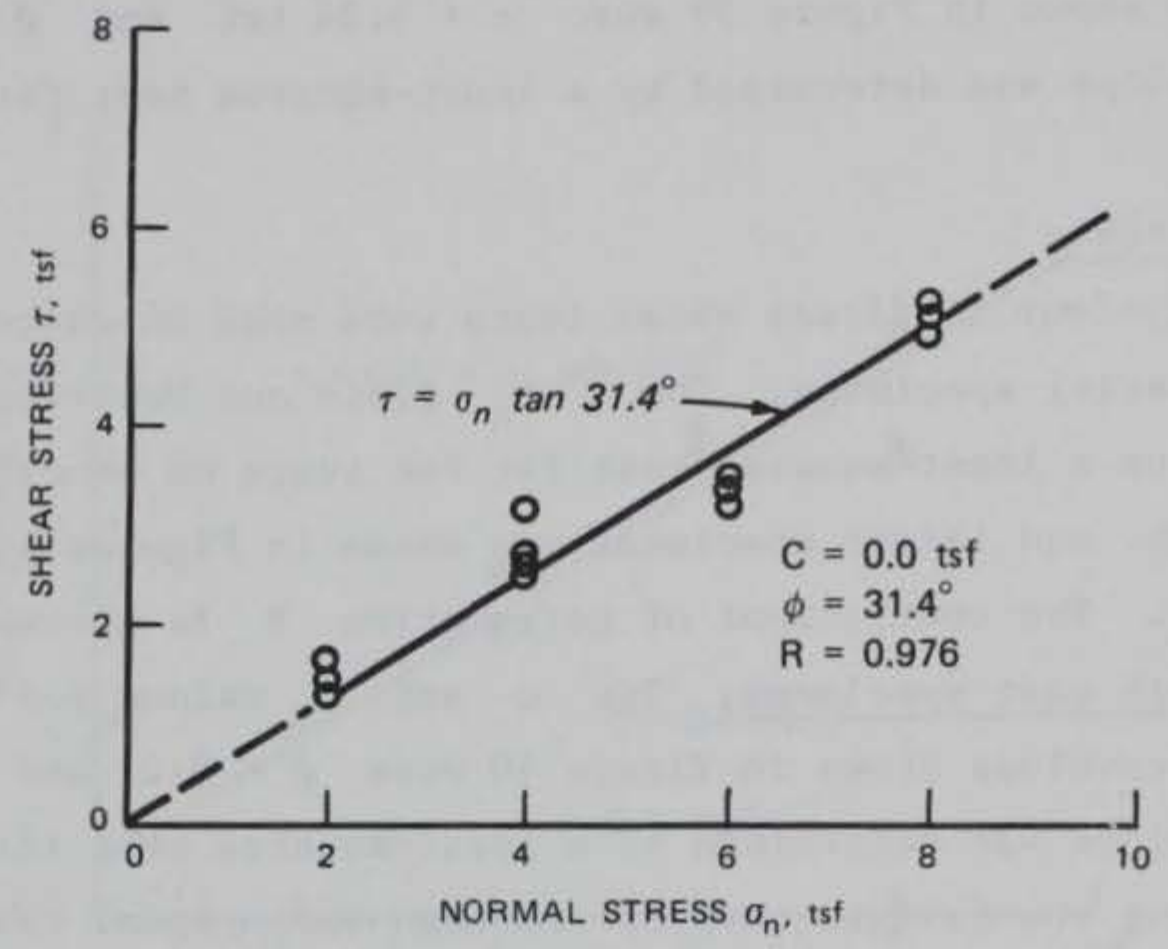

Figure 40. IC direct shear test results for model material smooth cast specimens

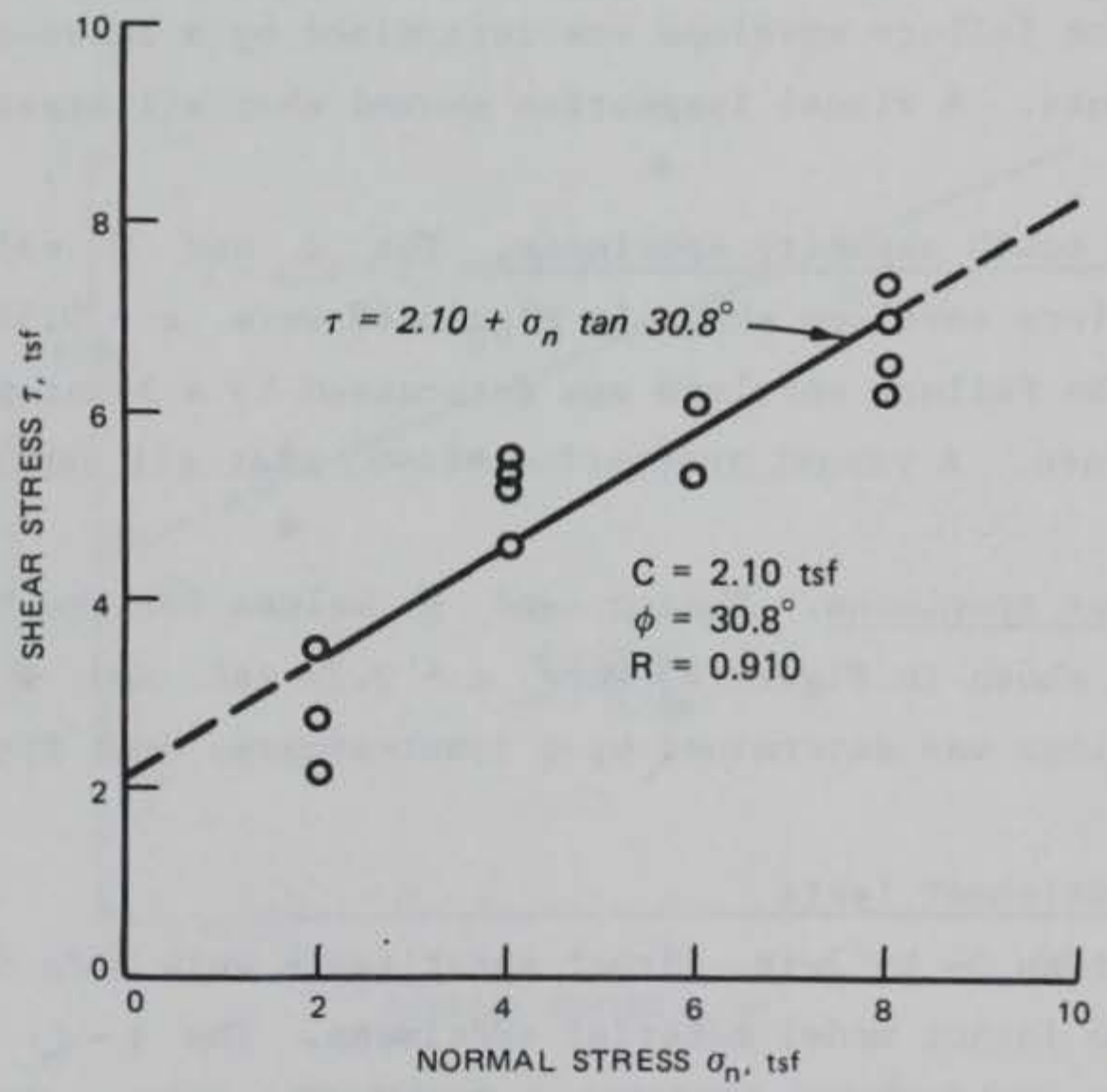

Figure 41. IC direct shear test results for model material even angle asperity specimens

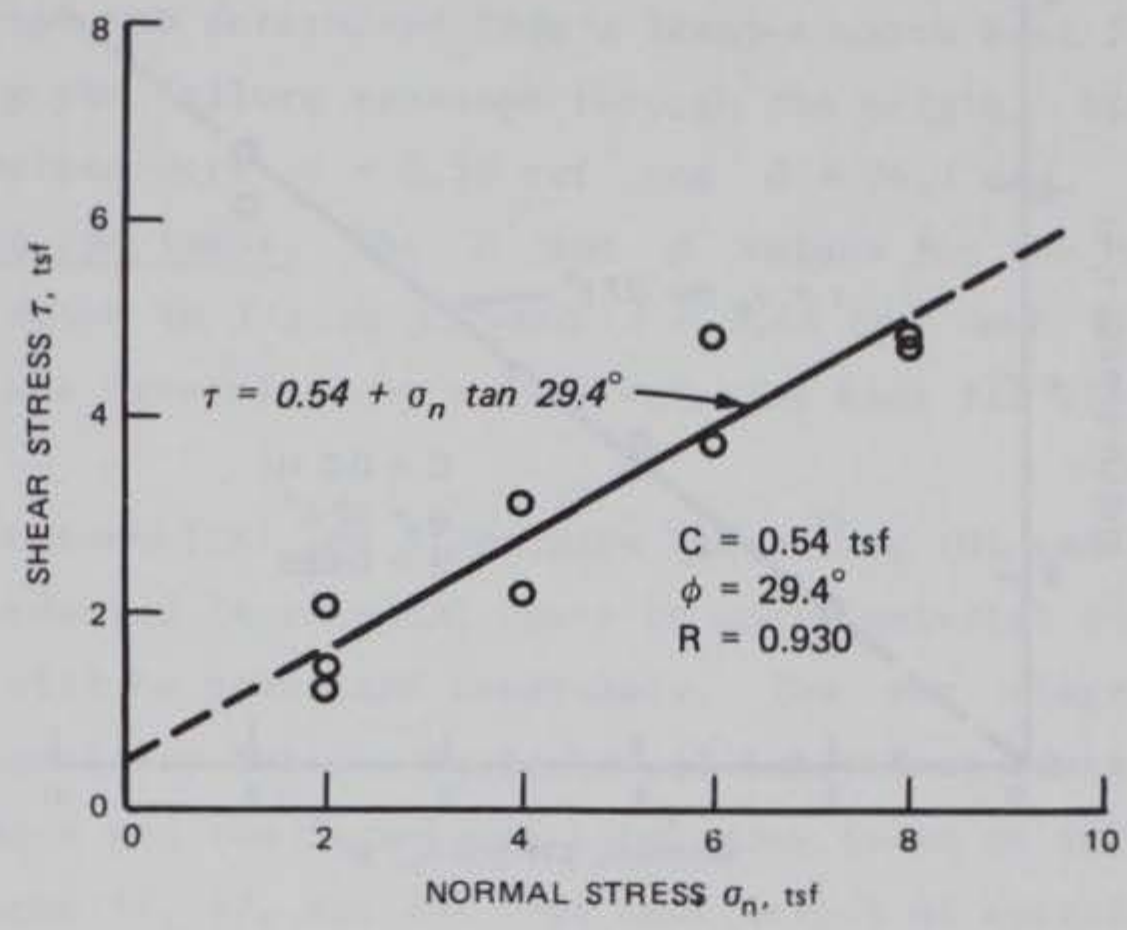

Figure 42. IC direct shear test results for model material rake tooth asperity specimens

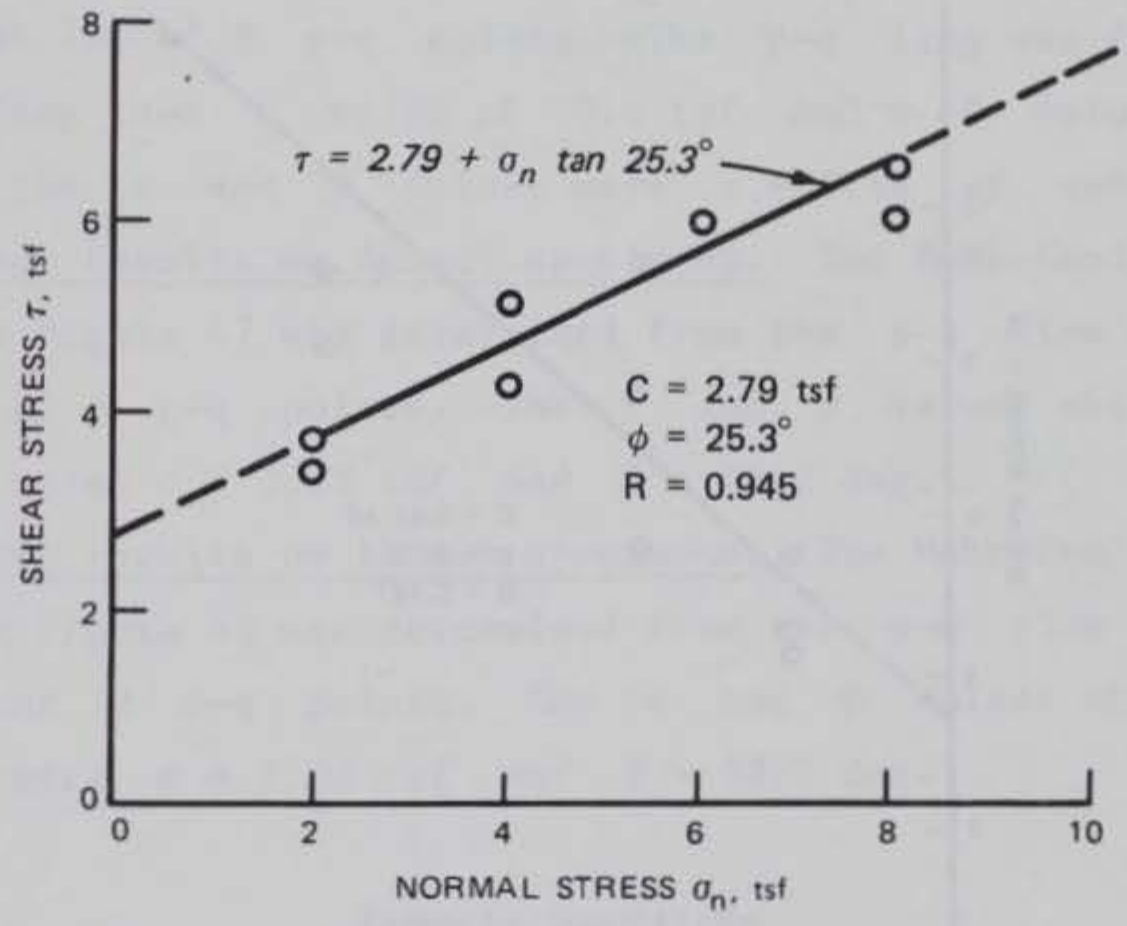

Figure 43. IC direct shear test results for model material intact specimens

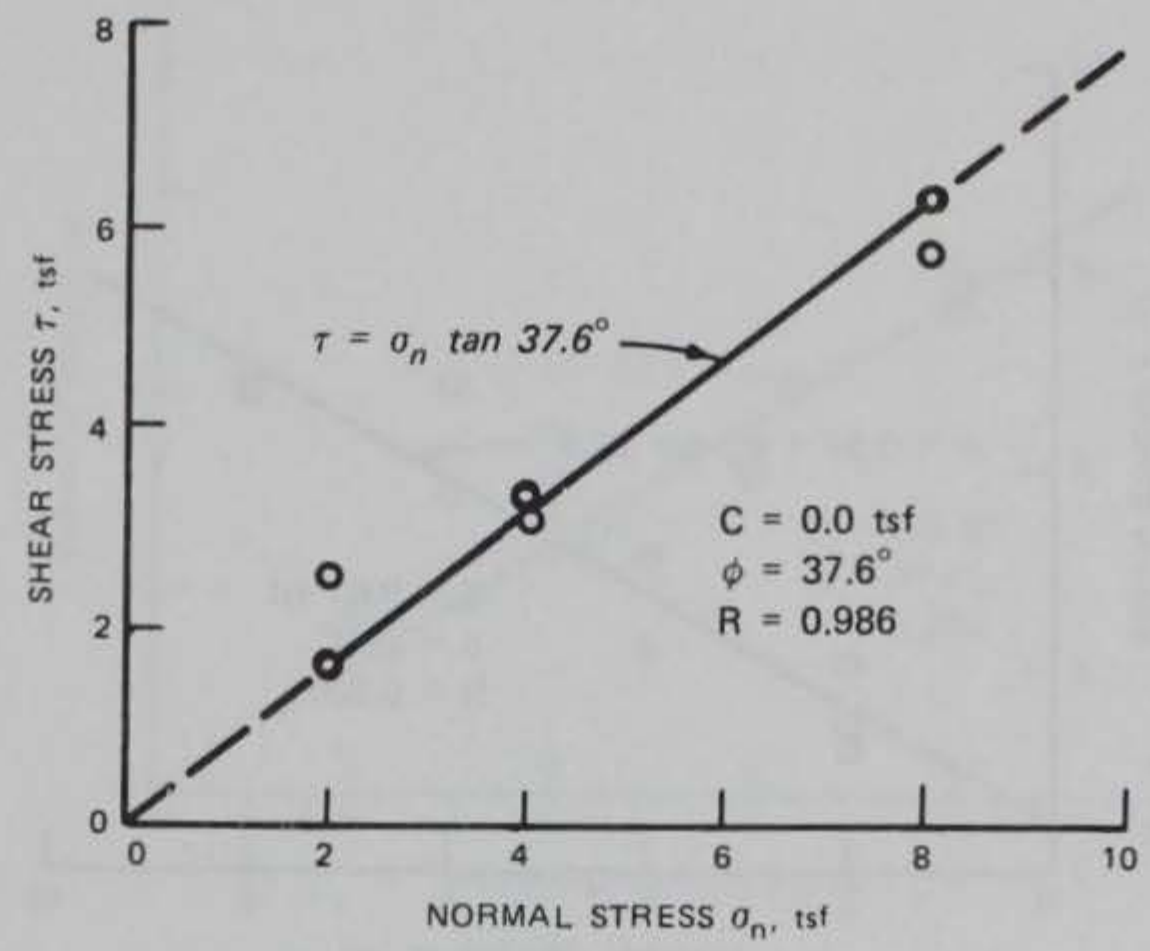

Figure 44. Three- by three-inch direct shear tests on model material smooth cast specimens

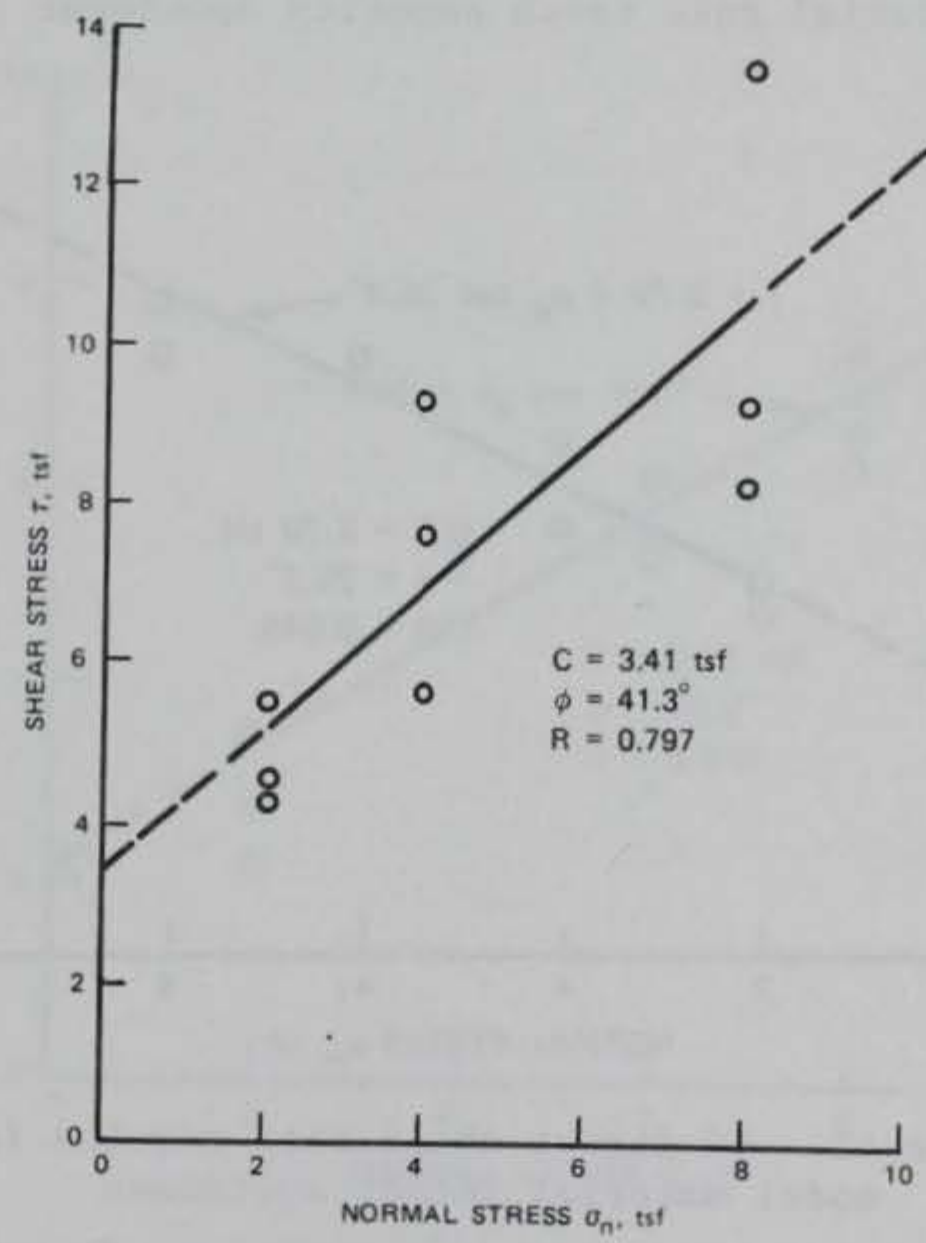

Figure 45. Three- by three-inch direct shear tests on model material intact specimens

153. Smooth cast specimens. The c and ϕ values for the Mohr-Coulomb failure envelope shown in Figure 44 were c = 0.0 and ϕ = 37.6 deg. The failure envelope was determined from a least-squares best fit of 9 $\tau - \sigma_n$ points and forcing the failure envelope through the origin. Wihtout forcing, the c and ϕ values were c = 0.50 tsf and ϕ = 34.7 deg.

154. Intact specimens. The c and ϕ values for the Mohr-Coulomb failure envelope shown in Figure 45 were c = 3.41 tsf and ϕ = 41.3 deg. The failure envelope was determined by a least-squares best fit of 9 $\tau - \sigma_n$ points.

Triaxial tests

155. The Geotechnical and Structures Laboratory (GL and SL, respectively) at WES conducted 24 triaxial tests on model material specimens. Each set of test data will be presented separately. The p-q diagrams and Mohr-Coulomb failure envelopes for the Geotechnical Laboratory tests on smooth cast and intact specimens and the Structures Laboratory tests on intact specimens are shown in Figures 46, 47, and 48. The coefficient of correlation R is given for each plot.

156. GL test results on smooth cast specimens. The Mohr-Coulomb failure envelope shown in Figure 46 was determined from the p-q line of least-squares best fit of 6 p-q points. The p-q line was forced through the origin resulting in a c value of 0.0 tsf and a ϕ value of 35.4 deg. Without forcing, the c and ϕ values were c = 0.44 tsf and ϕ = 37.0 deg.

157. GL test results on intact specimens. The Mohr-Coulomb failure envelope shown in Figure 47 was determined from the p-q line of least-squares best fit of 6 p-q points. The c and ϕ values obtained from the failure envelope were c = 3.28 tsf and ϕ = 43.2 deg.

158. SL test results on intact specimens. The Mohr-Coulomb failure envelope shown in Figure 48 was determined from the p-q line of least-squares best fit of 12 p-q points. The c and ϕ values obtained from the failure envelope were c = 1.02 tsf and ϕ = 58.2 deg.

Rangely Sandstone

In situ direct shear tests on natural joint specimens

159. The initial intent was to conduct one single-staged direct shear test on each of the three specimens recovered in the field. However, the

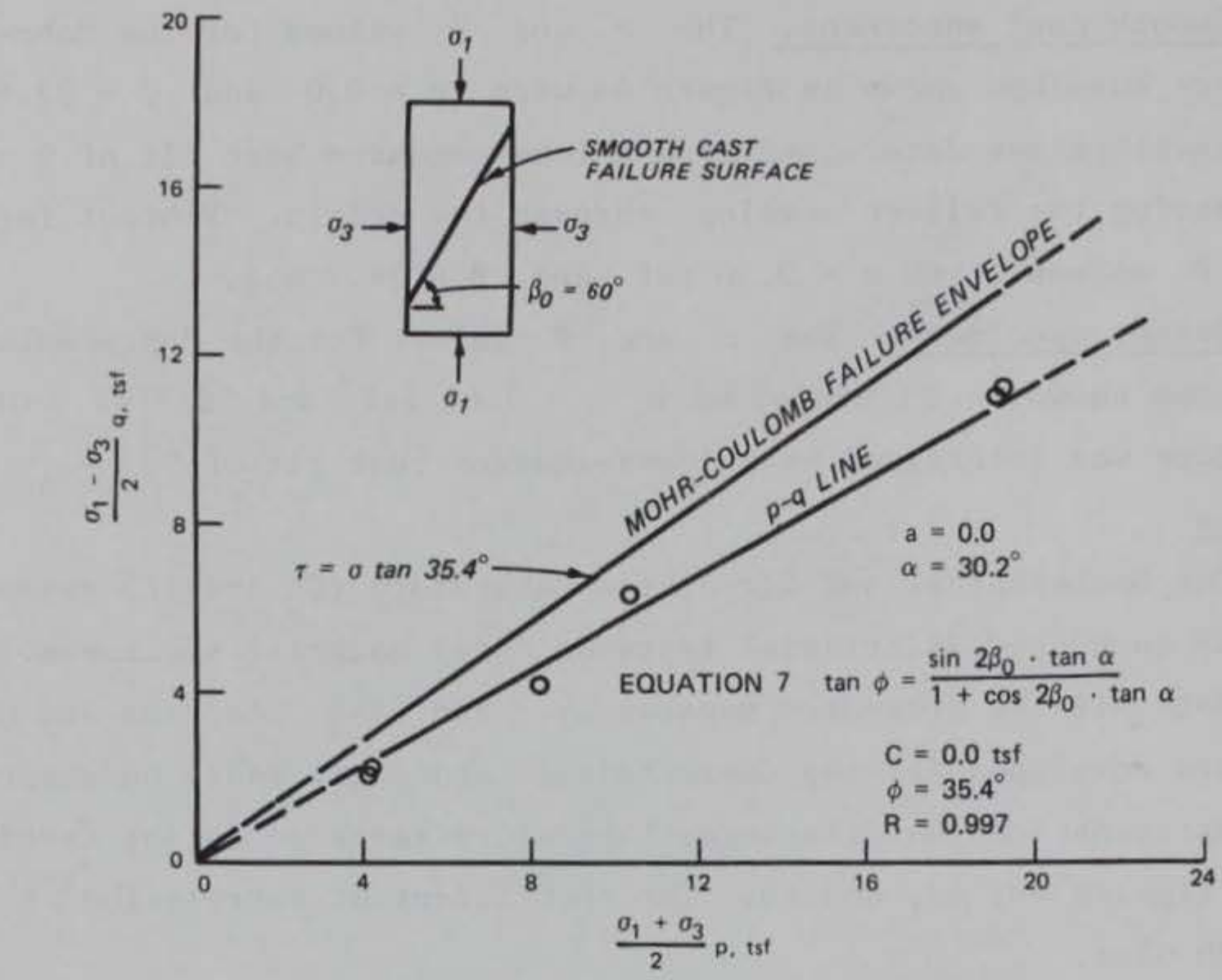

Figure 46. GL triaxial test results for model material smooth cast specimens

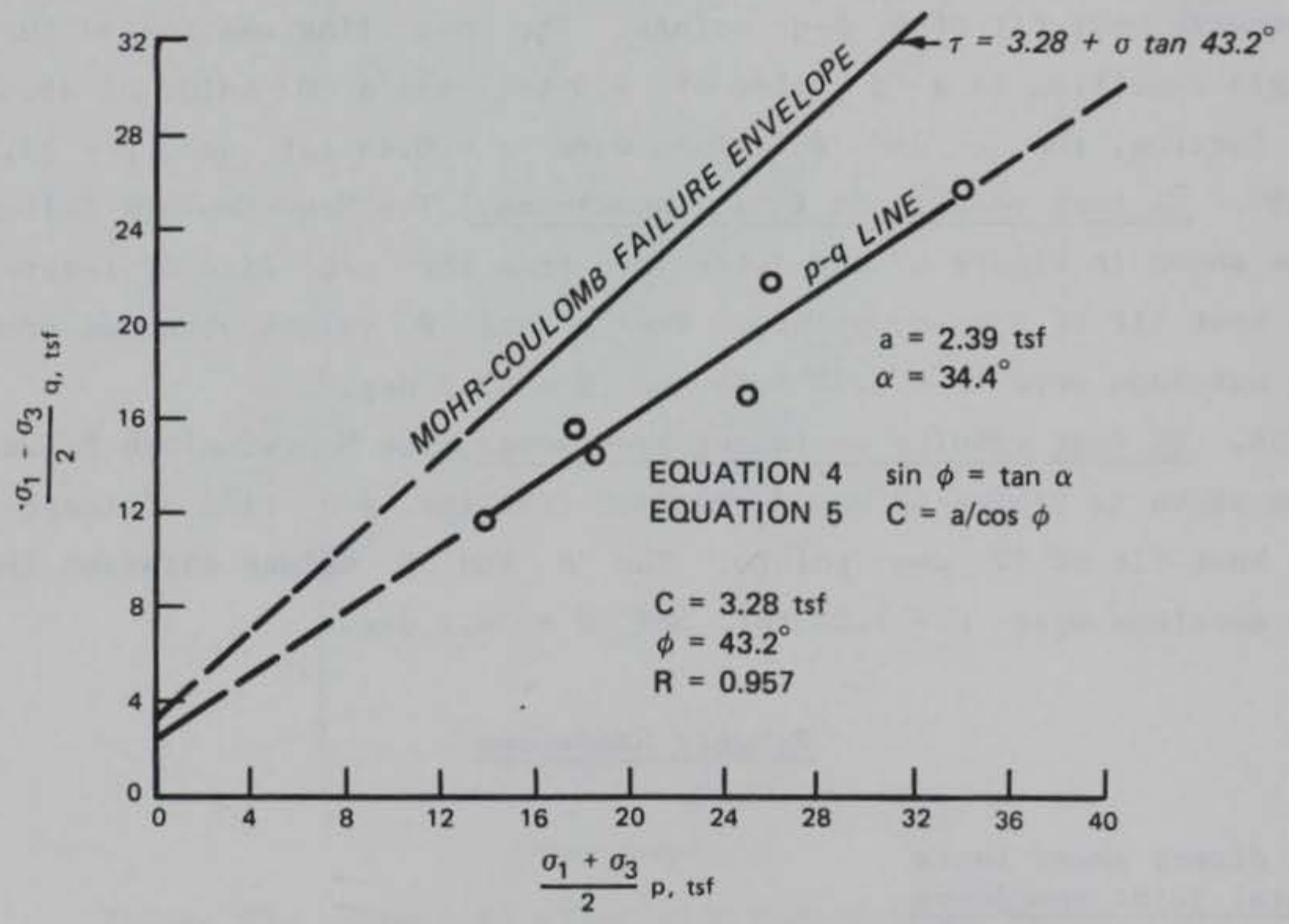

Figure 47. GL triaxial test results for model material intact specimens

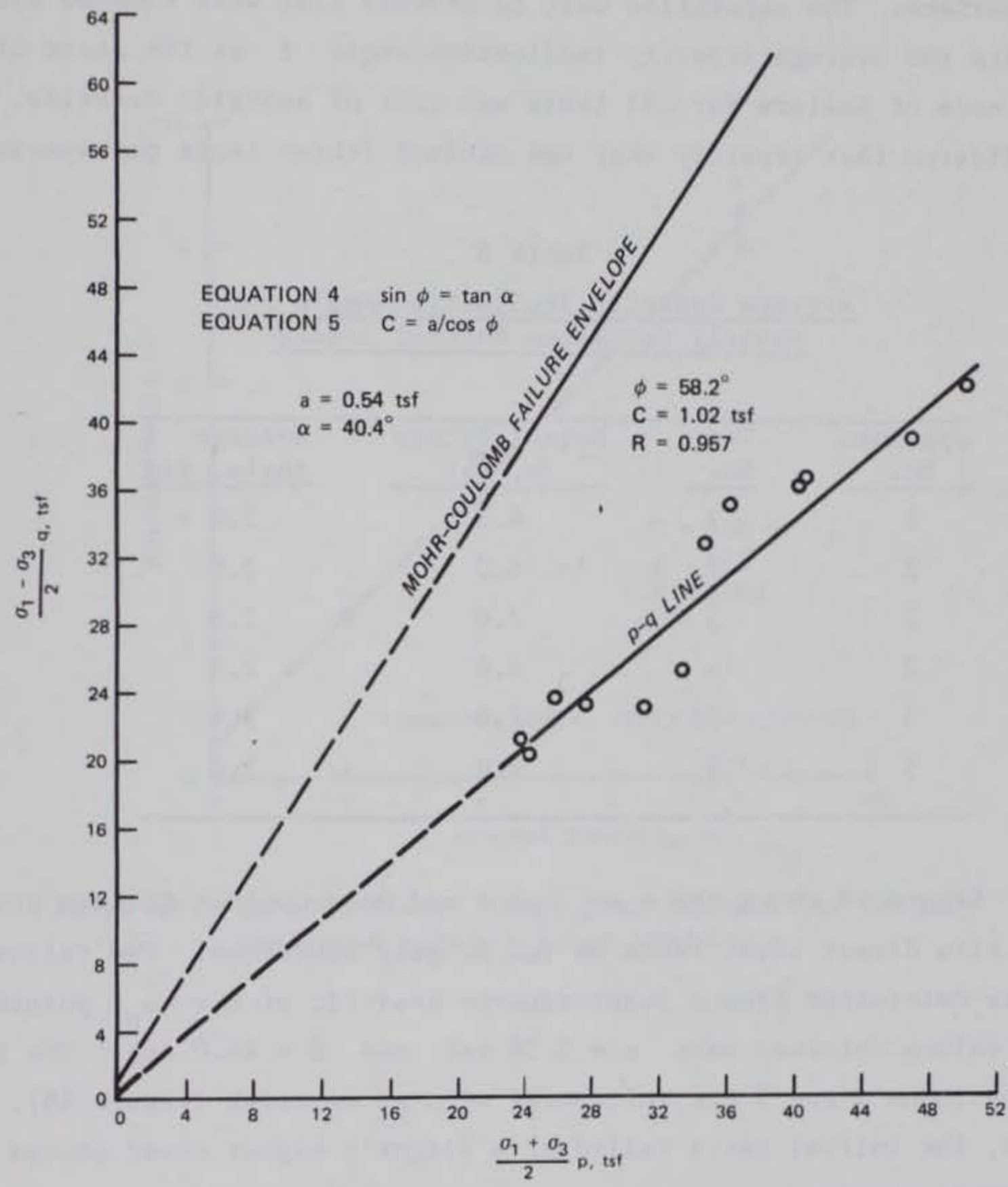

Figure 48. SL triaxial test results for model material intact specimens

first specimen was damaged prior to testing and three staged shear tests were conducted on each of the remaining two specimens.

160. Before each shear cycle, an asperity profile was made along three lines parallel to the direction of shear and located at the 1/4 points across the shear surface. The asperities were relatively flat with rounded apexes. Table 8 lists the average asperity inclination angle i at the start of each test. The mode of failure for all tests was that of asperity override. Table 8 indicates that asperity wear was minimal (three tests per specimen).

Table 8

Average Asperity Inclination Angle for Rangely Sandstone Natural Joints

Specimen No.	Test No.	Normal Stress σ_n, tsf	Average i Angle, deg
2	1	4.0	3.0
2	2	8.0	2.9
2	3	2.0	2.8
3	4	8.0	2.9
3	5	2.0	2.9
3	6	4.0	2.6

161. Figure 49 shows the $\tau - \sigma_n$ plot and Mohr-Coulomb failure envelope for the in situ direct shear tests on the Rangely sandstone. The failure envelope was determined from a least-squares best fit of 6 $\tau - \sigma_n$ points. The c and ϕ values obtained were c = 0.56 tsf and ϕ = 44.0 deg. The initial tests on specimens 2 and 3 are referenced with an asterisk (Figure 49). As can be seen, the initial tests failed at a slightly higher shear stress than the multistaged tests.

KC direct shear tests on natural joint specimens

162. Six KC direct shear tests were conducted on Rangely sandstone 6-in.-diam specimens with a natural joint transversing the vertical axis. The direction of shear was the same with respect to actual field orientation as the in situ direct shear tests discussed in paragraphs above.

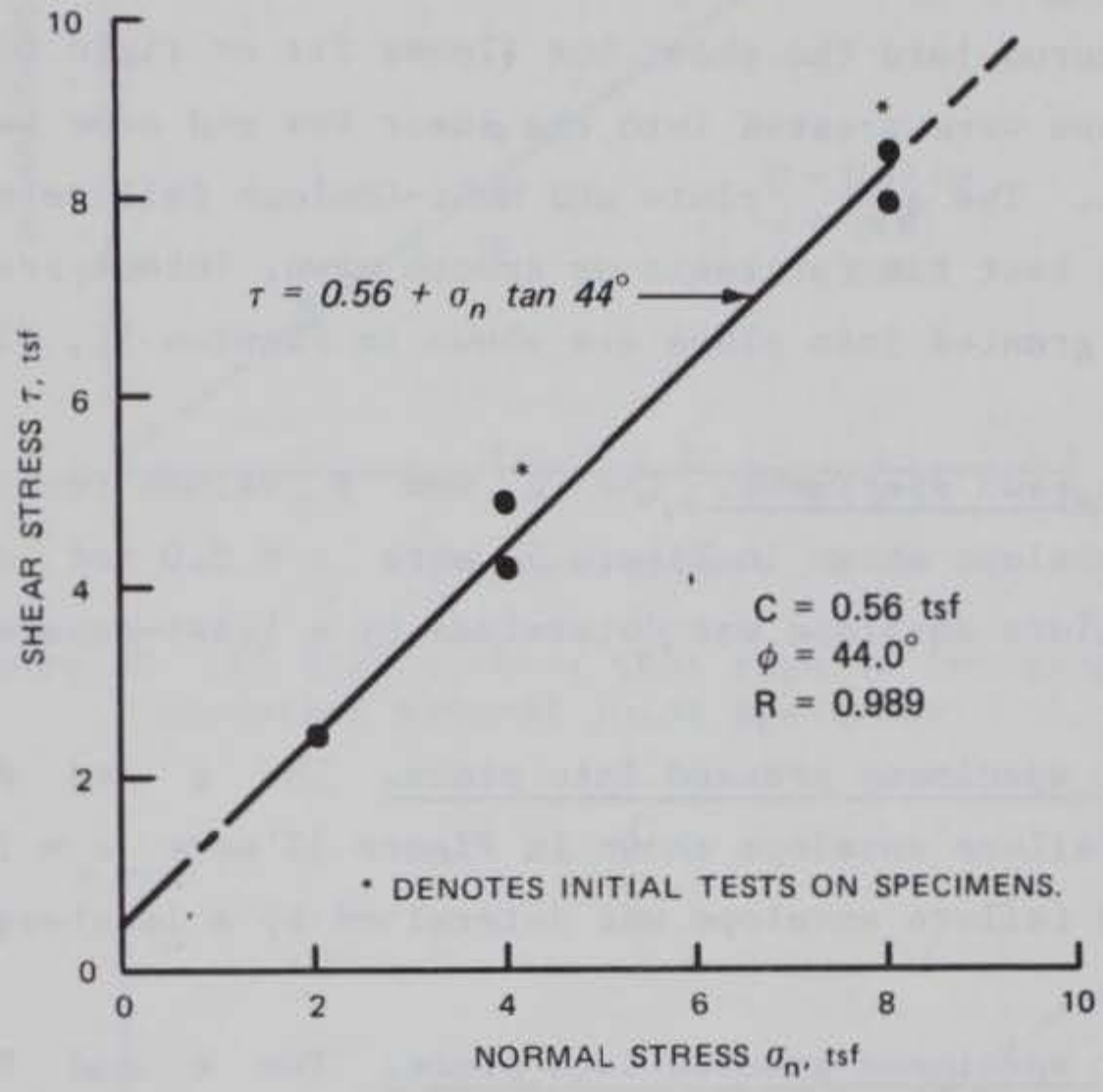

Figure 49. In situ direct shear test results for Rangely sandstone natural joint specimens

163. Figure 50 shows the $\tau - \sigma_n$ plot and Mohr-Coulomb failure envelope for the KC direct shear tests on the Rangely sandstone. The failure envelope was determined from a least-squares best fit of 6 $\tau - \sigma_n$ points. The c and ϕ values obtained were c = 0.07 tsf and ϕ = 36.9 deg.

3- by 3-in. direct shear tests

164. Fifteen 3- by 3-in. direct shear tests were conducted on smooth sawn and intact Rangely sandstone specimens. To study the effects of how the specimens were secured into the shear box (loose fit or rigid fit), some of the intact specimens were pressed into the shear box and some were grouted into the shear box. The $\tau - \sigma_n$ plots and Mohr-Coulomb failure envelopes based on a least-squares best fit for tests on smooth sawn, intact pressed into place, and intact grouted into place are shown in Figures 51, 52, and 53, respectively.

165. Smooth sawn specimens. The c and ϕ values for the Mohr-Coulomb failure envelope shown in Figure 51 were c = 0.0 tsf and ϕ = 32.6 deg. The failure envelope was determined by a least-squares best fit of 6 $\tau - \sigma_n$ points.

166. Intact specimens pressed into place. The c and ϕ values for the Mohr-Coulomb failure envelope shown in Figure 52 were c = 10.83 tsf and ϕ = 46.0 deg. The failure envelope was determined by a least-squares best fit of 6 $\tau - \sigma_n$ points.

167. Intact specimens grouted into place. The c and ϕ values for the Mohr-Coulomb failure envelope shown in Figure 53 were c = 4.68 tsf and ϕ = 57.4 deg. The failure envelope was determined by a least-squares best fit of 3 $\tau - \sigma_n$ points.

Terra Tek shear test results

168. Terra Tek (Swolfs, 1977) conducted two in situ staged shear tests with normal stresses of 7.31 and 14.62 tsf on a Rangely sandstone natural joint specimen. The test results, as applicable to this study, were inconclusive since neither test was sheared to a peak shear stress. However, shear stresses approximately equal to the normal stresses were just sufficient to cause shear deformations to occur. The state of stresses where shear stress and normal stress are equal can be defined by a 45-deg line in τ versus σ_n space. The only conclusion that can be made from these tests is that the actual envelope defining the state of stresses at peak failure will have a ϕ value at least equal to and no doubt greater than 45 deg.

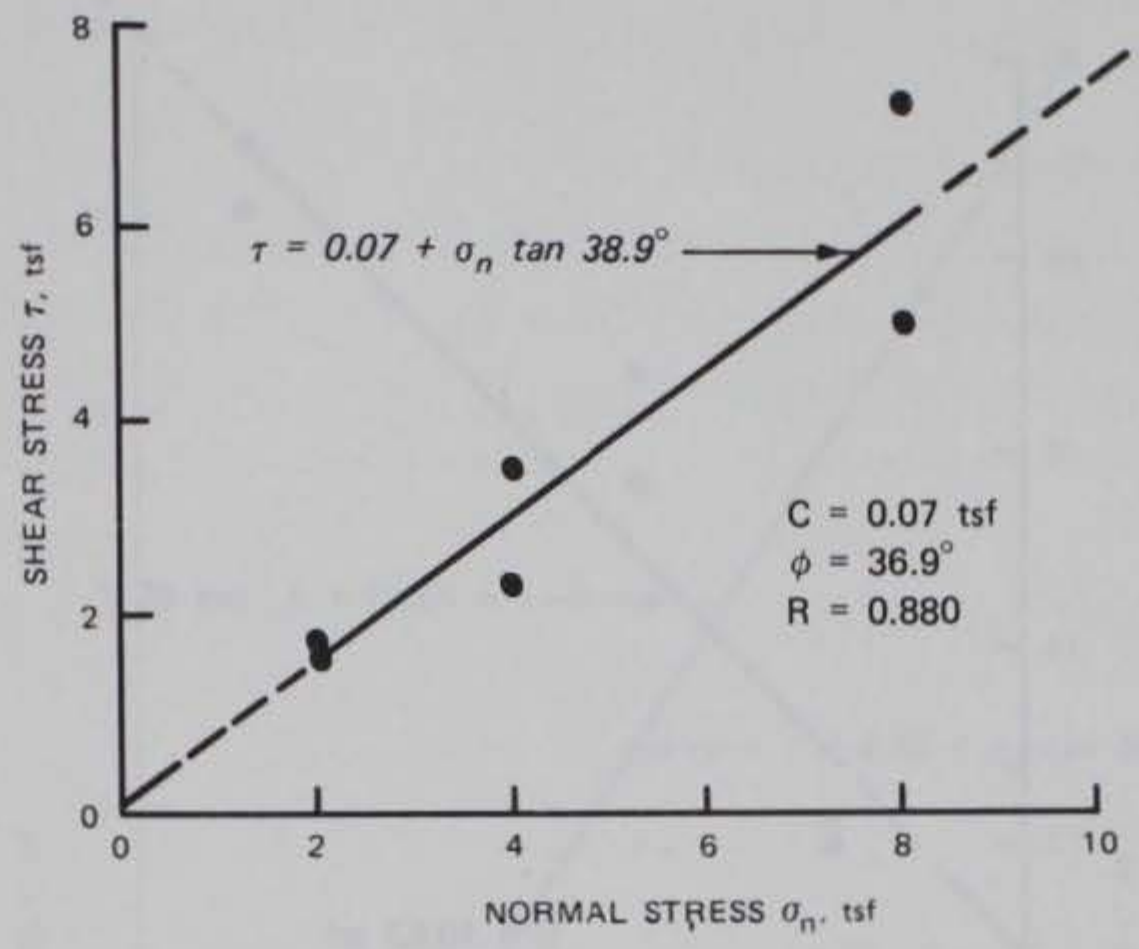

Figure 50. KC direct shear test results for Rangely sandstone natural joint specimens

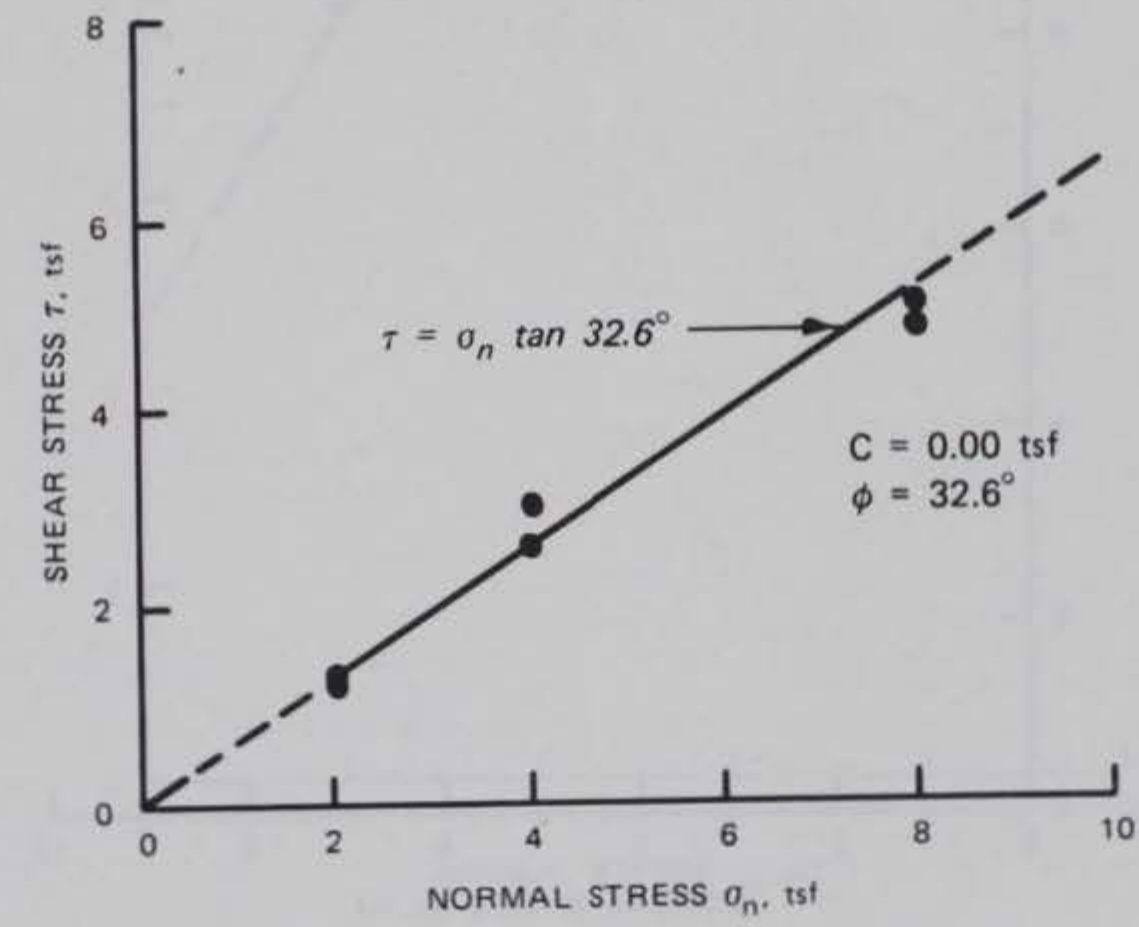

Figure 51. Three- by three-inch direct shear test results for smooth sawn Rangely sandstone specimens

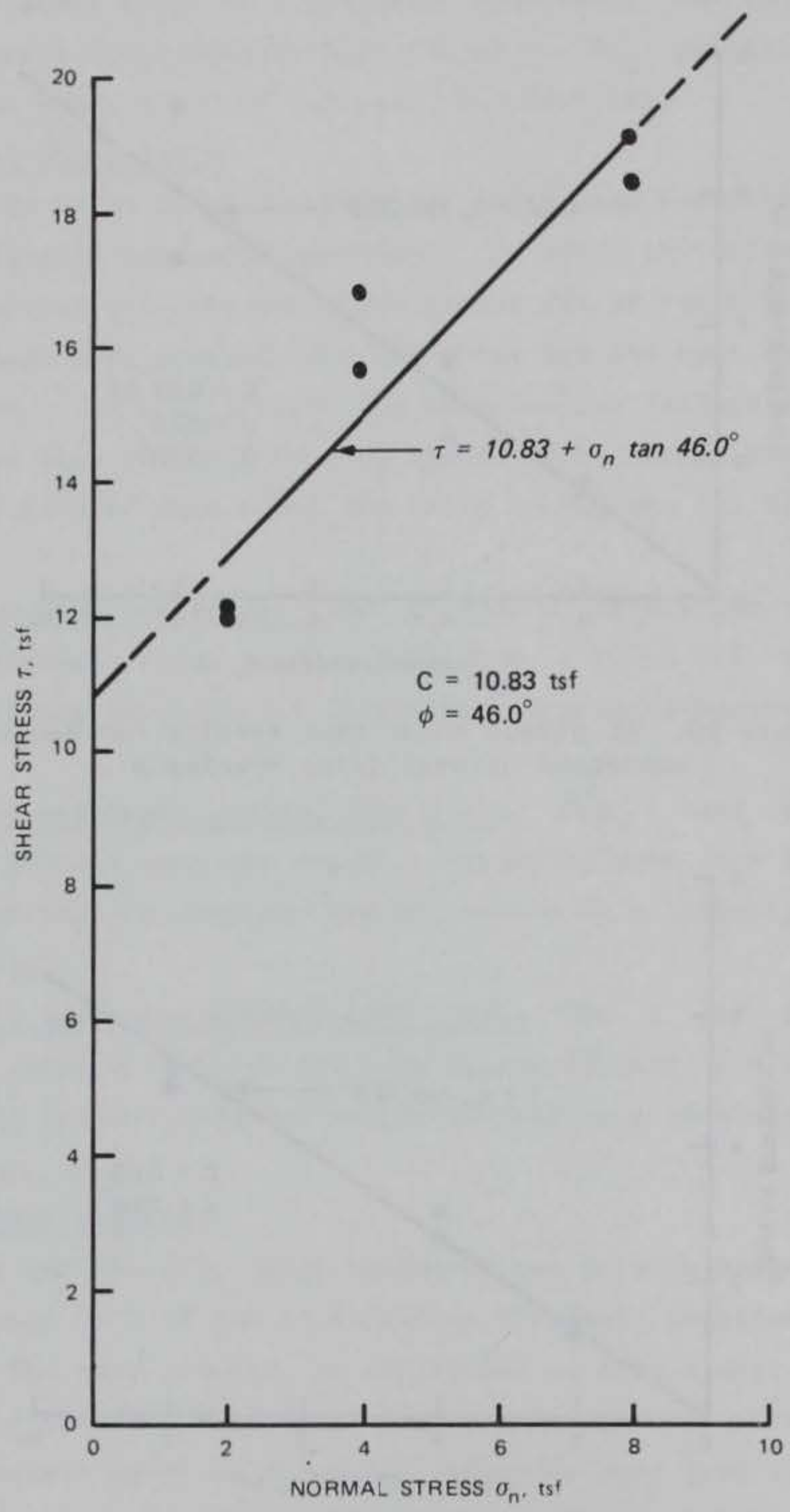

Figure 52. Three- by three-inch direct shear test results for intact Rangely sandstone specimens pressed into shear box

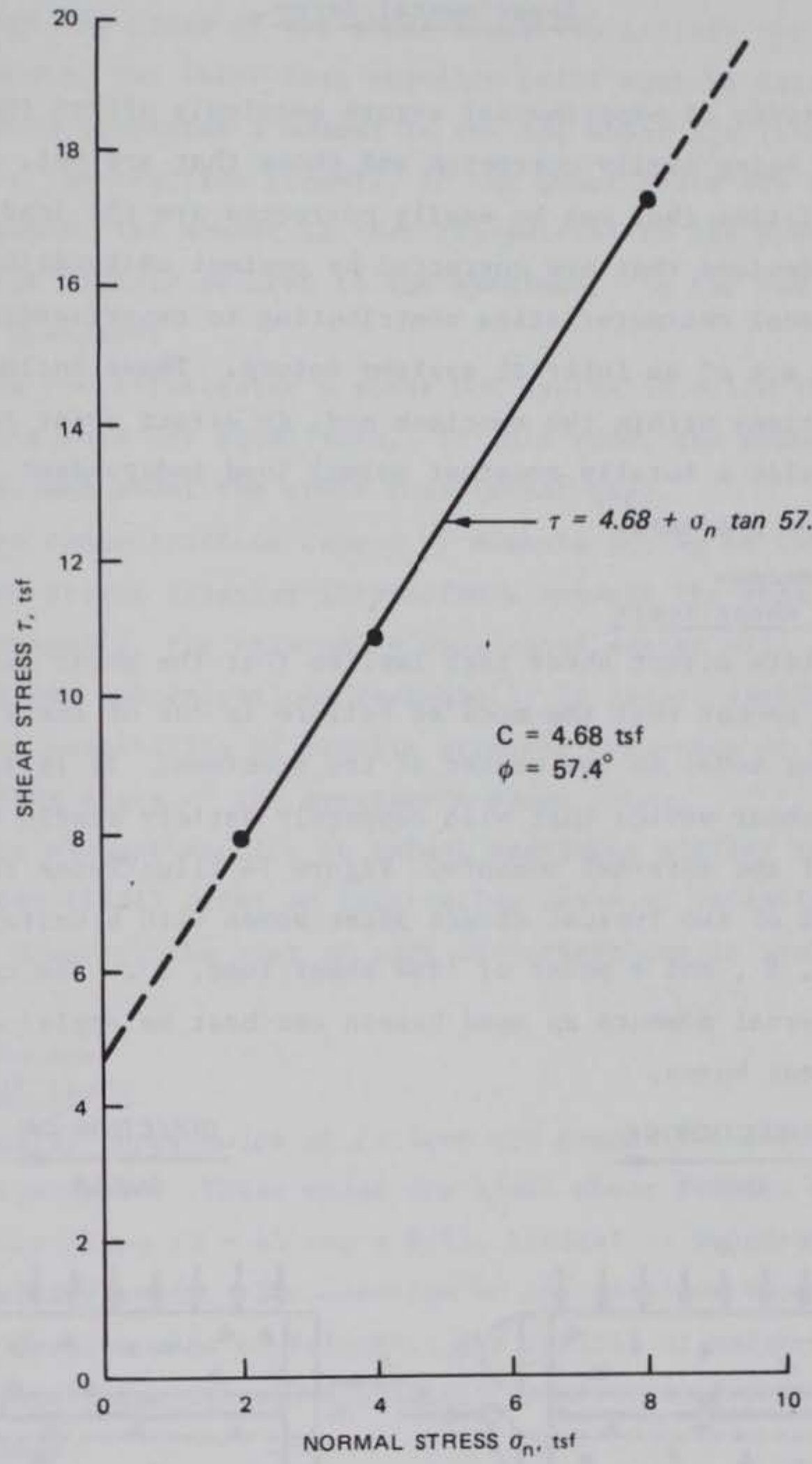

Figure 53. Three- by three-inch direct shear test results for intact Rangely sandstone specimens grouted into shear box

PART VIII: COMPARISON AND DISCUSSION OF TEST RESULTS

Experimental Error

169. Two types of experimental errors seemingly affect the test results: those capable of being easily corrected and those that are not. The operational characteristics that can be easily corrected are the load and displacement monitoring devices that are corrected by pretest calibrations of the system. Operational characteristics contributing to experimental errors not easily corrected are of an internal systems nature. These include adverse stress concentrations within the specimen and, in direct shear tests, the inability to provide a totally constant normal load independent of dilation or compression of the specimen.

Adverse stress concentrations, direct shear tests

170. The term direct shear test implies that the shear test is conducted in such a manner that the mode of failure is one of shear through a narrow zone (shear zone) in the center of the specimen. It is impossible to design a direct shear device that will competely satisfy static equilibrium for both internal and external moments. Figure 54 illustrates the basic design schematics of two typical direct shear boxes with a uniformly distributed normal load, N , and a point or line shear load, S . The concept of internal and external moments as used herein can best be explained by examining the two shear boxes.

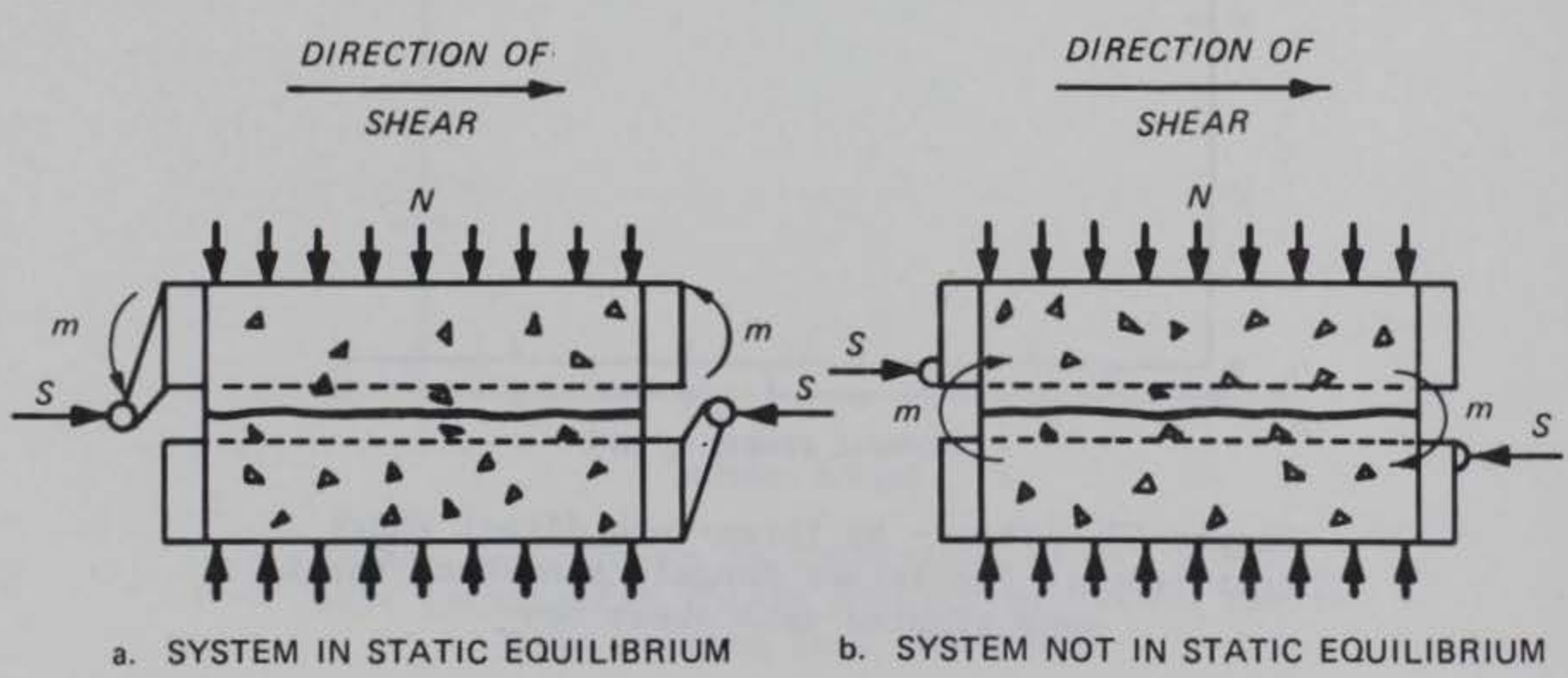

Figure 54. Schematic of typical direct shear devices

171. Figure 54a illustrates a shear box system in static equilibrium (Σ forces = 0 and Σ moments = 0) with the line of action of the shear force, S , passing through the plane of the shear zone. To satisfy the condition of zero external moments, the shear load reaction point must be cantilevered, as shown, which in turn generates a moment in the top shear box (the bottom is generally fixed by the reaction frame). If the shear boxes are rigidly secured to the specimen, the moment is then transmitted to the specimen. If the shear boxes are not rigidly secured to the specimen, the top box will tend to rotate about the specimen.

172. Figure 54b illustrates a shear box system in which the summation of external moments does not equal zero. In this case, the moment acts directly on the specimen about the shear zone (shear gap).

173. Stress concentrations caused by moments acting on the specimen are dependent upon the stress transfer interactions between the shear boxes and the specimen. Generally, the externally unbalanced system will generate more severe adverse stress concentrations (especially in intact specimens) because there is a greater possibility of tensile stresses occurring at both the trailing and leading edges of the specimen's shear zone.

174. Finite element studies on intact specimens similar to the one conducted by Kutter (1971) offer an interesting means of investigating stress concentrations. However, the cost of such investigations is prohibitive for routine testing.

Adverse stress concentrations, triaxial tests

175. Basically three modes of failure are commonly observed in triaxial tests on intact specimens. These modes are ideal shear failure along the theoretical failure plane (β = 45 deg + $\phi/2$), conical or wedge-shaped fragment failure, and axial splitting. The creation of the ideal or theoretical failure plane is the desired mode of failure. The conical or wedge-shaped fragment and axial splitting modes are attributed to adverse stress concentrations at the specimen ends.

176. Friction between the ends of the specimen and the rigid end caps restricts lateral deformation adjacent to these surfaces. This leads to a departure from the condition of uniform stress and strain. The effect of lateral restraint is often to initiate failure at the circumferential contact between the specimen and the rigid end caps at a value of load less than that

corresponding to the true strength of the specimen. This gives rise to the conical fragments sometimes observed.

177. Axial splitting of intact triaxial specimens is caused by radial tensile stress concentrations. Tensile stresses may be generated by material inserted between the specimen and end caps to reduce friction, irregular imperfections at the specimen ends, or eccentrically applied axial loads.

178. Triaxial friction tests on predeveloped failure planes, such as the smooth cast specimen tests presented herein, are also subject to stress concentrations. If β is near 90 deg or smaller than about 20 deg, the state of stress within the specimen may become tangent to the Mohr failure envelope of the intact rock (fail as an intact specimen) before the joint can slip. Also, the results of such a test can be useful only if the specimen is free to slide along the joint without frictional restraint from the ends. Rosengren (1968) showed that friction at the specimen ends adds new stress contributions on the joint. The effect of such a contribution is a tendency to decrease the apparent strength of the material.

Direct shear constant normal load

179. Shear stress is not only normal-stress dependent, but is also dependent upon total displacement. Generally, the higher the normal load, the smaller the shear displacement required for failure. Therefore, shear displacements at failure are dependent upon normal stress and material type. The interrelationship between shear stress, shear displacement, and normal stress dictates the need for a constant normal load system.

180. A direct shear device that will provide a constant normal load, independent of dilation or compression of the specimen during shear, is difficult to design. All of the direct shear devices investigated for this study, except the in situ direct shear device, used a hydraulic ram or jack to apply the normal load. A constant normal load was achieved by manually maintaining a constant hydraulic pressure, or by externally adjusting the hydraulic pressure required to generate a preselected normal load. Both methods have certain features which are undesirable.

181. Maintaining a constant hydraulic pressure does not necessarily guarantee a constant normal load. Hydraulic ram friction can be significant. Calibrations of load cells during the initial debugging of the in situ direct shear tests at the Eddy Bridge site, Fort Benning, Ga., indicated that ram friction could be as much as 10 to 12 percent of the total load generated by

hydraulic fluid pressure. At the Eddy Bridge site two hydraulic jacks fitted with load cells used for applying the normal load were placed face to face in a reaction frame and jacked against each other. It was found that ram friction, as determined by the difference between the total applied force (ram area times driving fluid pressure) and the measured force acting on the load cells varied with ram displacement, ram displacement rate, and magnitude of driving fluid pressure (less friction at higher pressures). Ram friction also varied between calibrations. In general, ram friction was not a constant factor that could be incorporated into shear data corrections. For this reason, test results from shear devices such as the ORD and IC devices which monitor normal loads (IC devices also monitor shear load) by measuring just fluid pressure should be used with caution.

182. Shear devices which incorporate constant normal load capabilities by externally manipulating hydraulic fluid pressures have a delay between the time a change in load is detected and adjustments to fluid pressures are made. The KC device investigated in this study used this method to maintain constant normal load. The delay between detection and correction can be critical, particularly when testing soft discontinuous specimens with asperities. A small increase in normal stress may change the mode of failure from overriding of asperities to shear through asperities.

Comparison of Test Results on Model Material

Direct and triaxial shear test results on smooth cast specimens

183. Figure 55 shows the Mohr-Coulomb failure envelopes from the direct and triaxial shear test results on smooth cast discontinuous specimens. The failure envelopes indicate a range in ϕ values from 38.5 to 28.2 deg (a spread of 10.3 deg). This relatively large spread in ϕ values is surprising because the results of the series of tests on smooth cast specimens should have been the most uniform since the absence of asperities minimizes scale effects and effects of cohesion. The spread in friction values can best be attributed to differences in operational characteristics of the devices.

184. The failure envelopes seem to fall into two distinct groups. The envelopes from the in situ, 3- by 3-in., and triaxial tests formed the upper boundary of ϕ values with a spread of 3.1 deg. Envelopes from the IC, KC,

TYPE OF TEST	ϕ , DEG	R
IN SITU	38.5	0.994
3"x 3"	37.6	0.986
TRIAXIAL	35.4	0.997
IC	31.4	0.976
KC	29.0	0.998
ORD	28.2	0.948

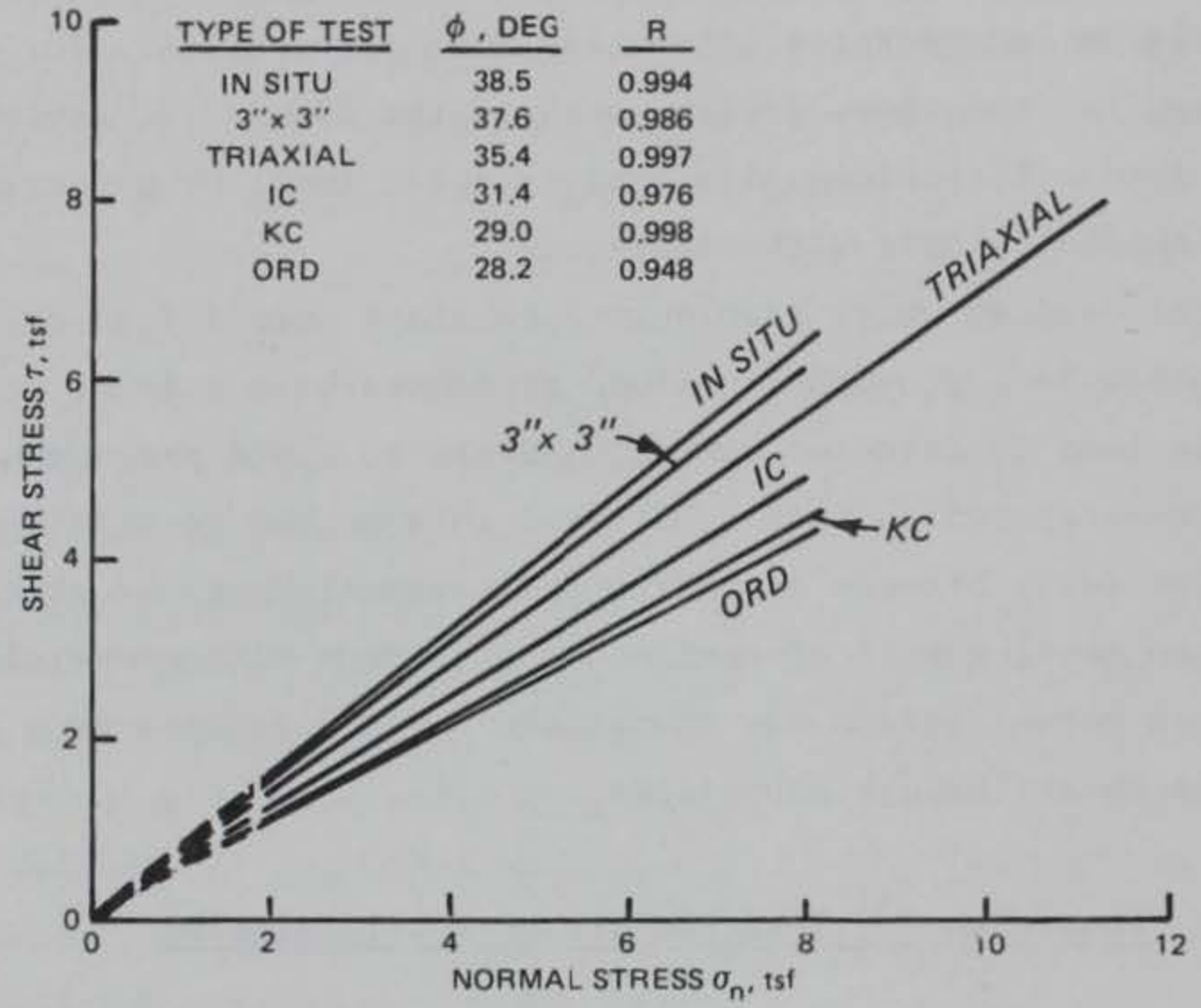

Figure 55. Comparison of direct and triaxial shear test results on model material smooth cast specimens

and ORD direct shear devices formed the lower boundary of ϕ values with a spread of 3.0 deg. The real problem at hand is to decide which envelope represents the true frictional strength of the material. Rosenblad (1971) reported a ϕ value of 41 deg based on direct and triaxial shear tests of smooth cast specimens for his model material. Rosenblad's (1971) model material was almost identical to the model material tested herein except that the sand was slightly more angular and contained approximately 5 percent less fine filler material. Based on the composition of the two model materials, one would expect a slightly lower ϕ value for the model material used in this study compared to Rosenblad's (1971) model material. The results from the in situ direct shear device appear to generate the most realistic failure envelope with a ϕ value of 38.5 deg. The 3- by 3-in. direct shear device, which has basically the same operational characteristics as the in situ device, generated almost the same envelope as the in situ device with less than 1 deg (0.9 deg) difference in the ϕ value. Although the ϕ value from the triaxial tests was the lowest of the upper boundary group, it also compared favorably with the in situ shear results. The lower triaxial ϕ value can be attributed to the end restraint effects previously discussed.

185. The 6-in.-diam rock core direct shear devices each have particular operational characteristics that are not desirable. The KC device generates an external moment and the IC and ORD devices monitor normal loads by measuring hyraulic fluid pressure. It is interesting to note that this group of devices generate ϕ values comparable to one another but 7 to 10 deg lower than the in situ shear ϕ value. If the IC and ORD normal stresses used in the $\tau - \sigma_n$ plots could be corrected for ram friction, the trend would be to shift normal stress values to the left and thereby increase the ϕ value. The effects of an external moment on the specimen in the KC device are difficult to determine. Such a moment would cause a nonuniform normal stress distribution across the face of the shear surface that becomes more severe with increasing shear loads.

Direct shear tests results
on even angle asperity specimens

186. The even angle asperity specimens were incorporated into the testing program to investigate the effect of asperity override as well as shear. The combination of failure modes (override and shear) over an interval of normal stress sufficient to define the two modes will generate a nonlinear

failure envelope. The $\tau - \sigma_n$ plots for the in situ, ORD, KC, and IC tests shown in Figures 27, 33, 37, and 41 indicate the $\tau - \sigma_n$ plots for the ORD and KC devices seem to be relatively linear while the $\tau - \sigma_n$ plots for the IC device and perhaps the in situ device can be fitted with a nonlinear relationship. It is of interest to note that the in situ and IC devices were the only two devices designed with built-in "soft" normal load systems.

187. Mohr-Coulomb failure envelopes. Figure 56 shows a comparison of the Mohr-Coulomb failure envelopes. Although the in situ and IC test results could be more realistically fitted with a curvilinear or bilinear relationship, they are shown here to illustrate the spread in c and ϕ values based on linear fits. The c values ranged from 0.72 to 2.10 tsf, a difference of 1.38 tsf, while ϕ values ranged from 47.8 to 30.8 deg, a difference of 17.0 deg. The trend in test results is similar to the results observed for the smooth cast specimens; the 6-in.-diam rock core shear tests generated failure envelopes with lower ϕ values than the in situ shear tests. The observed c values must be considered as apparent cohesive values since at zero normal load the even angle asperity configuration cannot initiate failure through the asperities.

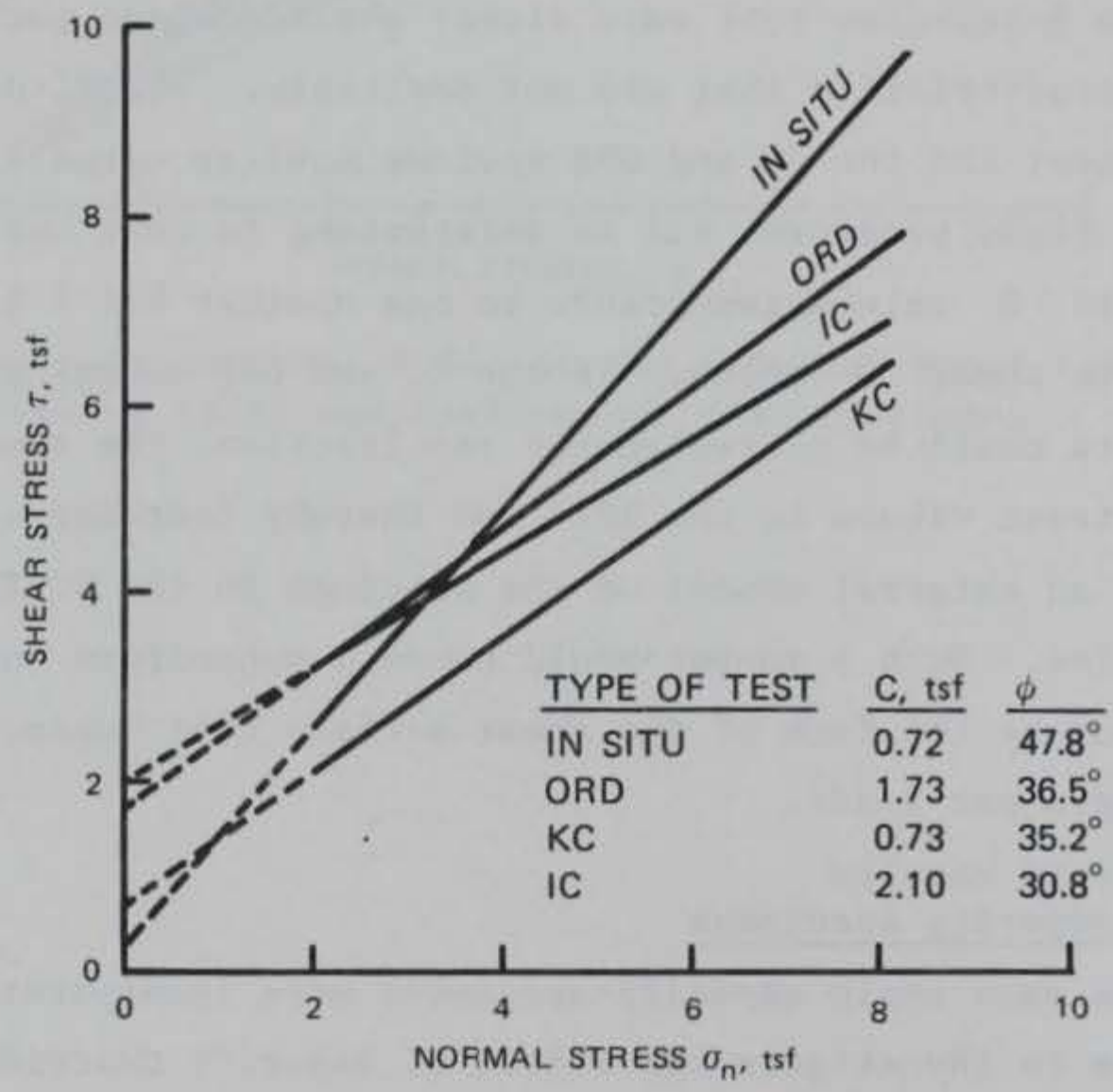

Figure 56. Comparison of direct shear Mohr-Coulomb failure envelopes for model material even angle asperity specimens

188. The significance of the spread in shear strength parameters can be evaluated from the modes of failure. The mode of failure may be determined by observing the normal deformations of the specimen during the shear cycle. Dilation of the specimen at failure denotes an overriding failure mode. No dilation or compression of the specimen at failure denotes a shear through failure mode. The in situ and ORD shear tests were the only tests conducted where normal deformations were conscientiously monitored. Table 9 presents a summary of normal deformations at failure for the in situ and ORD direct shear tests. Table 9 shows a slight trend for specimen dilation at failure up to a normal stress of 4 tsf for the in situ test. Above 4-tsf normal stress, the specimens are compressed at failure. Based on the normal deformations, one would expect a transition between override and shear through failure modes somewhere between 4- and 6-tsf normal load. An inspection of the in situ shear $\tau - \sigma_n$ plots (Figure 32) indicates that such a transition probably occurs at approximately 5- to 6-tsf normal stress. The nonlinear characteristics of the in situ direct shear tests results will be discussed in greater detail below. However, at this point it should be noted that the in situ test results ($\tau - \sigma_n$ plots and normal deformations) indicate that both overriding and shear through failure modes occurred over the normal stress test interval.

Table 9

Summary of In Situ and ORD Direct Shear Normal Deformations at Failure

Type of Test	Normal Load tsf	Range of Normal Deformations at Failure, in.
In situ	2	+0.003 (one test only)
In situ	3	+0.002 to +0.010 (two tests)
In situ	4	+0.0125 (one test only)
In situ	6	-0.015 (one test only)
In situ	8	-0.028 to -0.022 (two tests)
ORD	2	-0.007 to +0.004 (two tests)
ORD	4	+0.007 (two tests)
ORD	6	+0.002 to +0.006 (two tests)
ORD	8	-0.007 to -0.008 (two tests)

Note: + sign denotes dilation; - sign denotes compression.

189. Table 9 indicates a general trend for dilation at failure up to 6-tsf normal stress for the ORD direct shear tests. However, the results listed in Table 9 are deceptive. Figure 57 shows typical plots of τ versus shear deformation and normal deformation versus shear deformation from one suite of ORD shear tests at 2-, 4-, 6-, and 8-tsf normal load. From the plots, it can be seen that all the test specimens underwent compressive deformation until just prior to failure, indicating that failure was not due to an asperity override. This compressive behavior was not noted in the in situ shear tests. The absence of a definite bilinear or curvilinear trend in the ORD $\tau - \sigma_n$ plot (Figure 33) also gives the indication of some failure mode other than asperity override at low normal stresses. Consideration of the relatively linear nature of the $\tau - \sigma_n$ plots, even though dilation occurred immediately before failure, suggests that the actual mode of failure was progressive with failure initiating at either the trailing or leading edge and progressing across the specimen.

190. Although there are no supportive normal deformation data, the KC shear test $\tau - \sigma_n$ plot (Figure 37) indicates that the failure mode for this series of tests was similar to the ORD tests. The surprising feature of the KC tests is that although the normal stresses were carefully controlled (constant normal load), there does not appear to be any asperity override at low normal stresses.

191. No normal deformation measurements were made for the IC shear tests. However, the $\tau - \sigma_n$ plot (Figure 41) indicates an asperity override failure mode at low normal stresses. Like the ORD device, the IC device monitors hydraulic fluid pressures rather than loads. The fact that an override failure occurred can be attributed to the built-in "soft" normal load system. Also, the hydraulic load rams are smaller, requiring higher driving fluid pressures, which results in less ram friction than the ORD device.

192. Patton (1966) demonstrated that for an ideal shear through asperity failure mode the ϕ value should be approximately equal to the ϕ value obtained from residual shear test, ϕ_r, or from tests on smooth discontinuous specimens, ϕ_u, for most unweathered rock. For most materials, Patton demonstrated that $\phi_r \simeq \phi_u$. Cast model material specimens composed of a cementing matrix have a thin, almost glossy skin. Therefore, ϕ_r cannot necessarily be expected to equal ϕ_u. Rosenblad (1971) demonstrated that for his model material, shear tests on smooth cast specimens with the thin skin removed

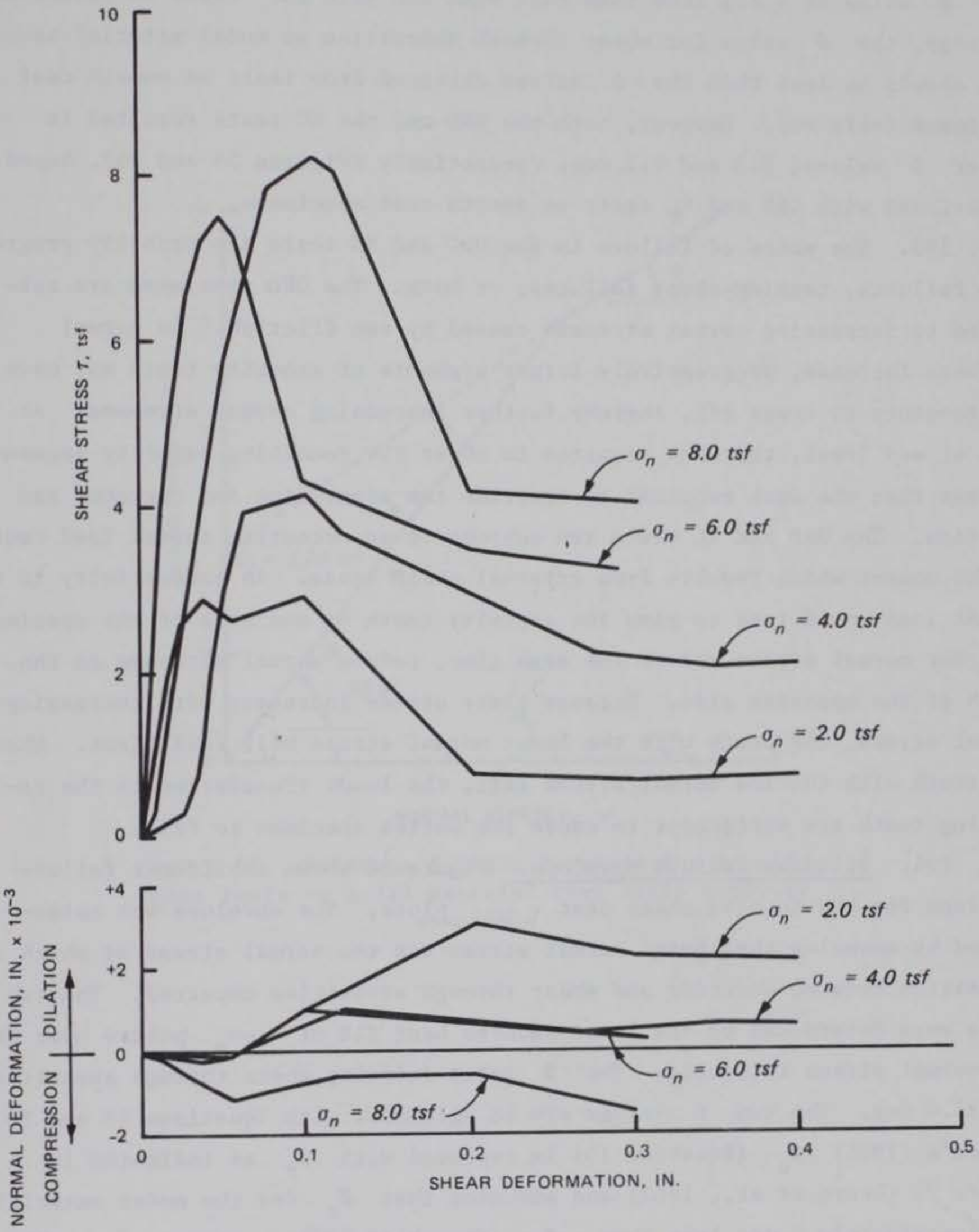

Figure 57. Typical plot of ORD shear stress and normal deformation versus shear deformation for tests on model material even angle asperity specimens

(equivalent to a residual where the shearing action removes the skin) resulted in a ϕ value of 4 deg less than that with the skin on. Based on Rosenblad's findings, the ϕ value for shear through asperities on model material specimens should be less than the ϕ values obtained from tests on smooth cast specimens (skin on). However, both the ORD and the KC tests resulted in higher ϕ values, 8.3 and 6.2 deg, respectively (Figures 55 and 56), based on comparisons with ORD and KC tests on smooth cast specimens.

193. The modes of failure in the ORD and KC tests are probably progressive failures, tension-shear failures, or both. The ORD specimens are subjected to increasing normal stresses caused by ram friction. As normal stresses increase, progressively larger segments of asperity teeth may have the tendency to break off, thereby further increasing normal stresses. At some stress level, the work required to shear the remaining asperity segment is less than the work required to override the asperities and overcome ram friction. The ORD and KC tests are subject to an eccentric normal load caused by the moment which results from external shear loads. An eccentricity in the normal load would tend to give the asperity teeth on one side of the specimen a higher normal stress and at the same time, reduce normal stresses on the teeth of the opposite side. Because shear stress increases with increasing normal stress, the teeth with the lower normal stress will fail first. When the teeth with the low normal stress fail, the loads transferred to the remaining teeth are sufficient to cause the entire specimen to fail.

194. Bilinear failure envelope. Figure 58 shows a bilinear failure envelope for the in situ shear test $\tau - \sigma_n$ plots. The envelope was established by assuming that 6-tsf normal stress was the normal stress at which the transition between override and shear through asperities occurred. The two lines were determined by the least-squares best fit of $\tau - \sigma_n$ points over the two normal stress intervals. The ϕ value defining shear through asperities was 35.0 deg. The two ϕ values are in agreement with Equations 15 and 16 if Patton's (1966) ϕ_u (Equation 15) is replaced with ϕ_r as indicated in Figure 22 (Deere et al., 1967) and assuming that ϕ_r for the model material is approximately 4 deg less than ϕ_u (Rosenblad 1971). With a ϕ_r value of 34.5 deg, the predicted (from Equations 15 and 16) values of ϕ for override and shear through asperities are 55 and 34.5 deg, respectively. The cohesion intercept for the shear through portion of the envelope (labeled C_j in Figure 58) was 3.79 tsf.

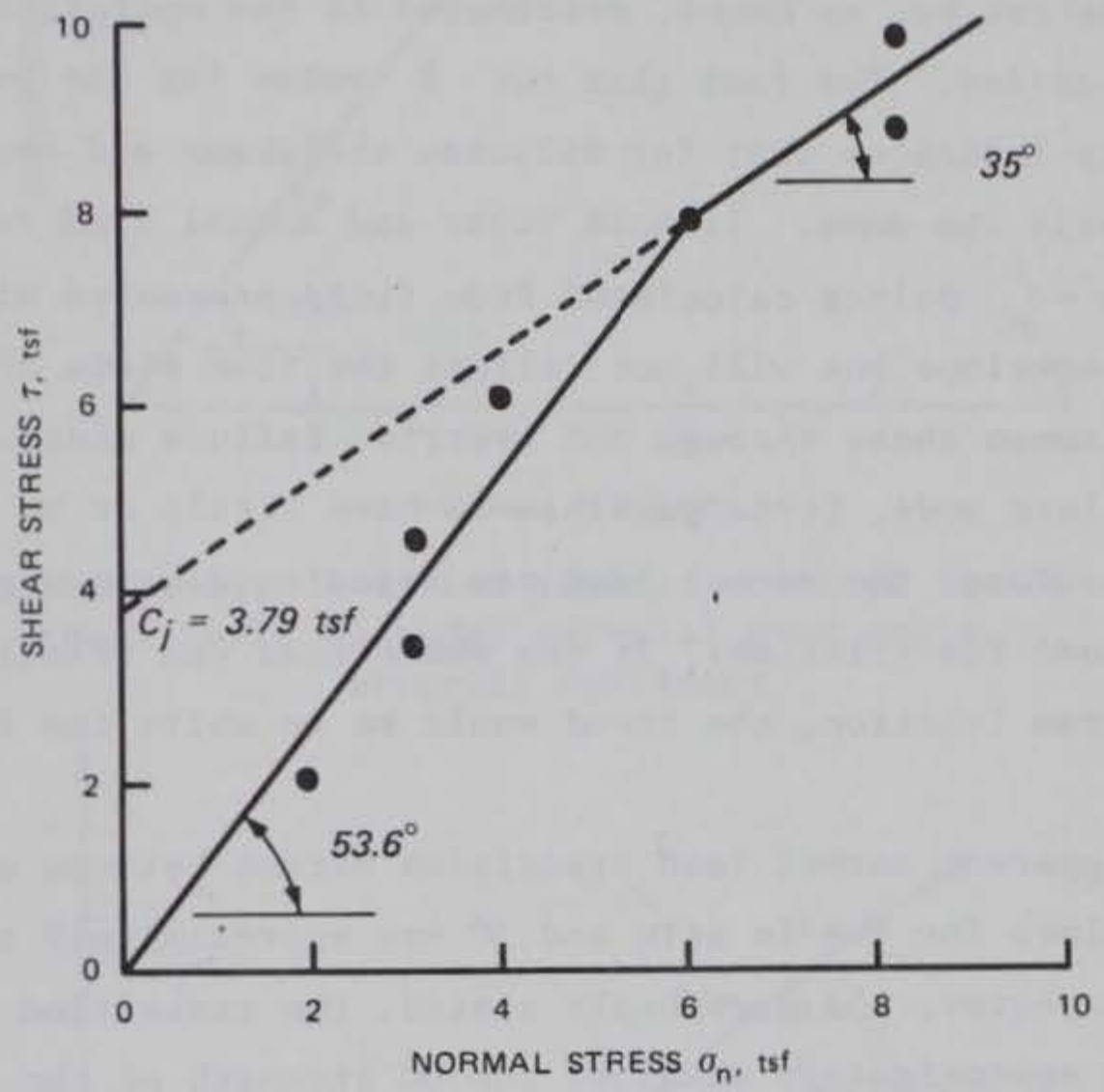

Figure 58. Bilinear failure envelope for in situ shear tests on model material even angle asperity specimens

195. Figure 59 shows a bilinear failure envelope for the IC shear test $\tau - \sigma_n$ plot. For the IC tests, the transition normal stress was assumed to be 4 tsf. The ϕ value for the override segment of the envelope was 52.1 deg, which is comparable to the 53.6 deg obtained from the in situ tests. The ϕ value for the shear through segment of the curve was 21.7 deg (approximately 13 deg lower than what might be expected). The discrepancy in shear through ϕ values can be, no doubt, attributed to the operational characteristics of the IC device. The fact that the ϕ value for the override failure mode is reasonable indicates that for dilation the shear and normal load ram frictions are nearly the same. If both shear and normal load ram frictions are equivalent, the $\tau - \sigma_n$ points calculated from fluid pressures will fall along the true failure envelope but will not reflect the true state of stress for the transition between shear through and override failure modes. For the shear through failure mode, it is possible to have little or no normal deformation. Therefore, the normal load ram friction can be significantly less than shear load ram friction. If the shear load ram friction is greater than normal load ram friction, the trend would be to shift the failure envelope down.

196. The apparent normal load transition stress between override and shear through failure for the in situ and IC was approximately seven to ten times less than expected. As previously stated, the transition stress for most materials is approximately equal to the UC strength of the joint wall material. For the model material tested the joint wall UC strength should be equivalent to the intact UC strength of approximately 40 tsf. The discrepancy in apparent and expected transitions may be due to scale effects between intact and asperity materials, unexplained behavioral characteristics of the model material, progressive failure of the even angle asperities, or misinterpretation of the test results due to data scatter.

197. Curvilinear failure envelope. Figure 60 shows a comparison of Barton's empirical curvilinear failure envelope (Equation 21) and the in situ direct shear test results on even angle asperity specimens. Curvilinear failure envelope A was established by assuming a JRC (joint roughness coefficient) of 20. A JRC of 20 is the highest value that can be assigned and corresponds to a rough undulating joint. The JCS (joint wall compressive strength) was assumed to be the mean intact UC strength at 6 days of 41.1 tsf.

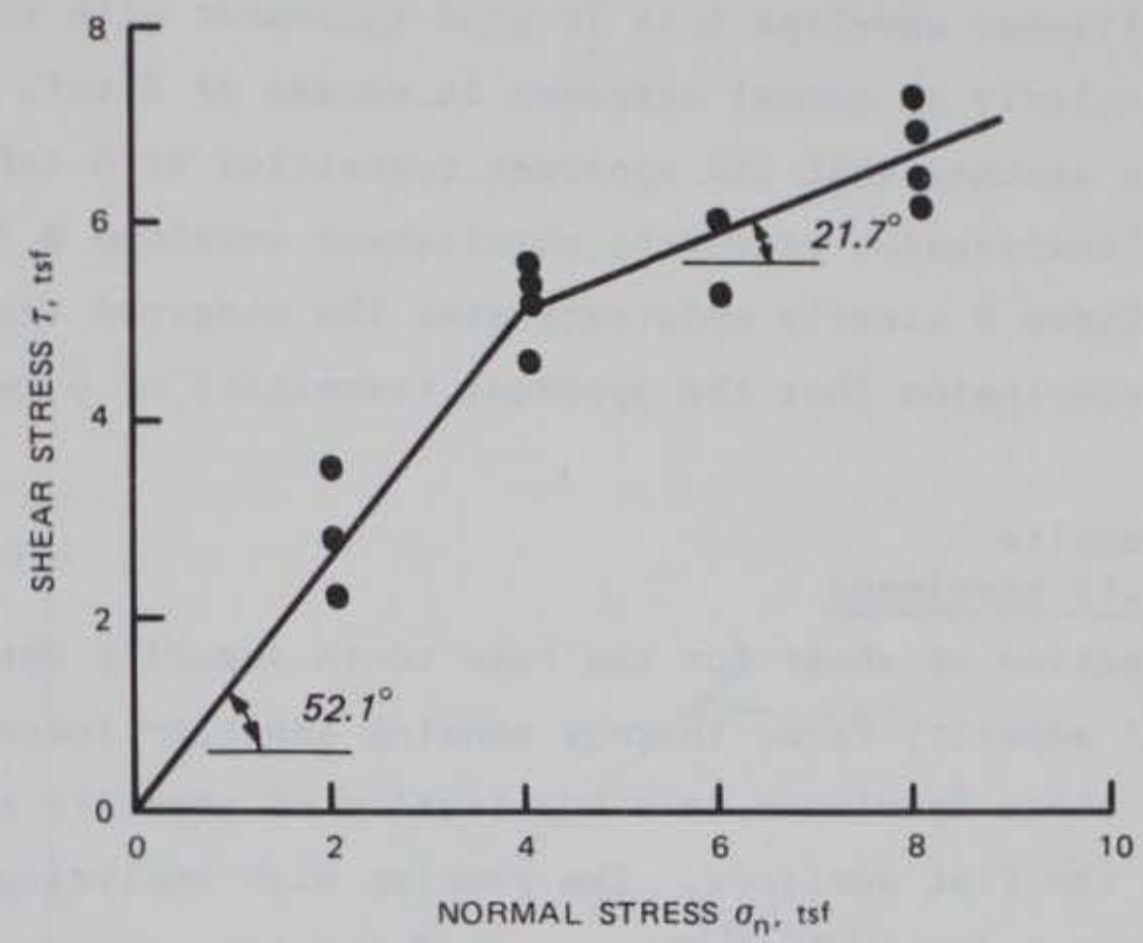

Figure 59. Bilinear failure envelope for IC shear tests on model material even angle asperity specimens

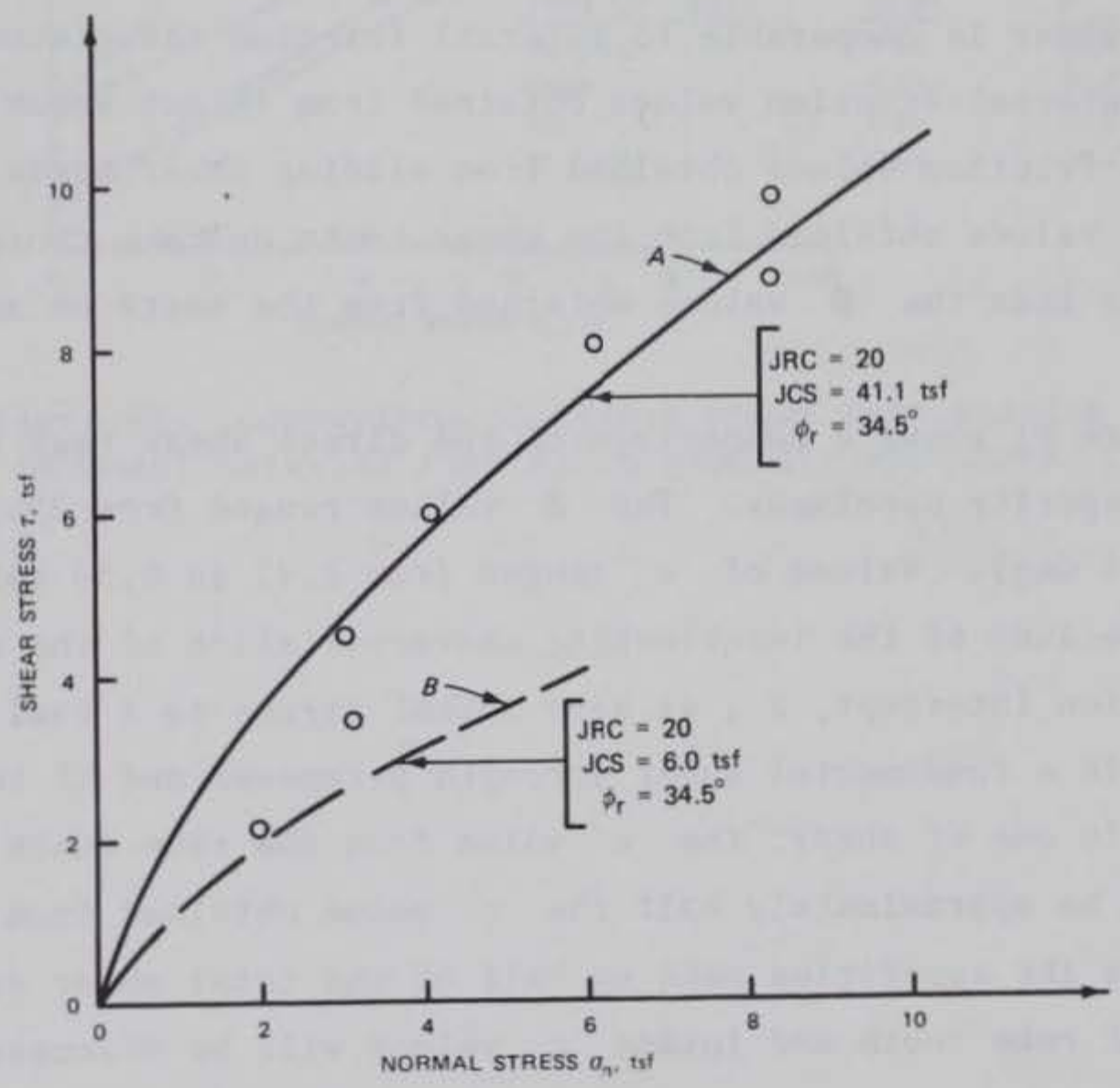

Figure 60. Comparison of Barton's curvilinear failure envelope with in situ direct shear test results on model material even angle asperity specimens

The ϕ_r value was assumed to be 34.5 deg (see paragraph 194). As can be seen in the figure, curvilinear envelope A is in good agreement with the plotted test results, particularly at normal stresses in excess of 2 tsf.

198. If it is assumed that the apparent transition at 6 tsf represents the true joint wall compressive strength, curvilinear envelope B is obtained from Equation 21. Curve B clearly underestimates the observed test results, which supports the conclusion that the apparent transition of 6 tsf is due to data scatter.

Direct shear test results
on rake tooth asperity specimens

199. The direction of shear for the rake tooth asperity specimens was against the vertical asperity face, thereby causing asperity interlock. The mode of failure for these specimens is a combination of asperity shear and sliding friction on the flat surfaces. The problem with analyzing test results based on failure modes is that the apparent friction component (slope of the failure envelope) of the total shear strength is actually composed of two separate and different friction components. The friction component attributed to the asperity shear is comparable to internal friction associated with intact shear. Internal friction values obtained from intact shear are generally higher than friction values obtained from sliding shear tests. Therefore, the expected ϕ values obtained from the shear tests on rake tooth specimens should be greater than the ϕ values obtained from the tests on smooth cast specimens.

200. Figure 61 shows a comparison of the direct shear test results on the rake tooth asperity specimens. The ϕ values ranged from 25.7 to 39.8 deg (a spread of 14.1 deg). Values of c ranged from 1.91 to 0.54 tsf (a spread of 1.37 tsf). Because of the interlocking characteristics of the asperity teeth, the cohesion intercept, c, at zero normal stress is a real parameter. In fact, if c is a fundamental shear strength parameter and if the asperity mode of failure is one of shear, the c value from the rake tooth asperity specimens should be approximately half the c value obtained from the intact shear tests since the asperities make up half of the total shear surface area. The comparison of rake tooth and intact c values will be discussed in greater detail below.

201. The ϕ values obtained from the rake tooth asperity tests were surprisingly close to those obtained from the smooth cast tests (Figures 55

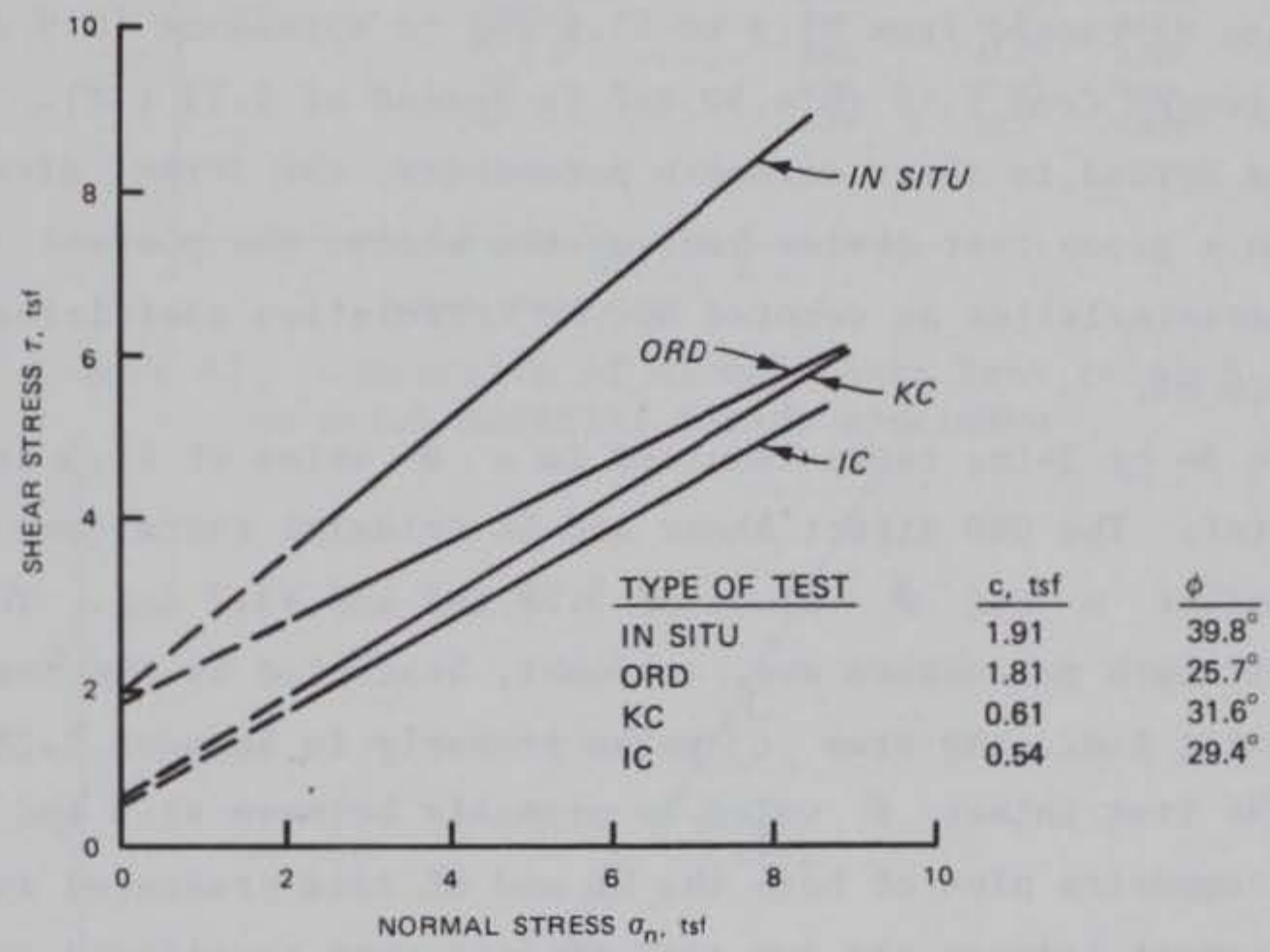

Figure 61. Comparison of direct shear test results on model material rake tooth asperity specimens

and 61). The in situ and KC shear tests, respectively, had ϕ values 1.3 and 2.6 deg higher than the smooth cast tests, while the IC and ORD tests had ϕ values 2.0 and 2.5 deg, respectively, lower.

Direct and triaxial shear
test results on intact specimens

202. Figures 62 and 63 show the direct and triaxial shear test results, respectively, for the tests on intact specimens. The intact specimen shear test results exhibited the greatest variation due to the type of direct shear tests of any types of specimen tested in the course of this study. The ϕ values in Figure 62 ranged from 21.9 to 41.8 deg (a spread of 19.9 deg). The c values ranged from 2.79 to 4.50 tsf (a spread of 1.71 tsf). In addition to the spread in shear strength parameters, the intact direct shear test from a given test device had, on the whole, the poorest $\tau - \sigma_n$ correlation characteristics as denoted by the correlation coefficients R listed in Figure 62.

203. The 3- by 3-in. tests resulted in a ϕ value of 41.3 deg and c value of 3.41 tsf. The ORD direct shear and GL triaxial tests (see Figure 45) resulted in similar c and ϕ values of 3.28 tsf and 43.2 deg. The true intact shear strength parameters are, no doubt, bracketed by the results from these three tests; i.e., the true c value probably is between 3.28 to 4.50 tsf and the true intact ϕ value is probably between 41.3 and 43.2 deg.

204. A composite plot of both the GL and SL data presented in Figure 63 shows good agreement between the two sets of data when considered together. The composite plot least-squares best fit (forced through the origin) ϕ value of 59.0 deg is in excellent agreement with the ϕ value of 58.2 deg obtained from the individual SL tests in Figure 48. The question must be asked as to which set of data is representative of the true strength. The only significant differences in the two tests procedures were the end caps used. The GL tests used aluminum end caps, whereas the SL tests used steel end caps. There did not appear to be any major differences in observed failure modes between the two tests. However, Figure 63 shows that at equivalent confining pressures the GL specimens failed at consistently lower levels of normal stress.

205. Both the KC and IC tests resulted in ϕ values approximately 17 to 20 deg lower than the probable true range of 41.3 to 43.2 deg. The discrepancy can best be attributed to the operational characteristics of the devices. The external moment associated with the KC device resulted in a

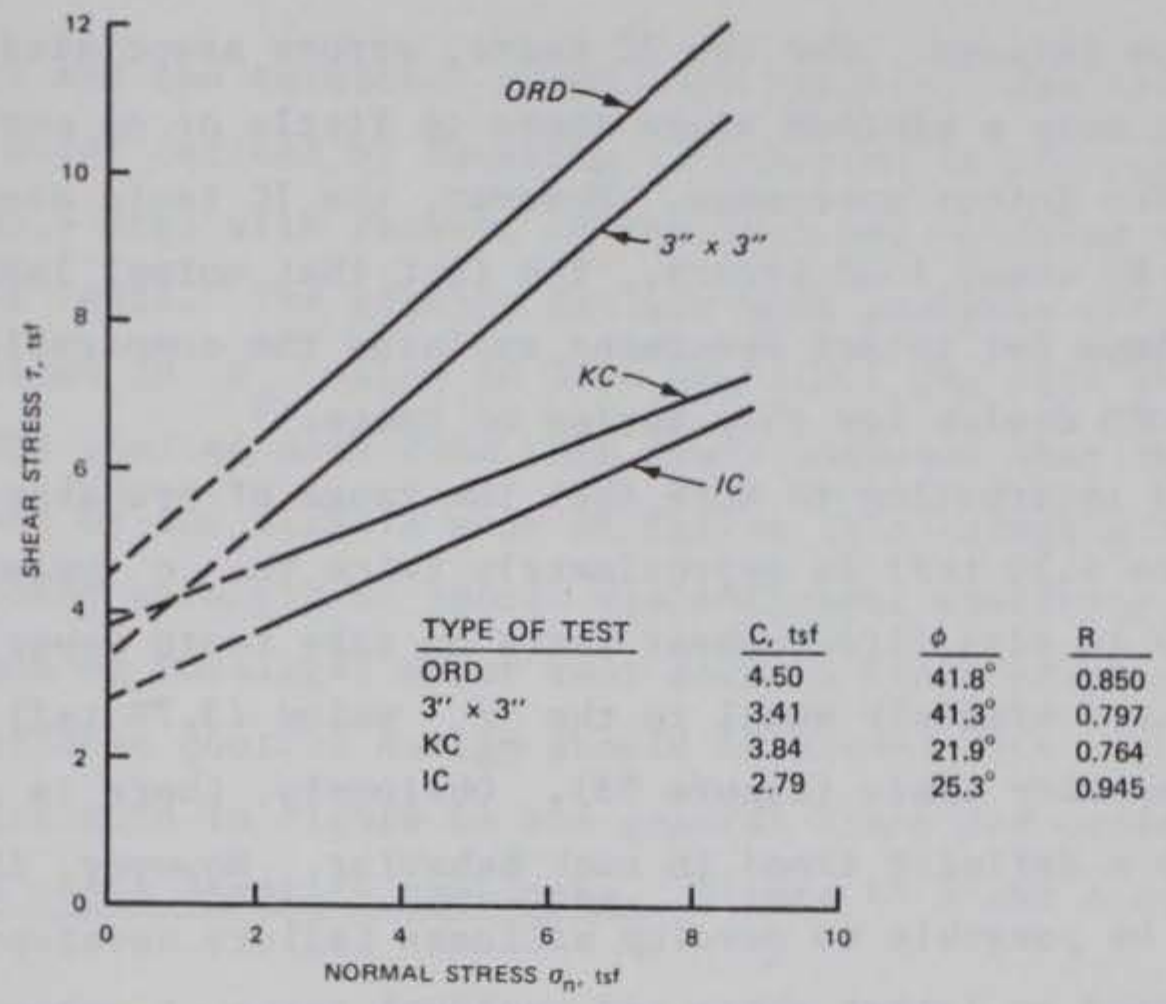

Figure 62. Comparison of direct shear test results on model material intact specimens

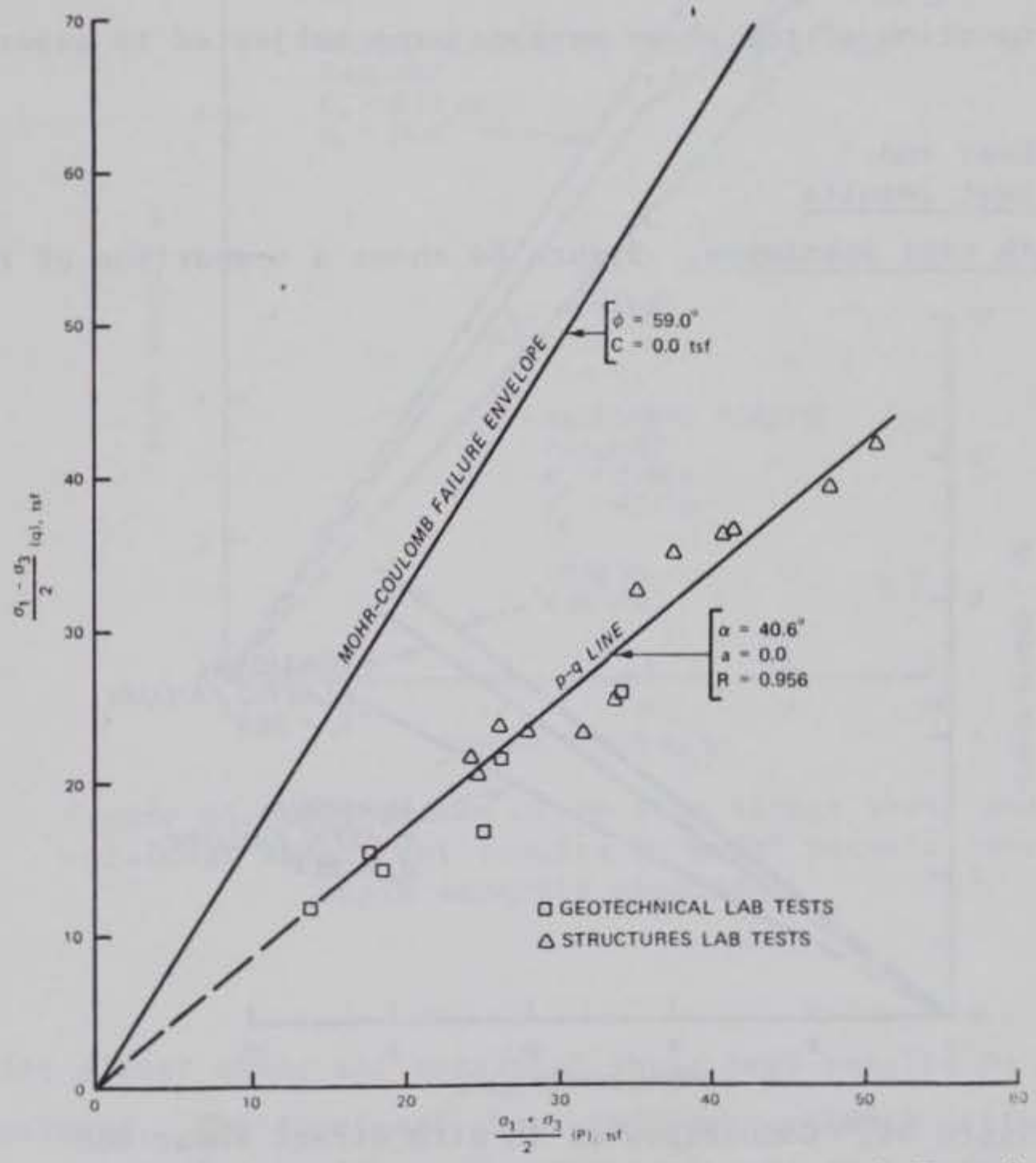

Figure 63. Composite p-q diagram of GL and SL triaxial tests on model material intact specimens

tension-shear type failure. For the IC tests, errors associated with normal load ram friction were a minimum since there is little or no normal deformation at failure for intact specimens. However, the IC tests are still adversely affected by shear load errors. The fact that normal load ram friction errors are a minimum for intact specimens explains the comparable results obtained by the ORD device for this series of tests.

206. It is interesting to note that the range of probable true intact c values (3.28 to 4.50 tsf) is approximately twice the c value (1.91 tsf) obtained from the in situ direct shear tests on rake tooth asperity specimens (Figure 28) and approximately equal to the c_j value (3.79 tsf) obtained from the even angle asperity tests (Figure 58). Obviously, there is insufficient data to establish a definite trend in such behavior. However, if such trends are real, it may be possible to develop bilinear failure envelopes for in situ natural joints based on intact shear and residual tests of material representative of the joint wall and by determining the effective asperity inclination angle and the proportion of the shear surface area subjected to asperity shear.

In situ direct shear and
torsional shear test results

207. Smooth cast specimens. Figure 64 shows a comparison of the in

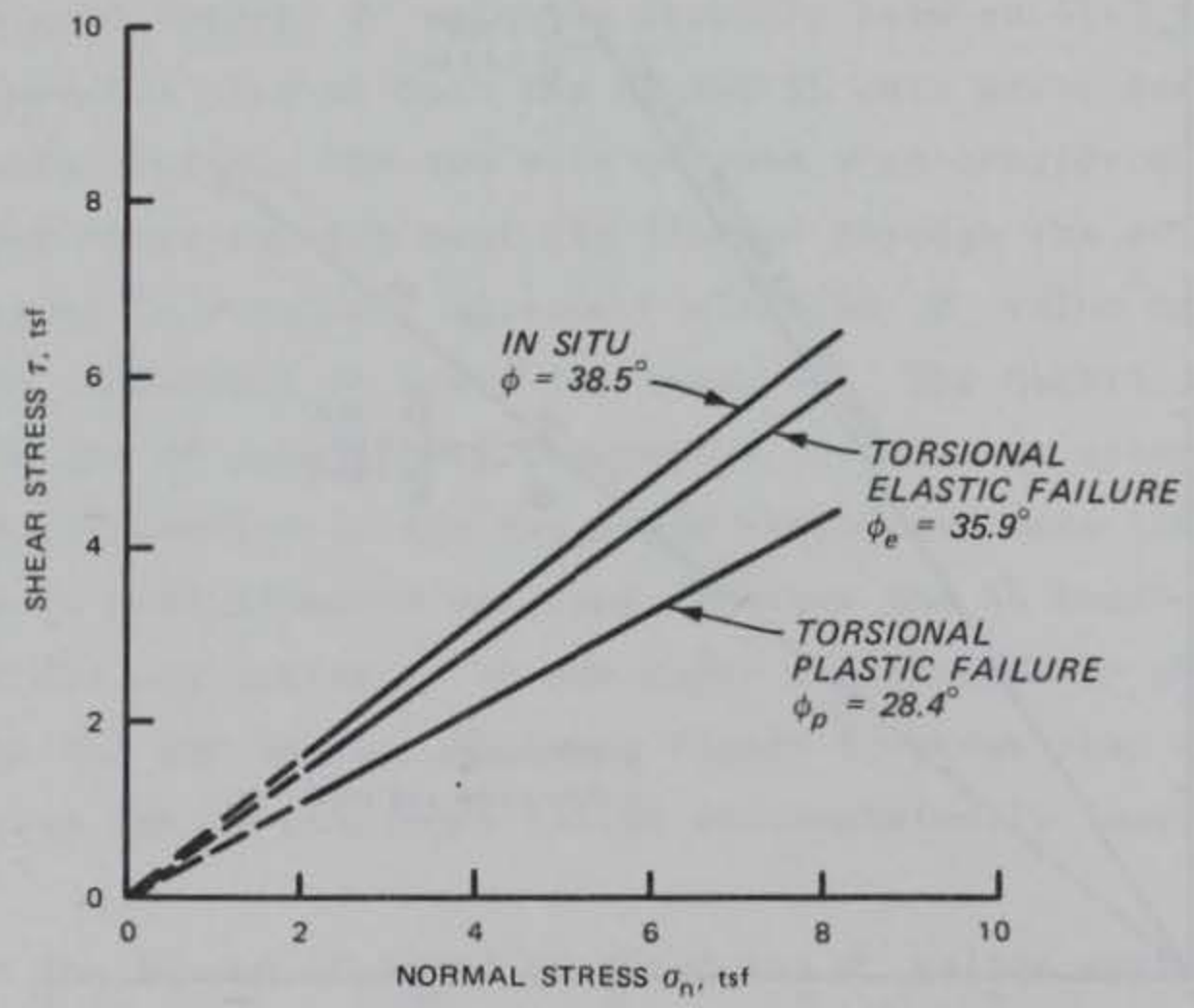

Figure 64. Comparison of in situ direct shear and torsional shear test results on model material smooth cast specimens

situ direct shear and the torsional shear test results. The torsional shear elastic failure model defined by Equation 10 resulted in the most comparative ϕ value (ϕ_e = 35.9 deg) with respect to the 38.5 deg obtained from the in situ direct shear tests. The plastic failure mode analysis defined by Equation 12 resulted in ϕ_p value of 28.4 deg (10.1 deg less than the direct shear value). The limited data from this study indicate that the torsional shear test defined by the elastic mode of failue is a suitable index test for predicting the shear strength of smooth discontinuous specimens. However, the direct application of torsional shear test data to field problems where smooth discontinuous surfaces control design should be viewed with circumspection since the data indicate in Figure 64 the general trend for conservatism.

208. Even angle asperity specimens. Figure 65 shows a comparison

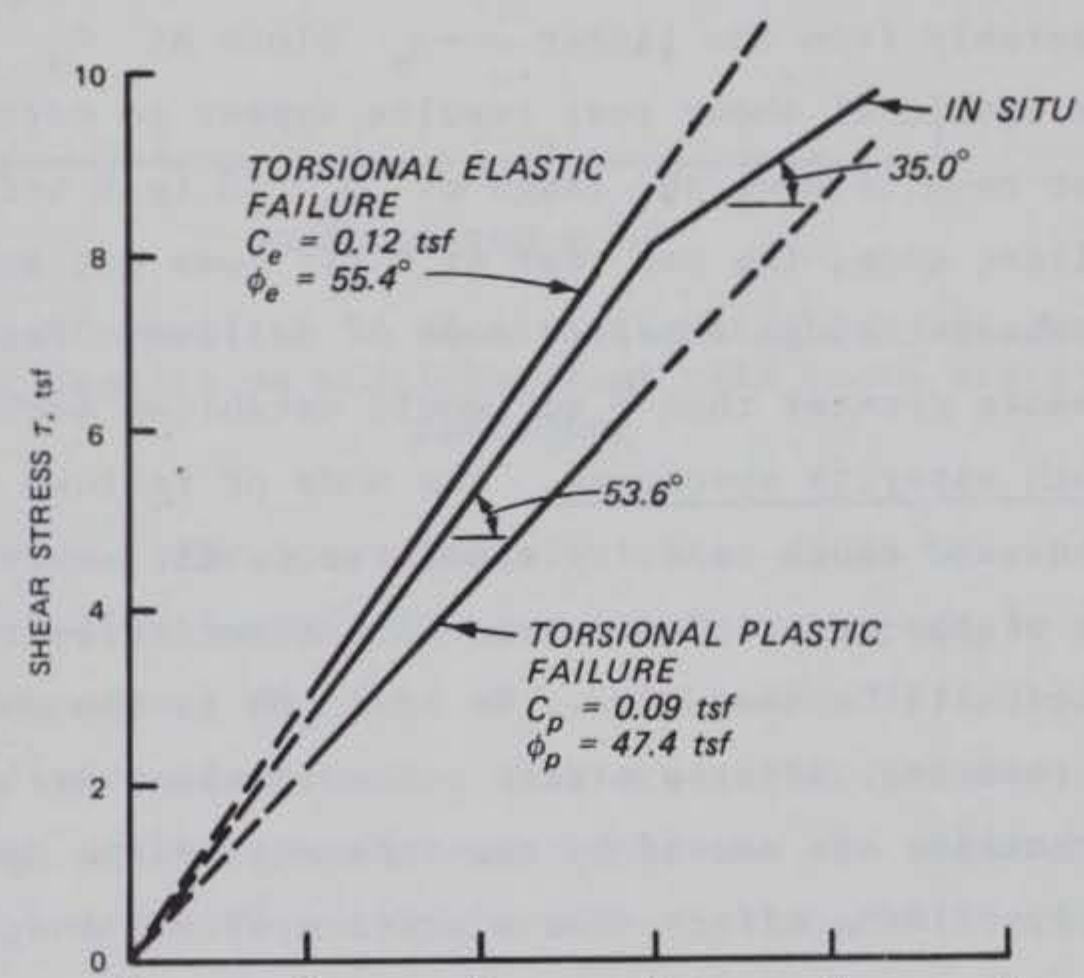

Figure 65. Comparison of in situ direct shear and torsional shear test results on model material even angle asperity specimens

of the in situ direct shear and torsional shear test results on even angle asperity specimens. The torsional shear failure envelopes defined by elastic and plastic failure modes bracketed the initial (override) bilinear direct shear failure envelope. The elastic failure mode analysis resulted in a c_e

of 0.12 tsf and a ϕ_e of 55.4 deg. The plastic failure mode analysis resulted in a c_p of 0.09 tsf and a ϕ_p of 47.4 deg. The cohesion intercepts obtained from the torsional shear test are probably apparent rather than real and are caused by the slight scatter in the test data. If the elastic and plastic envelopes are forced through zero, the ϕ values increase slightly to 55.9 and 47.9 deg for ϕ_e and ϕ_p, respectively. Considering the radial shear deformations associated with the torsional shear tests, the envelope defined by elastic failure mode is surprisingly close to the initial envelope obtained from the in situ tests and also the initial envelope (ϕ = 55 deg) predicted by Patton's bilinear failure criteria.

209. The elastic and plastic τ-σ_n plots shown in Figure 30 indicate that no test was conducted above 6-tsf normal stress. Actually, one test was conducted at 8 tsf but is not shown in Figure 30 because the results from that test differed considerably from the linear τ-σ_n plots at σ_n of 6 tsf or lower. Although the torsional shear test results appear to correlate well with the in situ test results over the range of σ_n (0 to 6 tsf) associated with an override failure mode, the one test at 8 tsf does not support a correlation trend of the shear through asperity mode of failure. Perhaps additional tests at normal stresses greater than 6 tsf would establish such a trend.

210. Rake tooth asperity specimens. The mode of failure for the torsional shear tests on rake tooth asperity specimens is extremely complex. The nonsymmetrical shape of the asperities causes both asperity override and asperity shear to occur at the same time. In addition to the combined override and shear failure modes, adverse stress concentrations are generated. These stress concentrations are caused by the tendency of the specimen to tilt due to the asperity overriding effect over a portion of the shear surface. The tilting tendency generates additional compressive forces on the opposite end of the asperities subject to override. To add to the complexity, the transition between asperity override and asperity shear and also the additional compressive forces are radius dependent.

211. Figure 66 shows the comparison of in situ direct and torsional shear test results on rake tooth asperity specimens. The torsional shear test results defined by the elastic failure analysis resulted in c_e and ϕ_e values of 1.63 tsf and 45.2 deg, respectively; plastic failure analysis resulted in c_p and ϕ_p values of 1.22 tsf and 37.1 deg, respectively. The cohesion intercept was somewhat lower than the 1.91 tsf reported for the in

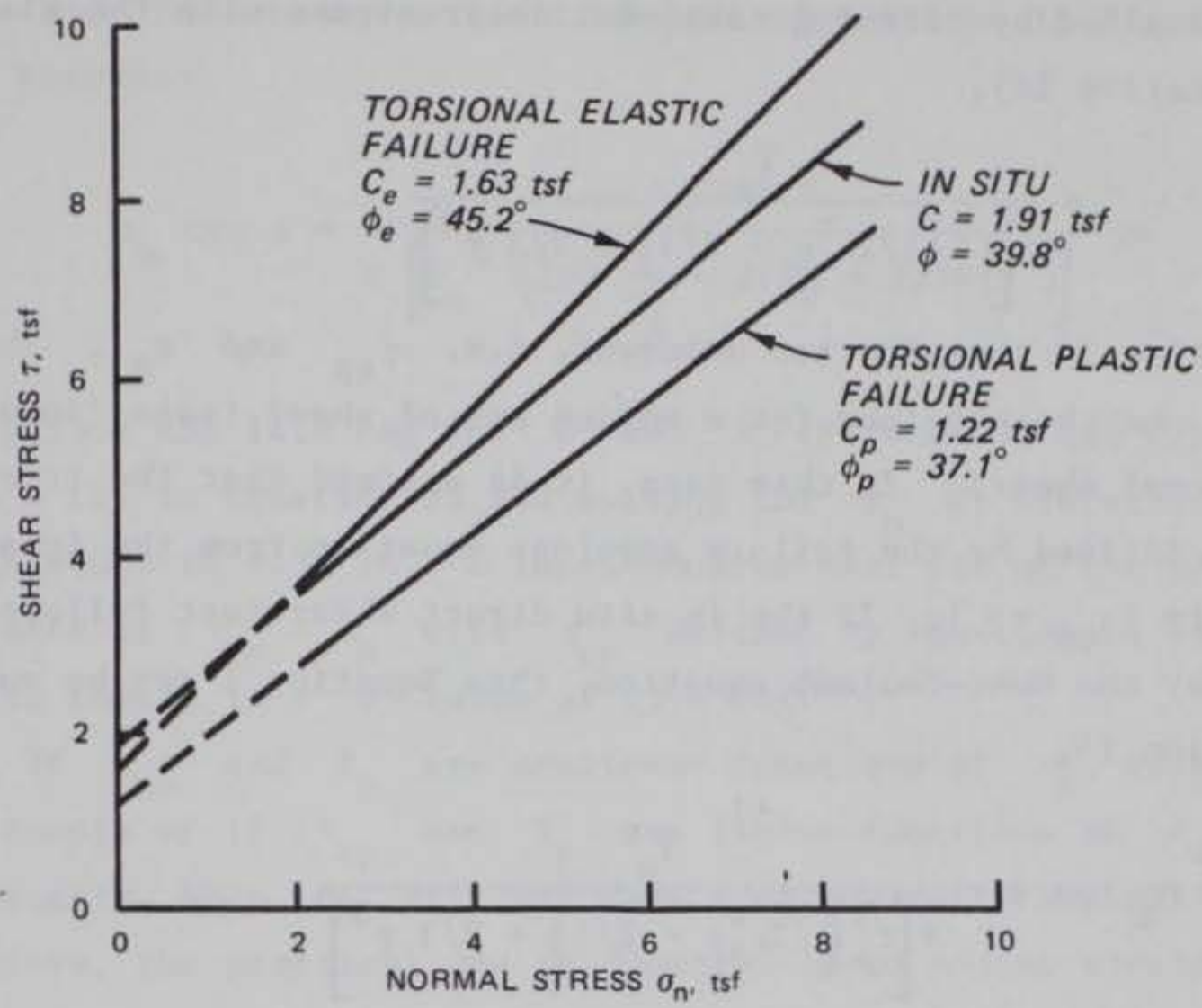

Figure 66. Comparison of in situ direct shear and torsional shear test results on model material rake tooth asperity specimens

situ direct shear test. The lower cohesion value is to be expected considering the multiple failure modes of the torsional shear test. The elastic and plastic friction components (ϕ_e and ϕ_p) bracket the ϕ value (39.8 deg) obtained from the direct shear test. However, unlike the test results on smooth cast and even angle asperity specimens, the ϕ value obtained from the plastic failure (ϕ_p) definition correlated best with the in situ direct shear test results.

212. Elastic-plastic comparison. The preceding paragraphs discussed the comparison of results between the in situ direct shear test and the torsional shear test as defined either in the pure elastic or pure plastic case. The pure elastic case compared well with the in situ direct shear results for the smooth cast and even angle asperity specimens, whereas the pure plastic case compared well with rake tooth specimens. The failure envelopes for the torsional shear tests on even angle and rake tooth asperity specimens defined by the pure elastic and pure plastic case bracketed the in situ direct shear envelopes for those tests. For the even angle and rake tooth asperity tests,

a closer correlation between the in situ direct shear and torsional shear test results may be obtained by defining torsional shear stress with the elastic-plastic case (Equation 14).

$$\tau_{ep} = \frac{T_p}{\pi\left[r_o^3\left(1/2\ \frac{r_o}{r} - 2/3\right) + 2/3\ r^3\right]} \tag{14}$$

213. Equation 14 contains two unknowns, i.e. τ_{ep} and r_o. The solution for r_o may be obtained for a unique set of shear tests (in situ direct and torsional shear). In this case, it is assumed that the true shear strength, τ, is defined by the failure envelope equation from the in situ direct shear tests ($\tau_{ep} = \tau$). If the in situ direct shear test failure envelope is defined by the Mohr-Coulomb equation, then Equation 1 may be substituted into Equation 14.

$$c + \sigma_n \tan \phi = \frac{T_p}{\pi\left[r_o^3\left(1/2\ \frac{r_o}{r} - 2/3\right) + 2/3\ r^3\right]} \tag{22}$$

For Equation 22 to be valid requires that the right side of the expression also be a linear function. If r_o is a unique value for a given set of comparative data, then T_p expressed as a function of ϕ_n must be linear and also the line equations for both $T_p - \phi_n$ and $\tau - \phi_n$ plots must pass through the origin as illustrated in Figures 58 and 67 (assumes c = 0).

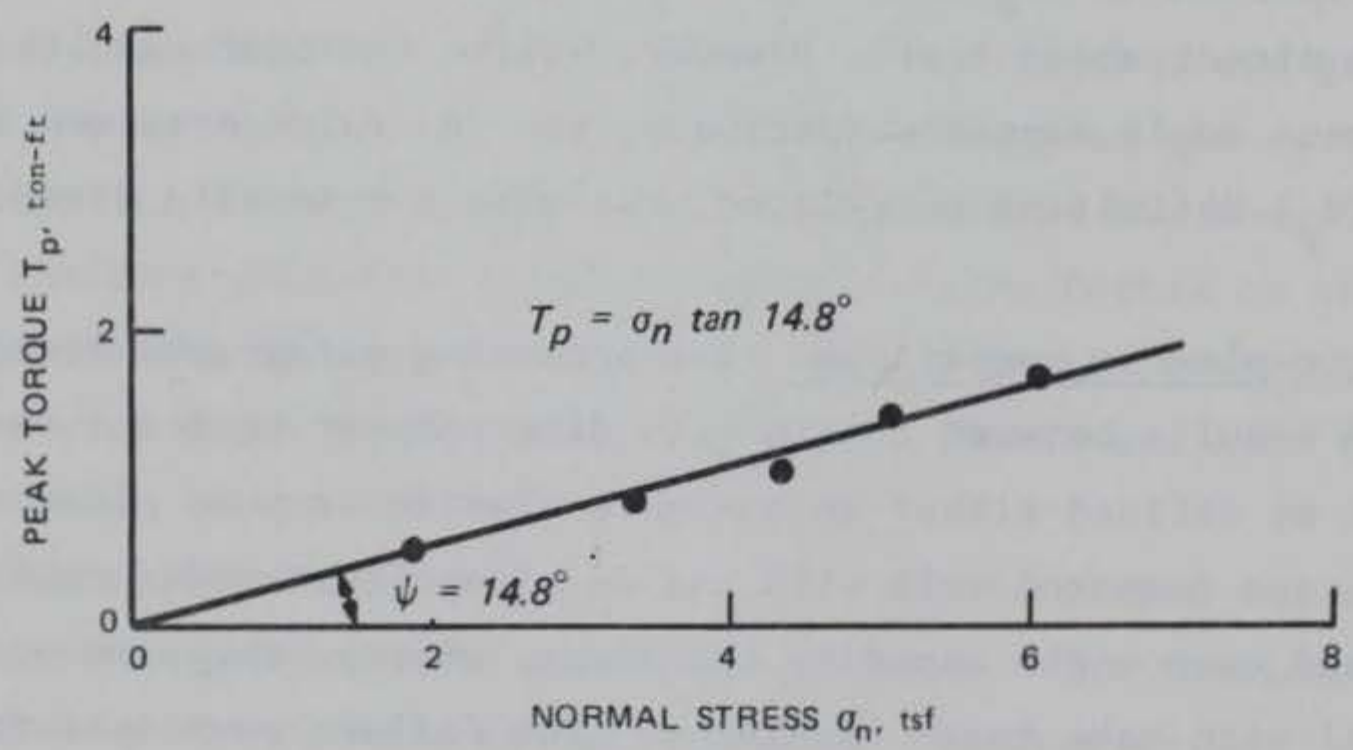

Figure 67. Plot of $T_p - \sigma_n$ from torsional shear tests on model material even angle asperity specimens

For the particular case of comparative in situ and torsional shear tests asperity override failure modes (initial part of envelope in Figure 58), Equation 22 becomes:

$$\sigma_n \tan \phi = \frac{\sigma_n \tan \Psi}{\pi \left[r_o^3 \left(1/2 \frac{r_o}{r} - 2/3 \right) + 2/3 \, (r^3) \right]} \tag{23}$$

Substituting 53.6 and 14.8 deg for ϕ and Ψ (Figures 58 and 67) and setting r equal to 6 in. in Equation 23 and solving for r_o by iteration reveals that r_o is equal to 4.32 in. A least-squares best fit of the torsional shear test data of $\tau_{ep} - \sigma_n$ with τ_{ep} defined by Equation 14 and r_o = 4.32 in. will result in a ϕ value of 53.4 deg.

214. If τ_{ep} and T_p are nonlinear functions of σ_n with or without Y-axis intercepts or if τ_{ep} and T_p are linear functions of σ_n with Y-axis intercepts, then r_o will not have a unique value but will vary with σ_n. Therefore, the practical use of Equation 14 to adjust torsional shear test data to fit any other comparative shear data is limited to the special case where the predominant failure mode is one of asperity override.

Comparison of Test Results on Rangely Sandstone

Direct shear test results on natural joints

215. Figure 68 shows a comparison of Mohr-Coulomb failure envelopes for the in situ and KC direct shear tests on the Rangely sandstone specimens. The KC test results have an approximately 7 deg lower friction angle than the in situ test results, which is the same trend observed for the test comparisons for model material specimens.

216. Visual observations of in situ direct shear specimens' shear surfaces after each test indicated that the failure mode was that of asperity override. Normal deformation measurements for the KC direct shear tests showed that three test specimens underwent dilation at failure (indicates asperity override) and three specimens underwent compression at failure (indicates asperity shear). The failure envelopes shown in Figures 50 and 68 were determined from a least-squares best fit of all six points. If each of $\tau - \sigma_n$ points and respective failure envelopes are considered according to their

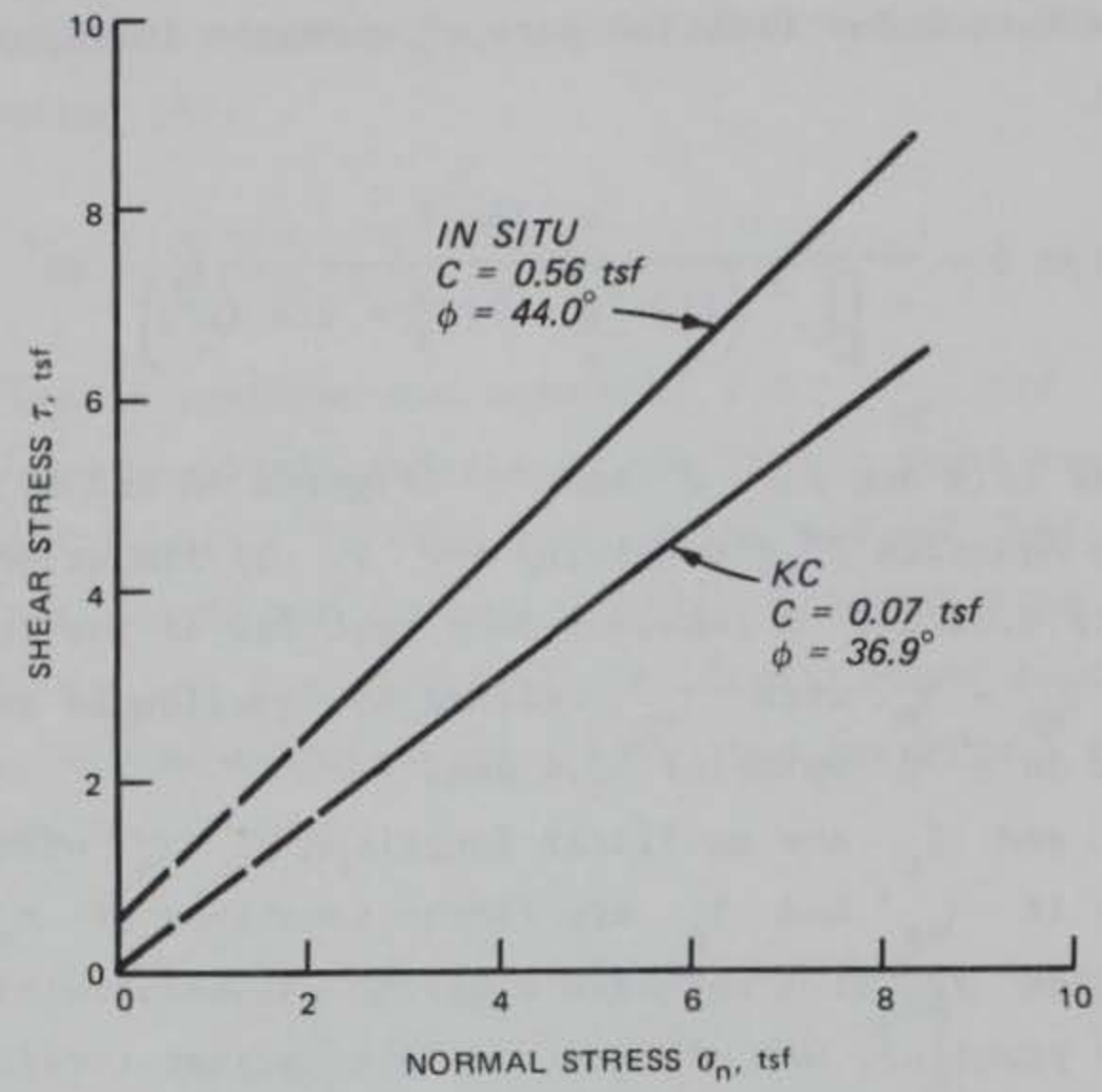

Figure 68. Comparison of in situ and KC direct shear test results on Rangely sandstone natural joint specimens

apparent failure modes, the KC test results compare very well with the in situ results and the results from the 3- by 3-in. direct shear tests on smooth sawn specimens as shown in Figure 69.

217. If the series of KC tests that experienced compression at failure truly underwent an asperity shear through mode of failure, then according to Patton's findings, the ϕ value obtained should be equal to the ϕ_r value obtained from residual shear tests or approximately equal to the ϕ_u value obtained from sliding friction tests similar to the 3- by 3-in. tests on smooth sawn surfaces. Figure 69 indicates that the KC failure envelope had a ϕ value of 3.2 deg lower than the 3- by 3-in. tests (29.4 versus 32.6 deg, respectively). Since the joint surfaces (shear surfaces) consisted of smooth, relatively flat, undulating asperities, cohesion intercepts should be considered as apparent rather than real. If the lower KC envelope is forced through zero, the resulting ϕ value is 31.5 deg or only 1.1 deg lower than the 32.6 deg obtained from the 3- by 3-in. tests.

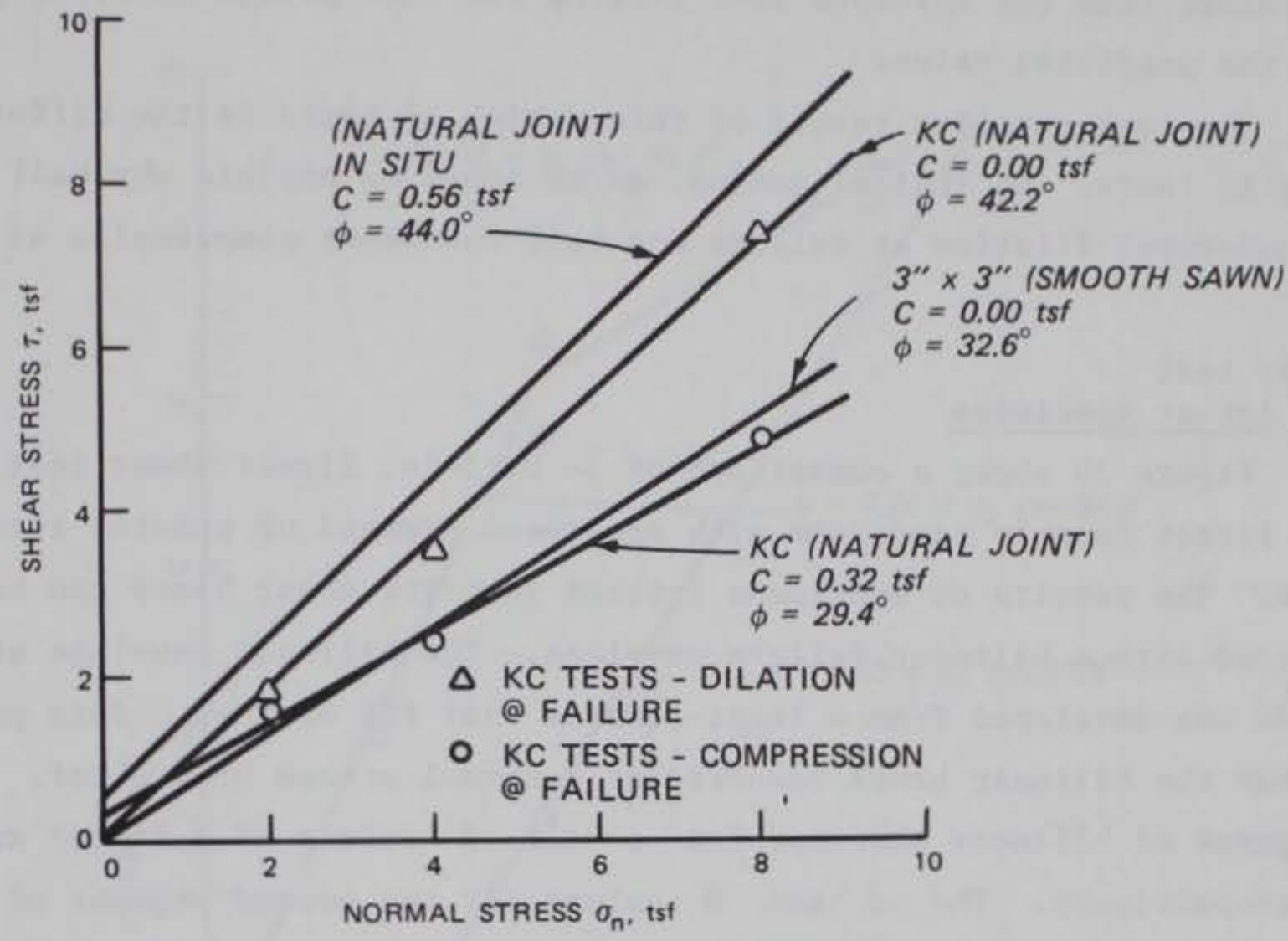

Figure 69. Comparison of in situ, 3- by 3-in. and KC direct shear tests on Rangely sandstone smooth sawn and natural joint specimens

218. The c and Ø values obtained from the in situ direct shear envelope are 0.56 tsf and 44.0 deg, respectively. The Terra Tek large field shear tests on a similar joint indicated that the true in situ Ø value was at least 45 deg. If the in situ envelope is forced through zero, the resulting Ø value is 46.4 deg, which is more in line with the probable field findings. Both the in situ and KC Ø values were higher than expected based on Patton's predictions of Ø override equal to $\emptyset_u + i$. The average second-order asperity inclination angle i for in situ specimens ranged from 2.6 to 3.0 deg. Therefore, the expected value of Ø should be approximately 35.5 deg based on average i values. The first-order asperity inclination angles ranged from 4 to 6 deg. Even considering the maximum first-order i angle of 6 deg, which would result in a maximum expected Ø value of approximately 38.5 deg, the test results indicate that the Ø values are still 4 to 6 deg higher than Patton's predicted results. The findings of the in situ and KC upper envelope tests are contrary to the findings of the in situ tests on

model material even angle asperities where the initial (override mode) ϕ value determined from the envelope best fitting the data points is 1.4 deg lower than the predicted value.

219. The most puzzling result of this series of tests is the difference between the KC tests. No logical reason can be found to explain why half the specimens underwent dilation at failure and half underwent compression at failure.

Direct shear test
results on intact specimens

220. Figure 70 shows a comparison of 3- by 3-in. direct shear test results on intact Rangely sandstone with specimens pressed or grouted into the shear boxes. The results on specimens pressed into the shear boxes can best be represented with a bilinear failure envelope. The bilinear envelope shown in Figure 70 was developed from a least-squares best fit of $\tau - \sigma_n$ data points assuming that the bilinear break occurred at a normal stress of 4.0 tsf. The initial segment of bilinear envelope had c and ϕ values of 7.94 tsf and 64.2 deg, respectively. The c and ϕ values for the second segment of the bilinear envelope were 13.72 tsf and 31.9 deg, respectively. Although shear test failure envelopes for intact specimens tend to become curvilinear or bilinear with increasing normal stress, there are no conclusive explanations as to why the tests on specimens pressed into the shear boxes exhibited a bilinear envelope at such a low normal stress (4.0 tsf). The bilinear relationship may have been caused by tensile stresses generated by a tendency for the pressed-into-place specimens to rotate in the shear box at normal stresses above 4.0 tsf. However, tensile stresses do not explain differences in the initial bilinear envelope cohesion (7.94 tsf) and the linear envelope cohesion (4.68 tsf). In any case, additional tests are needed to determine whether the two series of test results were coincidental or typical of a general trend.

Summary of Test Results

221. Table 10 presents a summary of the direct, torsional, and triaxial shear test results for the various types of shear devices and specimens investigated for this study. An inspection of Table 10 indicates a surprisingly large deviation in shear strength parameters obtained from supposedly companion type tests on identical (insofar as possible) specimens.

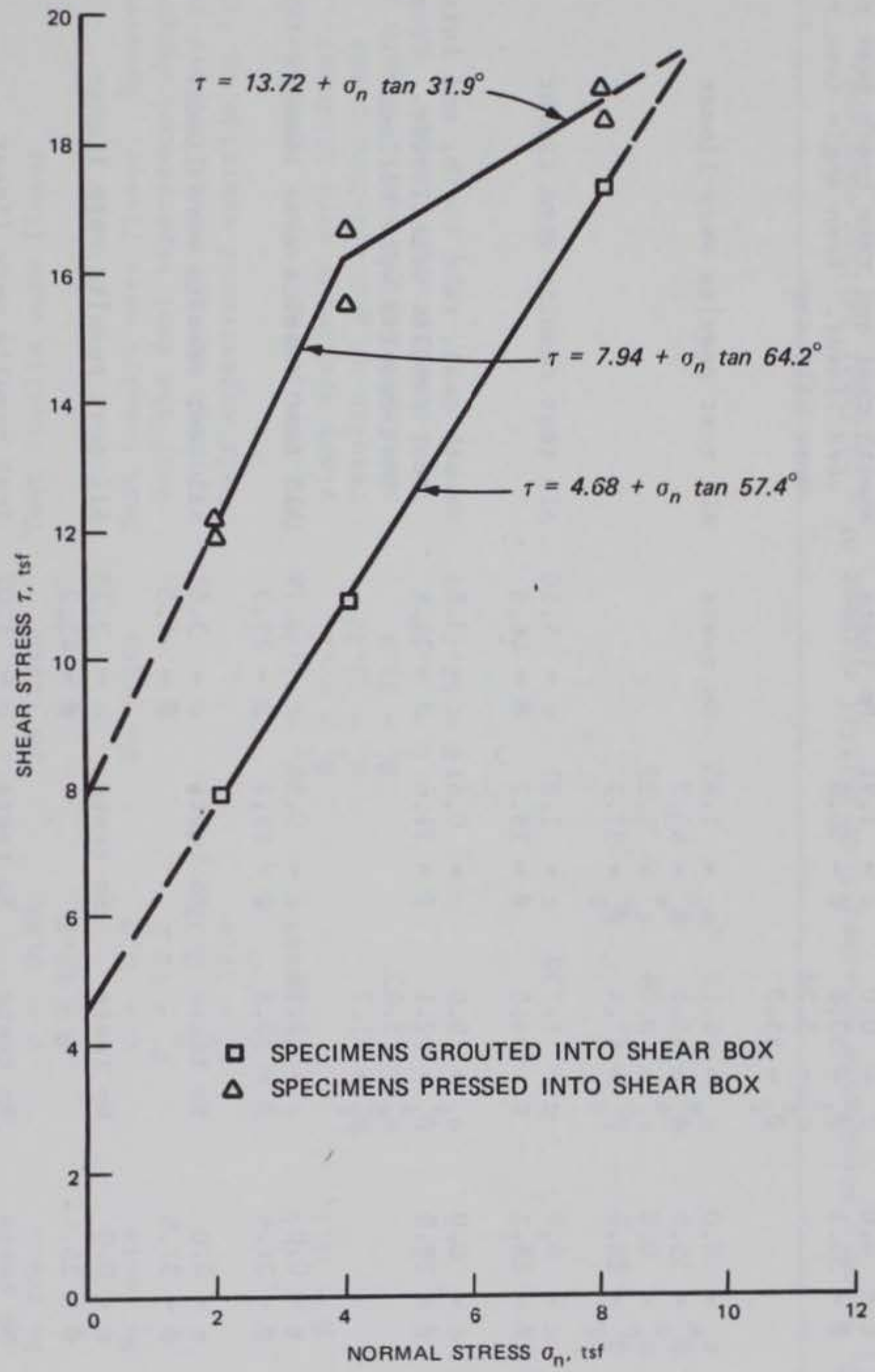

Figure 70. Comparison of 3- by 3-in. direct shear test results on intact Rangely sandstone specimens pressed and grouted into shear boxes

Table 10

Summary of Direct, Torsional and Triaxial Shear Test Results

Type of Test	Values of c (tsf) and ϕ (deg) for Type of Model Material Specimen: Smooth Cast	Even Angle	Rake Tooth	Intact	Remarks
In situ direct shear	$c = 0.0$ $\phi = 38.5$	$c_i = 0.0$ $\phi_i = 53.6$ $c_f = 3.79$ $\phi_f = 35.0$	$c = 1.91$ $\phi = 39.8$	No tests	Smooth cast and rake tooth test results were linear. Even angle test results were bilinear
Torsional shear	$c_e = 0.0$ $\phi_e = 35.9$ $c_p = 0.0$ $\phi_p = 28.4$	$c_e = 0.12$ $\phi_e = 55.4$ $c_p = 0.09$ $\phi_p = 47.4$	$c_e = 1.63$ $\phi_e = 45.2$ $c_p = 1.22$ $\phi_p = 37.1$	No tests	All test results were linear
ORD direct shear	$c = 0.0$ $\phi = 28.2$	$c = 1.730$ $\phi = 36.5$	$c = 1.81$ $\phi = 25.7$	$c = 4.50$ $\phi = 41.8$	All test results were linear
KC direct shear	$c = 0.0$ $\phi = 29.0$	$c_i = 0.0$ $\phi_i = 52.1$ $c_f = 3.42$ $\phi_f = 21.7$	$c = 0.61$ $\phi = 31.6$	$c = 3.84$ $\phi = 21.9$	Smooth cast, rake tooth, and intact test results were linear. Even angle test results were bilinear
IC direct shear	$c = 0.0$ $\phi = 31.4$	$c = 2.10$ $\phi = 30.8$	$c = 0.54$ $\phi = 29.4$	$c = 2.79$ $\phi = 25.3$	All test results were linear
3- by 3-in. direct shear	$c = 0.0$ $\phi = 37.6$	No tests	No tests	$c = 3.41$ $\phi = 41.3$	All test results were linear
GL triaxial	$c = 0.0$ $\phi = 35.4$	No tests	No tests	$c = 3.28$ $\phi = 43.2$	All test results were linear
SL triaxial	No tests	No tests	No tests	$c = 1.02$ $\phi = 58.2$	Test results were linear

(Continued)

Table 10 (Concluded)

Type of Test	Rangely Sandstone Test Results: Values of c (tsf) and Ø (deg) for Type of Specimen — Smooth Sawn	Natural Joint	Intact	Remarks
In situ direct shear	No tests	$c = 0.56$ $\phi = 44.0$	No tests	Test results were linear
KC direct shear	No tests	$c = 0.0$ $\phi_s = 42.2$ $c_o = 0.32$ $\phi_o = 29.4$	No tests	Test results were linear. However, half the test experienced shear-through asperities at failure and half experienced override at failure
3- by 3-in. direct shear	$c = 0.0$ $\phi = 32.6$	No tests	$c_i = 7.94$ $\phi_i = 64.2$ $c_f = 13.72$ $\phi_f = 31.9$ $c = 4.68$ $\phi = 57.4$	Test results on intact pressed-into-place specimens were bilinear. Test results on grouted-into-place specimens were linear. Smooth sawn test results were linear

NOTE: c_i and ϕ_i denote parameters obtained from initial segment of a bilinear failure envelope.

c_f and ϕ_f denote parameters obtained from final segment of a bilinear failure envelope.

c_s and ϕ_s represent parameters for probable shear through asperity mode of failure.

c_o and ϕ_o represent parameters for probable overriding of asperity mode of failure.

222. The in situ direct shear tests on model material and Rangely sandstone specimens were assumed to be the primary datum base to which the various other tests were compared. The in situ direct shear device's design and operational characteristics minimize internal and external moments and thus minimize adverse stress concentration within the specimen generated by such moments; its "soft" normal load system provides for a constant normal load. The data acquisition system permits continuous monitoring of shear and normal loads and deformations. Of the shear devices evaluated, only the 3- by 3-in. soils direct shear and the triaxial devices were comparable in features. The validity in the datum base assumption is supported by the results from the in situ, 3- by 3-in., and the triaxial tests on smooth cast model material specimens (Figure 55). The in situ test results on smooth cast model material specimens also compared well with similar tests conducted by Rosenblad (1971) on a similar model material.

223. To illustrate the variations with respect to the datum base test results, it is convenient to compare the percent difference in predicted shear strength as defined by the respective failure envelopes. Since in situ direct shear tests were not conducted on intact model material specimens, the average c and $\emptyset$ values obtained from the 3- by 3-in. direct shear and the GL triaxial shear tests were used as the datum base for intact model material tests.

Model material smooth cast specimens tests

224. All failure envelopes from tests on smooth cast specimens were linear and had a zero cohesion intercept (c = 0.0). Therefore, the percent differences between predicted shear strength for the datum base (in situ direct shear) tests and the index tests were constant for each type of device and all values of normal stress. Table 11 summarizes the percent differences in predicted shear strength.

225. The 3- by 3-in. direct shear test results gave the best correlation with predicted shear strengths, 3.2 percent lower than the in situ direct shear results. The torsional shear (defined by elastic failure) and the triaxial shear test results had differences of -9.0 percent and -10.7 percent, respectively. The 6-in.-diam shear devices (ORD, KC, and IC) had differences ranging from -23.3 percent to -32.7 percent.

Model material even angle asperity tests

226. All failure envelopes from tests on even angle asperity were either bilinear or linear with cohesion intercepts. Therefore, the percent

Table 11

Percent Difference Between Predicted Shear Strength from Index Tests and Datum Base Tests on Smooth Cast Specimens

Type of Test	Percent Difference in Shear Strength*
Torsional (elastic failure)	- 9.0
ORD	-32.7
KC	-30.2
IC	-23.3
3- by 3-in.	- 3.2
Triaxial	-10.7

* Minus sign denotes shear strengths were lower than strengths from datum base tests.

differences between predicted shear strength for the datum base tests and the index tests vary with normal stress and cohesion. Figure 71 presents a plot of normal stress versus percent difference between predicted shear strengths.

227. The IC shear device test results (bilinear failure envelope) gave a good correlation with a -5.3 percent difference up to the transition normal stress of 4 tsf (see Figure 59). Above 4-tsf normal stress the percent difference in IC test results becomes increasingly more negative with a percent difference of -30.0 percent at 8.0-tsf normal stress.

228. The percent difference for the test results from the ORD and KC direct shear devices are similar. Percent differences ranged from +21.4 percent at normal stress of 2 tsf to a -30.2 percent at a normal stress of 6 tsf. The general plus to minus trend is caused by the apparent cohesion intercept of the two failure envelopes for these tests (see Figure 56).

229. The torsional shear test results defined by elastic failure had a range of percent difference between +11.4 percent at a normal stress of 2.0 tsf to +8.35 percent at a normal stress of 6.0 tsf. Trends in percent differences cannot be predicted for normal stresses higher than 6 tsf since no conclusive torsional shear tests on even angle asperities were conducted above that normal stress.

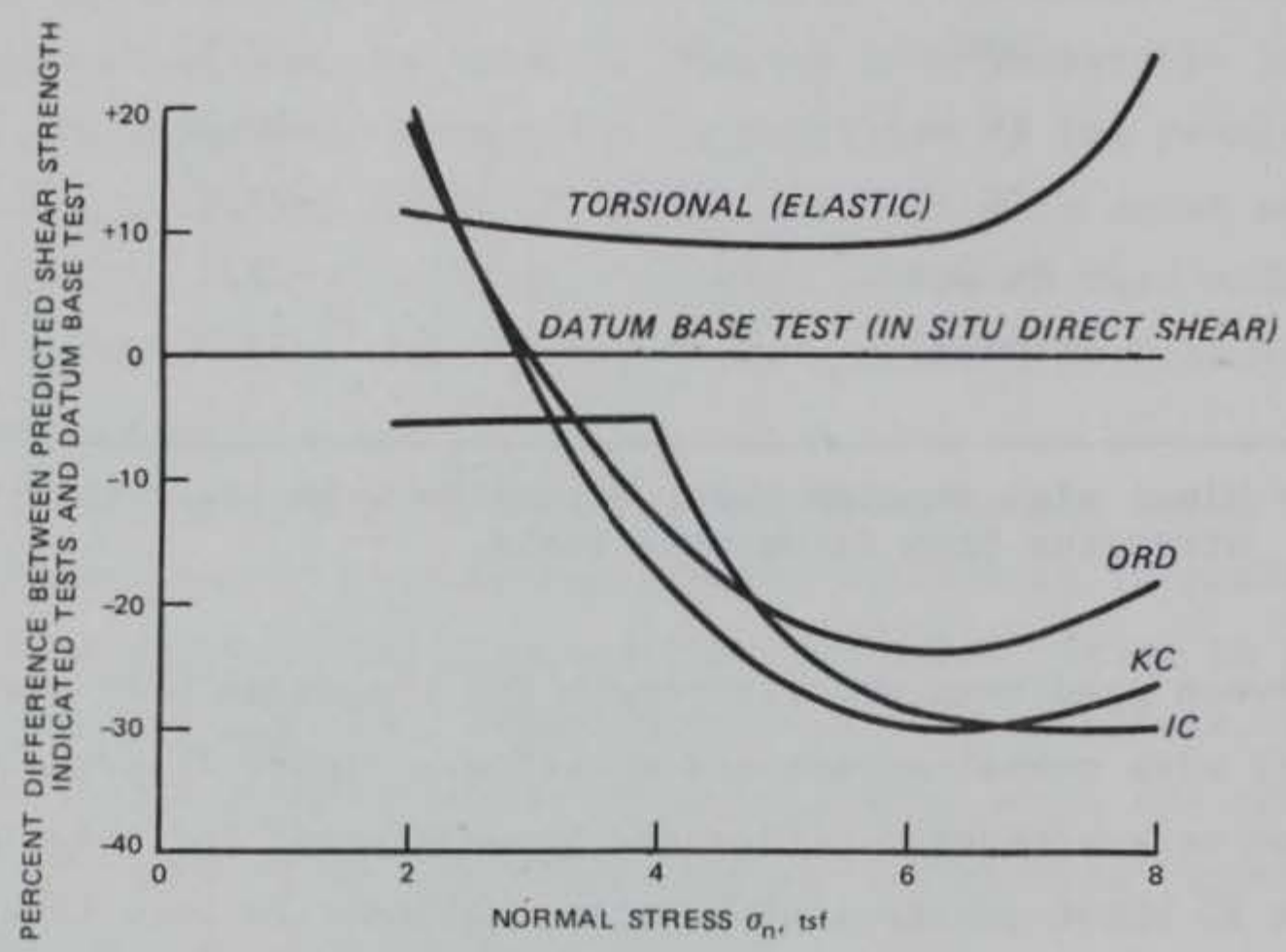

Figure 71. Normal stress versus percent difference between predicted shear strength from indicated tests and datum base test on model material even angle asperity specimens

Model material rake tooth asperity tests

230. All failure envelopes from tests on rake tooth asperities were linear with cohesion intercepts (c = 0.0). Therefore, the percent differences between predicted shear strength for the datum base tests and the index tests vary with normal stress. Figure 72 presents a plot of normal stress versus percent difference between predicted shear strengths.

231. The torsional shear test results (defined by plastic failure) gave the best correlation with respect to the datum base tests. The percent difference in predicted shear strength ranged from -23.7 percent at a normal stress of 2.0 tsf to -15.3 percent at a normal stress of 8.0 tsf.

232. The ORD direct shear test results yielded the second best correlation, with a predicted percent difference in shear strength of -22.6 percent at a normal stress of 2 tsf and -34.0 percent at a normal stress of 8 tsf.

233. The KC and IC direct shear test results were very similar. The predicted percent difference in shear strength for the KC tests ranged from -48.6 percent at a normal stress of 2.0 tsf to -35.5 percent at a normal stress of 8.0 tsf. The IC tests were -5.0 percent to -7.0 percent lower than the KC tests.

Model material intact specimens

234. All failure envelopes from tests on intact specimens were linear with cohesion intercepts. Therefore, the percent differences of predicted shear strength with respect to the datum base tests varied with normal stresses and cohesion. Figure 73 presents a plot of normal stress versus percent difference between predicted shear strengths.

235. The ORD direct shear test results gave the best correlation with respect to the datum base tests. The percent difference in predicted shear strength ranged from +21.9 percent at a normal stress of 2.0 tsf to +9.8 percent at a normal stress of 8.0 tsf. The ORD test results had a friction angle of 41.8 deg, which is 0.5 deg lower than the 42.3-deg average friction angle for the two datum base tests (soils triaxial and the 3- by 3-in. direct shear). The prediction by the ORD failure envelope of a higher shear strength than the datum base test is attributed to the higher cohesion intercept of 4.50 tsf (see Table 10).

236. The KC direct shear test results gave a percent difference in predicted shear strength ranging from -10.1 percent at a normal stress of 2.0 tsf to -33.5 percent at a normal stress of 8.0 tsf. The IC direct shear

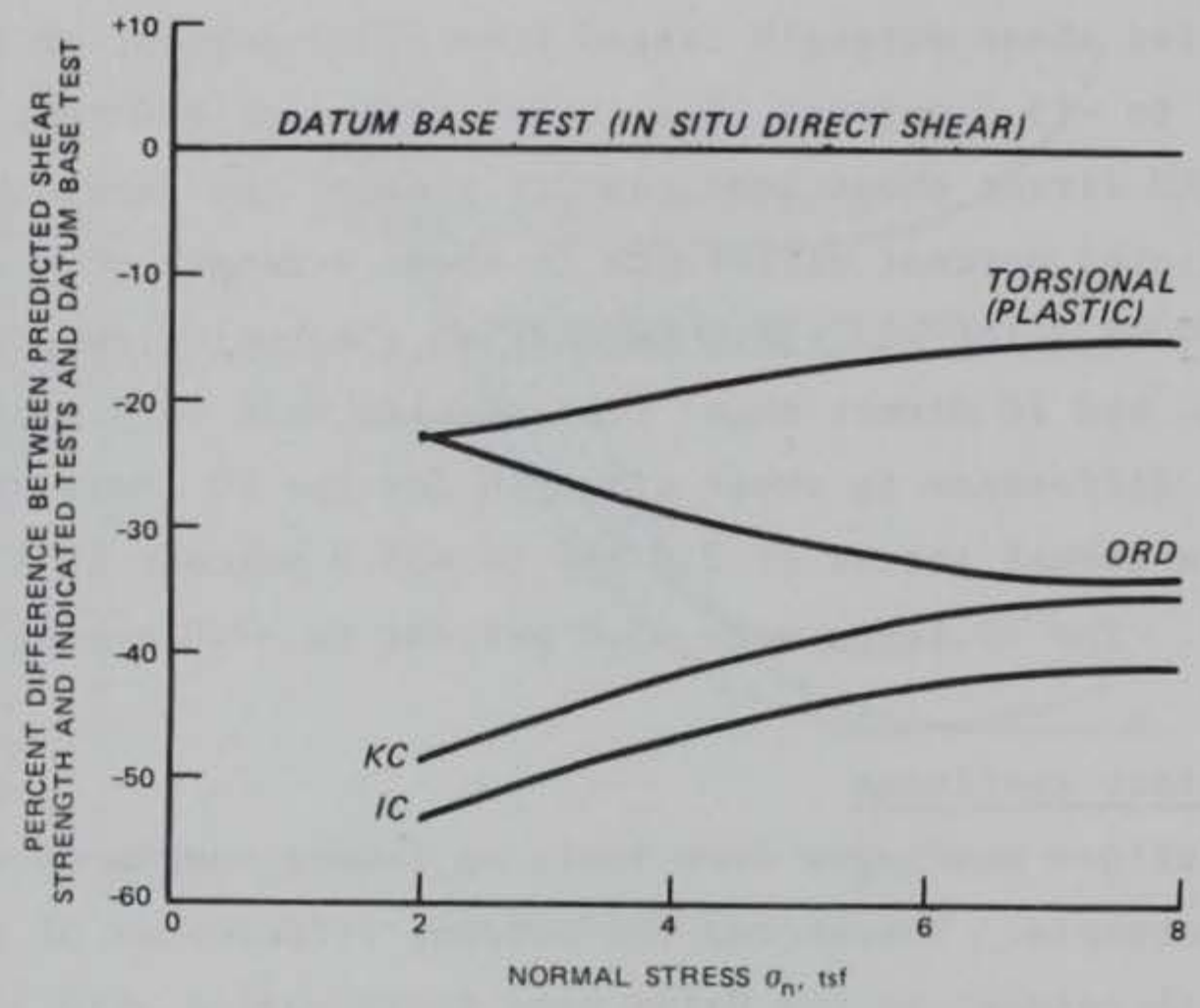

Figure 72. Normal stress versus percent difference between predicted shear strength from indicated tests and datum base test on model material rake tooth asperity specimens

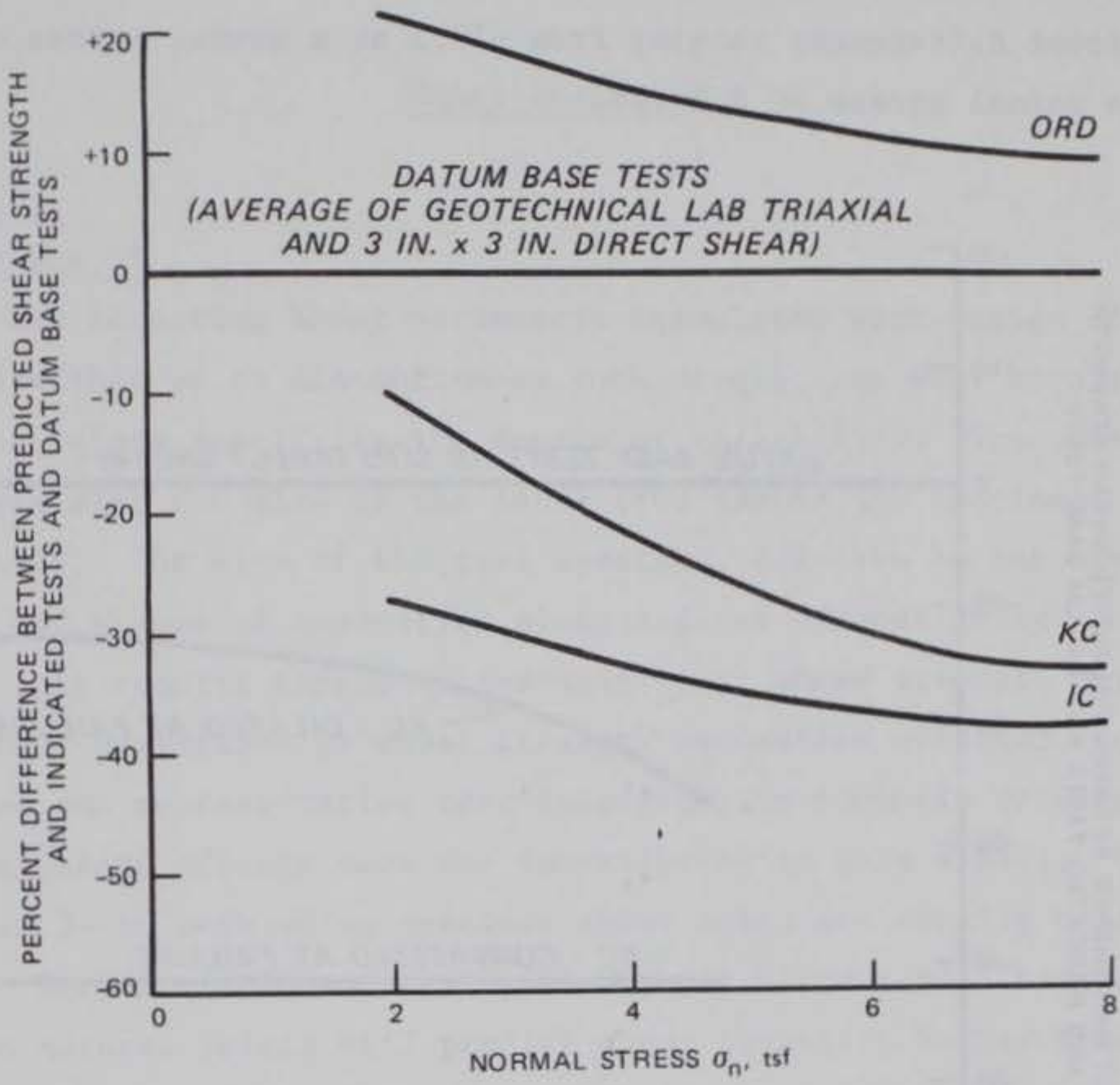

Figure 73. Normal stress versus percent difference between predicted shear strength from indicated tests and datum base tests on model material intact specimens

test results gave a percent difference ranging from -27.5 percent at a normal stress of 2.0 tsf to -38.1 percent at a normal stress of 8.0 tsf.

Rangely sandstone natural joint specimens

237. Failure envelopes for both the in situ and KC direct shear were linear. The KC tests were unique in that two different failure envelopes were obtained, depending upon whether the specimen dilated or compressed at failure. As discussed earlier, dilation or compression at failure is associated with override or shear through modes of failure. Figure 74 presents a plot of normal stress versus percent difference in predicted shear strength between the KC test results and the in situ datum base tests. The KC tests that underwent compression at failure resulted in a failure envelope that predicts an almost constant percent difference in shear strength of -41.7 to -41.9 with respect to the datum base tests. The KC tests that underwent dilation

(as did the in situ datum base tests) resulted in a more favorable correlation with percent differences ranging from -27.3 at a normal stress of 2.0 tsf to -12.5 at a normal stress of 8.0 tsf.

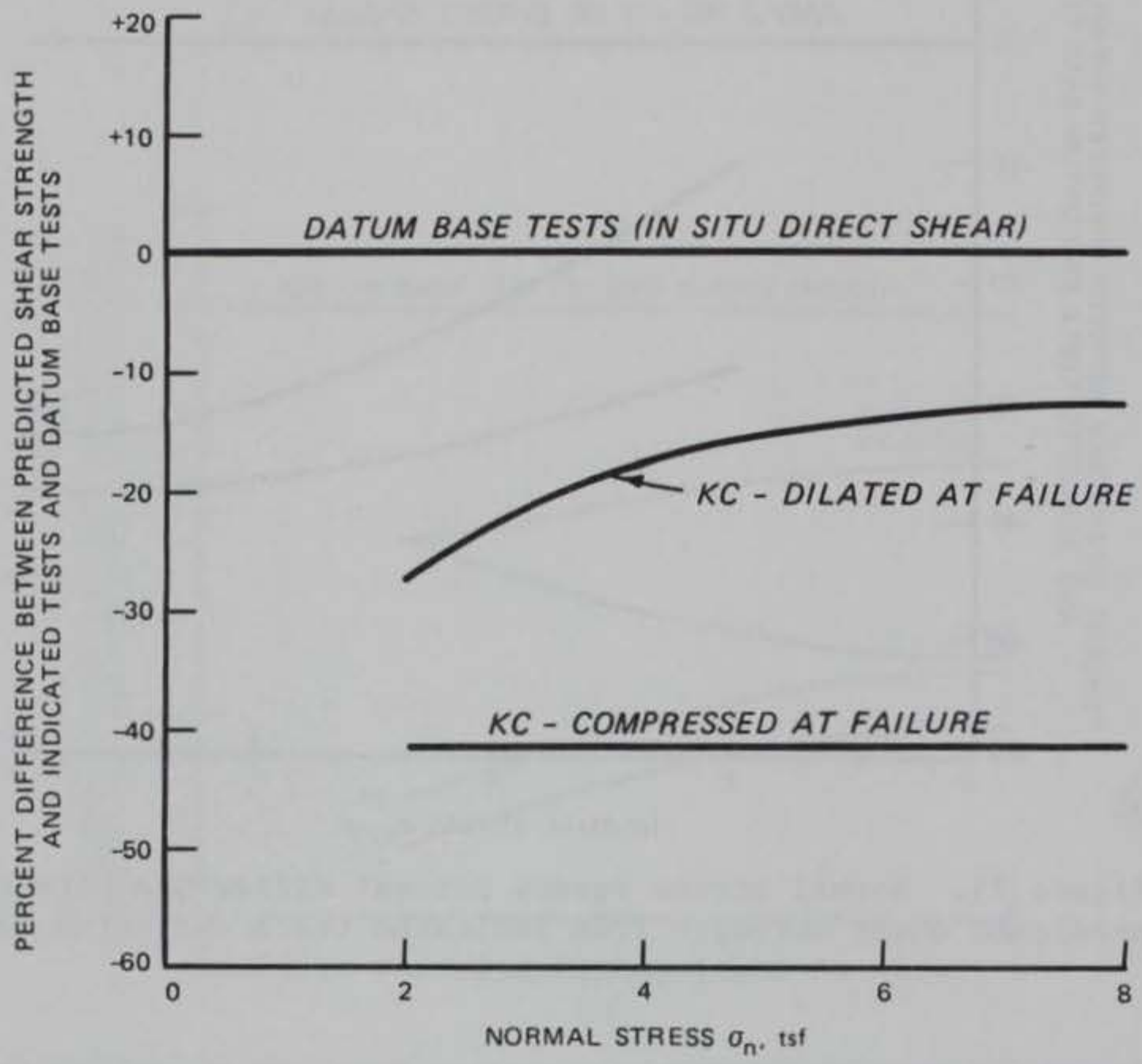

Figure 74. Normal stress versus percent difference between predicted shear strength from indicated tests and datum base tests on Rangely sandstone natural joint specimens

PART IX: CONCLUSIONS

Shear Devices

Shear devices in common use by the CE

238. When selecting shear parameters associated with design of structures founded within or on discontinuous rock masses, one must consider the cost of a test before specifying the degree of reliability. The cost of shear tests increases with the size of the tests (the larger the specimen, the higher the cost). The size of the test specimen, relative to the overall distribution and shapes of asperities along a given discontinuity, determines how well the test results represent the additional shear strength derived from the asperities. Deviations in shear strength parameters obtained from non-representative and representative test specimens are commonly referred to as scale effects (scale effects were not investigated in this study). Because of scale effects, 3- to 6-in.-diam specimen shear tests are usually considered as index tests. Barton (1973) and Pratt, Black, and Brace (1974) have shown that such tests on natural joints will predict shear strengths higher than actual prototype strengths.

239. The CE commonly uses three types of 2.8- to 6-in.-diam specimen tests. These are the 2.8-in.-diam triaxial tests and the 6-in.-diam ORD and KC direct shear tests. The IC direct shear test is also gaining some acceptance as a field index test. In the past, these shear devices have been used with little consideration given to the reliability of the parameters produced. The study presented herein demonstrates significant deviations in predicted shear strength parameters obtained from ORD, KC, and IC direct shear test devices. As a rule, the frictional component, ϕ , obtained from these three devices on smooth cast specimens were on the order of 8 to 10 deg lower than datum base (in situ shear) ϕ values.

Categorization of shear devices

240. Categorization of the various shear devices evaluated in this study is difficult since deviations in predicted shear strength appeared to be a function of the type of specimens tested, i.e. smooth cast, even angle, rake tooth, or intact. For example, the ORD direct shear test results on smooth cast specimens yielded the poorest correlation with the datum base tests, but

had the best correlation for the intact specimens. The inconsistent correlation for a given shear device and specimen type is attributed to unique operational characteristics of each device. Nevertheless, Table 12 attempts to list the various shear devices in order of their apparent ability to produce reliable data based on the test results of model material and Rangely sandstone specimens.

Improved direct shear device

241. The comparative study presented herein has demonstrated that both the ORD and KC devices are deficient in their ability to produce reliable shear strength behavior for soft discontinuous rock. The 3-in. by 3-in. soil direct shear device and the triaxial device produce reliable results but are limited in certain respects. The 3- by 3-in. device is limited to a maximum normal and shear stress of 20 tsf which is insufficient for most intact rock. The triaxial test costs approximately two to three times the cost of a direct shear test.

242. This study has demonstrated a need within the CE for a reliable direct shear device capable of testing 6-in.-diam or smaller rock core specimens, both intact and discontinuous. Ideally, such a device should be self-operational, self-monitoring, have provisions for a soft normal load system, be sufficiently rigid to permit tests suitable for input to finite element computer codes, and have a normal and shear stress range up to 100 tsf. As a result of this study, a new laboratory direct shear device (Figure 75) was designed and built at the WES. The design objectives included the following:

a. Provide for a constant shear displacement rate.

b. Provide for a constant normal load using a soft system.

c. Provide a self-contained test system.

d. Provide for minimum sample disturbance during specimen preparation.

e. Provide for automatic data collection.

243. The devised configuration is similar in design to the 3- by 3-in. soils direct shear device; i.e., it is a straight pull-through device with the shear force acting horizontally through the center of the test specimen. Important features of the device are as follows:

a. Shear displacement is controlled by a screw feed with transmission.

b. Maximum shear load is 50 kips.

c. Shear displacement rate is adjustable from <0.004 in./min.

Table 12

Various Shear Devices Listed in Order of Their Apparent Ability to Produce Reliable Shear Strength Parameters

Order	Type of Shear Device	Remarks
1	In situ direct shear	Design of the device permits good control of shear displacement rates and normal stresses. Size of specimen minimizes scale effects. Comparisons of test results with similar tests by Rosenblad (1971), Patton (1966), and Swolfs (1977) indicate excellent agreement. Design and construction of a shear load reaction frame is necessary to allow field testing. For maximum specimen size, shear stress range is limited to 15 tsf. Gear box modification is necessary to allow drained type tests. Expensive tests
2	3- by 3-in. soils direct shear	Design features of the device are similar to the in situ device. Comparison of test results with similar in situ and triaxial tests indicated good agreement. Can perform drained tests. Maximum shear and normal stress is limited to 20 tsf. Scale effects can be significant because of specimen size. Inexpensive tests
3	Triaxial shear	Devices of this type provide good control of principal stresses. Maximum range of shear stresses is higher than most direct shear devices. Stress concentrations due to end cap restraints can be a problem. Test results may be influenced by scale effects because of specimen size. Slightly more expensive than small direct shear test
4	Torsional shear	Size of specimen minimizes scale effects. The device provides good control of normal stresses. The rotational nature of failure makes it difficult to determine failure associated with sliding friction or asperity override. Elastic failure criteria appear to provide reasonable strength predictions. More study is needed to define failure criteria for asperity shear failure mode. More expensive than triaxial tests

(Continued)

Table 12 (Concluded)

Order	Type of Shear Device	Remarks
5	ORD	Tests in this device are inexpensive to run. Shear gap can be varied to suit particular needs. Normal stresses are subject to hydraulic ram friction effects. Test results may be influenced by scale effects
6	KC	Tests in this device are inexpensive to run. The device maintains good control of shear deformation rates and shear stress. Test specimens are subject to external moments. The device as used in this study required manual control of normal stresses
7	IC	Tests in this device are inexpensive to run. The device was designed for field tests on 4-in.-diam or smaller specimens. Both shear and normal stresses are subject to hydraulic ram friction effects. The test results on model material gave the poorest correlation with respect to the datum base tests

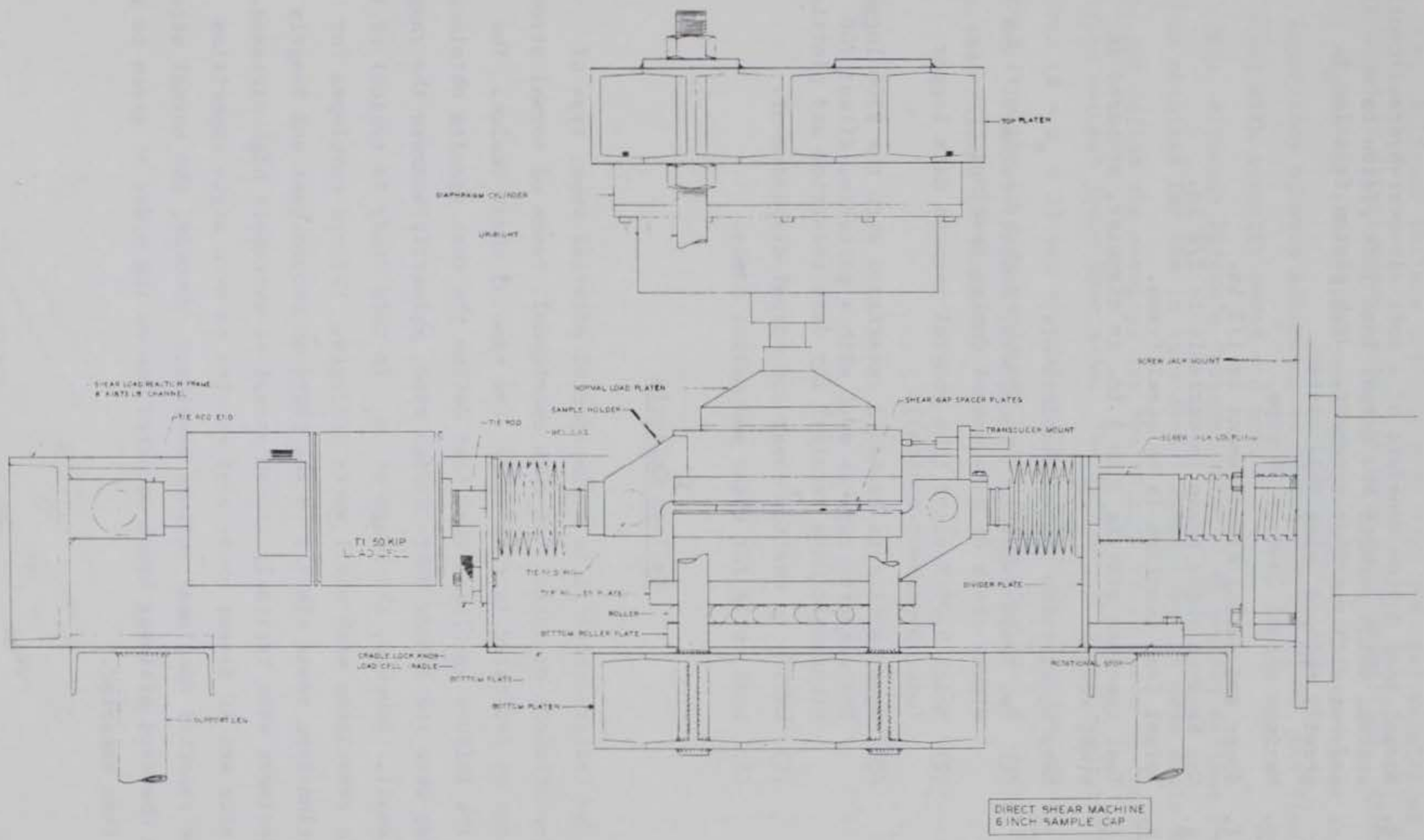

Figure 75. The WES laboratory direct shear device

d. Normal load device consists of a soft air-over-hydraulic-oil system, which permits the normal load jack piston to move in and out with specimen movement. Jack piston friction is greatly reduced using this system.

e. Maximum normal load is 30 kips.

f. Shear and normal displacement is 1/2 in.

g. Gap between shear boxes is variable to 1/2 in.

h. Normal load reaction is by steel frame.

i. Test specimen size is 3 to 6 in. in diameter, prepared in steel rings.

j. Data acquisition system consists of:

(1) Two 7046A X-double Y recorders, Hewlett-Packard. Use for visual check of data output during testing.

(2) Model 9300 Monitor Labs general purpose data logger (microprocessor control).

(3) Model 816A data cassette interfaced with the 9300 logger. The cassette tape is used with a portable, silent 700 electronic data terminal for data reduction and plotting.

(4) LVDT's to monitor shear and normal displacement.

(5) Load cells for shear and normal loads.

Failure Criteria

244. The failure criteria is a function of material type, type of specimen (discontinuous or intact for rock specimens), range of normal stress at failure, and as indicated in this study, the type of shear device. The majority of the failure envelopes that best define the test results obtained for this study were the linear Mohr-Coulomb type, primarily because the range of σ_n was small. However, the range of σ_n in this study is typical of the stress levels associated with civil works projects. Failure envelopes for sliding-friction-type tests similar to the tests on smooth cast and Rangely sandstone specimens were typically linear except at extremely high stresses. Only the in situ and KC direct shear test results on even angle asperities exhibited the expected nonlinear failure envelope. However, the normal stress at which the observed bilinear break occurred was on the order of seven to ten times lower than expected.

245. Bilinear failure criteria best fits the test results at failure for the in situ direct shear tests with even angle asperities. Although the initial segment of the failure envelope for KC direct shear tests on even angle asperities behaved according to Patton's predictions, the final segment associated with asperity shear did not.

246. Although Patton's failure criteria adequately defined the failure envelope obtained for the in situ direct shear tests on even angle asperities, it did not define the envelope for the in situ or KC tests on the Rangely sandstone natural joint specimens. The initial ϕ value predicted by Patton's criteria ($\phi = \phi_u + i$) was approximately 8 deg lower than the actual ϕ value obtained from the in situ tests and 6 deg lower than the ϕ value from the KC tests that dilated at failure.

REFERENCES

Barton, N. 1971. "A Relationship Between Joint Roughness and Joint Shear Strength," Rock Fracture Proceedings of the International Symposium on Rock Mechanics, Nancy, Vol 1, Theme I-8.

_____. 1973. "Review of a New Shear Strength Criterion for Rock Joints," Engineering Geology, Elsevier, 7, pp 287-332.

_____. 1976. "The Shear Strength of Rock and Rock Joints," International Journal of Rock Mechanics and Mining Sciences and Geomechanics Abstracts, Vol 13, No. 9, pp 255-279.

Bernaix, J. 1966. "Contribution a' L'etude de la Stabilite des Appuis des Barrages, Etude Geotechnique de la Roche de Malpasset," Ph.D. thesis, Paris.

Brown, D. M. R. and Walton, G. 1975. "A Portable Shear Box for Testing Rock Joints," Rock Mechanics, Journal of the International Society for Rock Mechanics, Vol 7, No. 3, pp 129-153.

Deere, D. R. et al. 1967. "Design of Surface and Nearsurface Construction in Rock," Proceedings, 8th Symposium on Rock Mechanics, American Institute of Mining Engineers, University of Minnesota, pp 232-302.

Fairhurst, C. 1964. "On the Validity of Brazilian Test for Brittle Materials," International Journal of Rock Mechanics and Mining Sciences, Vol 1, pp 535-546.

International Society of Rock Mechanics. 1974. "Suggested Methods for Determining Shear Strength," Commission on Standardization of Laboratory and Field Tests, Document No. 1, Lisboa Codex, Portugal.

Jaeger, J. C. 1971. "Friction of Rocks and the Stability of Rock Slopes - Rankine Lecture," Geotechnique, Vol 21, p 97.

Kenty, J. D. 1970. "Suggested Method of Test for Direct Shear Strength of Rock Core Specimens," Special Procedures for Testing Soil and Rock for Engineering Purposes, 5th ed., American Society for Testing and Materials Special, Technical Publication 479, Philadelphia, Penn., pp 613-617.

Kutter, H. K. 1971. "Stress Distribution in Direct Shear Test Samples," Proceedings of the International Symposium of Rock Fracture, International Society of Rock Mechanics, Nancy, paper 2-6.

Ladanyi, B. and Archambault, G. 1970. "Simulation of Shear Behavior of a Jointed Rock Mass," Proceedings, Eleventh Symposium on Rock Mechanics, American Society of Mining Engineers, pp 105-125.

Mogi, K. 1974. "On the Pressure Dependence of Strength of Rock and the Coulomb Fracture Criterion," Tectonophysics, Vol 21, pp 273-285.

Patton, F. D. 1966. "Multiple Modes of Shear Failure in Rock and Related Materials," Ph.D. thesis, University of Illinois.

Pratt, H. R., Black, A. D. and Brace, W. F. 1974. "Friction and Deformation of Jointed Quartz Diorite," Proceedings of the Third Congress of the International Society of Rock Mechanics, Denver, Vol II, Part A, pp 306-310.

Rosengren, K. J. 1968. "Rock Mechanics of the Black Star Open Cut, Mount Isa," Ph.D. thesis, Australian National University, Canberra.

Rosenblad, J. L. 1971. "Geomechanical Model Study of the Failure Modes of Jointed Rock Mass," Technical Report MRD-1-71, Missouri River Division, U. S. Army Engineer District, CE, Omaha, Nebr.

Sellers, J. B. 1973. "Measurement of In Situ Shear Strength Using the Torsional Shear Method," American Society for Testing and Materials, Special Technical Publication 554, Field Testing and Instrumentation of Rock, pp 147-155.

Swolfs, H. S. 1977. "Field Experiments on the Castlegate Sandstone, Rangely Anticline, CO," Technical Report 77-105, Published by Terra Tek for the U. S. Army Research Office, Salt Lake City, Utah.

U. S. Army Engineer Waterways Experiment Station, CE. 1949. "Handbook for Concrete and Cement," CRD-C 227-78, Vicksburg, Miss.

_____. 1970. "Soil Mechanics Testing Facilities at the Waterways Experiment Station," U. S. Army Engineer Waterways Experiment Station, Vicksburg, Miss.

_____. 1980. "Rock Testing Handbook," Test Standards, Vicksburg, Miss.

Zeigler, T. W. 1972. "In Situ Tests for the Determination of Rock Mass Shear Strength," Technical Report S-72-12, U. S. Army Engineer Waterways Experiment Station, CE, Vicksburg, Miss.